

6. SITE 737¹

Shipboard Scientific Party²

HOLE 737A

Date occupied: 30 December 1987
Date departed: 31 December 1987
Time on hole: 1 day, 12 hr, 45 min
Position: 50°13.67'S; 73°01.97'E
Bottom felt (rig floor: m, drill-pipe measurement): 574.5
Distance between rig floor and sea level (m): 10.5
Water depth (drill-pipe measurement from sea level, m): 564.0
Total depth (rig floor, m): 847.7
Penetration (m): 273.2
Number of cores: 29
Total length of cored section (m): 273.2
Total core recovered (m): 181.64
Core recovery (%): 66
Oldest sediment cored:
Depth sub-bottom (m): 263.5
Nature: diatom nannofossil ooze
Earliest age: late Miocene
Measured velocity (km/s): 1.57

HOLE 737B

Date occupied: 31 December 1987
Date departed: 4 January 1987
Time on hole: 3 days, 19 hr, 45 min
Position: 50°13.67'S; 73°01.95'E
Bottom felt (rig floor: m, drill-pipe measurement): 574.5
Distance between rig floor and sea level (m): 10.5
Water depth (drill-pipe measurement from sea level, m): 564.0
Total depth (rig floor, m): 1290.0
Penetration (m): 715.5
Number of cores: 52
Total length of cored section (m): 715.5
Total core recovered (m): 298.35
Core recovery (%): 41
Oldest sediment cored:
Depth sub-bottom (m): 715.5
Nature: clayey limestone
Earliest age: middle Eocene
Measured velocity (km/s): 3.06
Principal results: Site 737 (50°13.67'S, 73°01.95'E; target Site KHP-3) is on the northern Kerguelen-Heard Plateau, about 100 km south-

east of Site 736, in a water depth of 564 m. The 715.5-m-thick middle Eocene through lower Pliocene section cored in two holes at Site 737 begins almost exactly (3.4 Ma) where coring terminated at Site 736, so together, the two sites form a valuable reference section for the upper Paleogene and Neogene at about 50°S.

Coring commenced on 30 December 1987 in Hole 737A with the advanced piston corer (APC) to 167 m below seafloor (mbsf). Average core recovery approached 100% for this interval. Below 167 mbsf, extended core barrel (XCB) coring continued to a depth of 273.2 mbsf. Core recovery averaged 22% in this lower sequence. The poor recovery in the lower part of Hole 737A resulted in the decision to terminate the hole and switch to the rotary core barrel (RCB) in Hole 737B. Hole 737B was washed down to 114.5 mbsf, and two cores were taken between 114.5 and 133.8 mbsf to sample the Miocene/Pliocene boundary, which was not recovered in Hole 737A. The hole was then washed from 113.8 to 253.5 mbsf. The remainder of the hole was cored with the RCB to total depth (715.5 mbsf). The recovery was variable, averaging 62%. Most of the recovered cores were only slightly deformed or fractured.

Six lithologic units were recognized at Site 737. The topmost 1.5 m consists of a Quaternary glauconitic lag sand that rests on a 234-m-thick sequence of diatom ooze. From 234 to 250 mbsf increasing amounts of calcareous nannofossils change the sediment to a diatom nannofossil ooze, which extends to 313 mbsf. The diatom and diatom-nannofossil oozes seem to be a continuous lower Pliocene to upper Miocene (3.4–8.2 Ma) section from 1 to 263 mbsf. A hiatus covering the time from 8.2 to 10 Ma between the upper Miocene and the middle Miocene is indicated at the base of this level. The sedimentation rate was significantly lower for the middle Miocene diatom-nannofossil ooze interval from 264 to 315 mbsf than for the younger section in Holes 737A and 737B.

The oozes are underlain by a 355-m-thick sequence of variably bioturbated glauconitic calcareous claystones forming an almost continuous hemipelagic and turbidite-redeposited section from the upper Eocene to upper Oligocene. The top of this sequence is therefore a major hiatus covering the interval from 15 to 23 Ma. This hiatus probably shows up as the important reflector A of Munschy and Schlich (1987), who propose that it marks that division between pre-rifting and post-rifting sequences on the Kerguelen Plateau. The age of reflector A is thus clearly younger than the middle Eocene age expected.

The deepest part of Hole 737B, from 670 to 715 mbsf, unveiled a clayey pelagic limestone with scattered thin (10-cm-thick) layers of middle Eocene age chert. The upper part of this layer is correlated with a strong seismic reflector, possibly reflector M of Munschy and Schlich (1987). Minor amounts of volcanic material occur throughout the cored section.

Siliceous microfossils are abundant and well preserved and the diatom assemblages are highly diversified in the siliceous upper part (middle Miocene to Quaternary) of the sequence. Calcareous nannofossils are abundant throughout the Eocene-Oligocene lower part of the cored sequence. Below 245 mbsf all core-catcher samples yield foraminifers, chiefly planktonic. A detailed magnetostratigraphy has been established for the Oligocene interval.

BACKGROUND AND OBJECTIVES

Termination of Coring at Site 736

A combination of factors were responsible for the decision to terminate coring at Site 736 (target Site KHP-1) and to relocate *JOIDES Resolution* to Site 737 (target Site KHP-3). Below 127.1 mbsf, core recovery at Site 736 decreased considerably (from an

¹ Barron, J., Larsen, B., et al., 1989. *Proc. ODP, Init. Repts.*, 119: College Station, TX (Ocean Drilling Program).

² Shipboard Scientific Party is as given in the list of Participants preceding the contents.

average of 95% above to 29% below), presumably because the sediment was too stiff to penetrate with the XCB but too unconsolidated to recover without substantial loss. In an attempt to improve the core recovery, the drill string was tripped and Hole 736C commenced with the RCB system. Although core recovery improved slightly (averaging 47.1%), the sediment remained poorly consolidated and exhibited moderate to severe drilling disturbance. These conditions continued downhole without any sign of improvement for more than 100 m below the depth at which XCB coring was terminated (253.3 mbsf).

The sediment recovered at Site 736 consists of diatom ooze with varying volcanic-detrital content and low carbonate content. Sediment-accumulation rates averaged nearly 100 m/m.y. Thus, at 370 mbsf, the sediment is estimated to be younger than 4 Ma. Geophysical results at Site 736 suggested that the stratigraphic interval from 0 to 260 mbsf represents a major part of the S1 seismic sequence of Munsch and Schlich (1987). Comparison with the seismic records completed during the site survey of target Site KHP-3 and seismic lines completed between target Sites KHP-1 and KHP-3 suggest that although most, if not all, of seismic sequence S1 would be removed at target Site KHP-3, an estimated 320 m of lower and lower upper Neogene seismic sequence S2 would be present.

It was also reasoned that the upper part of this S2 sequence could be recovered with the APC at target Site KHP-3 and that the expected enriched Miocene carbonate sediments may be less diagenetically altered than they are at Site 736. Recovery of well-preserved carbonate sediments is necessary for completing detailed isotopic analysis.

In as much as discordance A of Munsch and Schlich (1987) was projected to occur at 320 mbsf at Site 737—compared with an estimated depth of 910 mbsf at Site 736—it was reasoned that this coring objective could be better achieved at Site 737 than at Site 736. Similarly, coring at Site 737 provided the possibility to recover more of the pre-rift sediments (?Eocene) that lie below discordance A. Recovery of these sediments will provide a northern point to the paleoceanographic transect for the pre-Neogene sediments and will allow comparisons of this region with sediments recovered from Ninetyeast and Broken Ridge during Leg 121.

Objectives

The drilling objectives for Site 736 also apply for Site 737. The primary objective at Site 737 is to date discordance A of Munsch and Schlich (1987). Other objectives include (1) recovery of a high-resolution reference section from the northern end of the Kerguelen Plateau-Prydz Bay transect (ODP Legs 119 and 120) for both biostratigraphic and paleoceanographic analyses, (2) documentation of the depositional processes previously and presently active at this site, and (3) determination of the tectonic history of this region of the plateau.

SITE GEOPHYSICS

Site Survey

A geophysical survey line was run from Sites 736 to 737 (ODP line 119-02, Fig. 1) using the standard navigation, seismic, and magnetic equipment (see "Explanatory Notes" chapter, this volume). About 3 km prior to crossing the proposed site a sonobuoy was deployed and recorded to a total offset of 8 km. A beacon was dropped on the initial crossing of the proposed site. The high-resolution (3.5-kHz) seismic data at this site indicated disruption of the upper 100 m of the sedimentary section, and the sonobuoy reflection data showed localized higher-velocity sediment. Consequently, Site 737 was moved from the proposed location to the point at which the sonobuoy had been deployed and where shallow sediments were not disrupted.

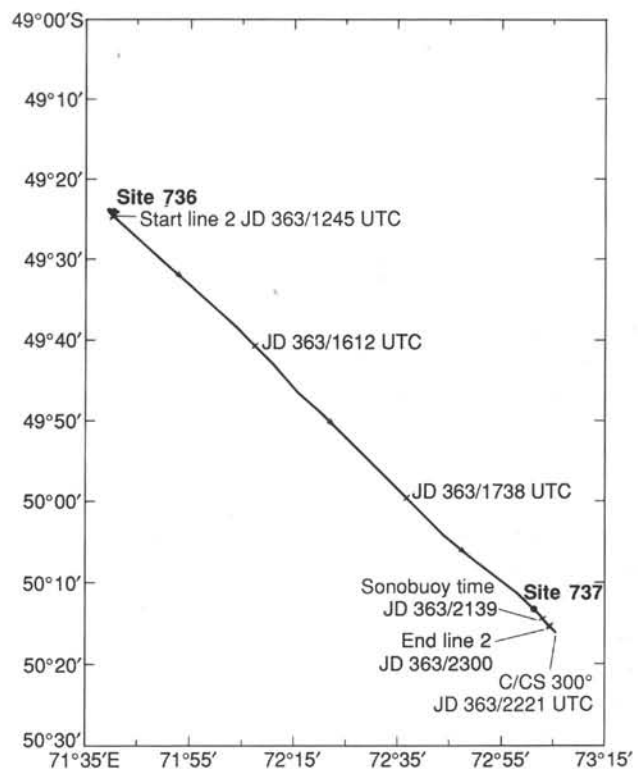


Figure 1. Index map of seismic lines recorded during site surveys for Site 737.

Upon completion of the sonobuoy run, the ship returned to the relocated site on a reciprocal course. Midway along the return line, the seismic gear was recovered. The final approach to the site was made with Global Positioning System (GPS) satellite navigation. The seismic results are discussed in the "Seismic Stratigraphy" section (this chapter).

Sonobuoy Data

The sonobuoy was deployed to assist in locating the drilling site and to acquire wide-angle reflection- and refraction-velocity data to compute depths prior to, rather than during, drilling operations.

Strong wide-angle reflection and refraction arrivals were recorded during the sonobuoy deployment (Fig. 2). Interval velocities for five layers (AA to FF) were computed using wide-angle reflections to offset distances of 4.5 km. Refraction arrivals were observed for three of the layers and underlying basement to offset ranges of 8 km. The interval and refraction velocities computed from the sonobuoy reflectors and refractors (Fig. 3) are given in Table 1.

The sonobuoy results indicate that low-velocity sedimentary strata (1.49–1.64 km/s) extend from the seafloor to the high-amplitude reflector at 1.1 s (CC, Fig. 3). The absence of detectable refraction arrivals from horizons AA and BB and the large horizontal offset to the first refractor (from CC) provide additional evidence that velocities are low and increase slowly with depth in the uppermost sedimentary section. The next two deeper layers form a distinct acoustic unit (CC to EE) that has only slightly higher interval velocities (1.89–2.14 km/s).

An abrupt increase in refraction velocity to 3.7 km/s occurs at 1.5 s (EE, Figs. 3 and 4), the top of acoustic basement in multichannel seismic-reflection profiles. The refractions from

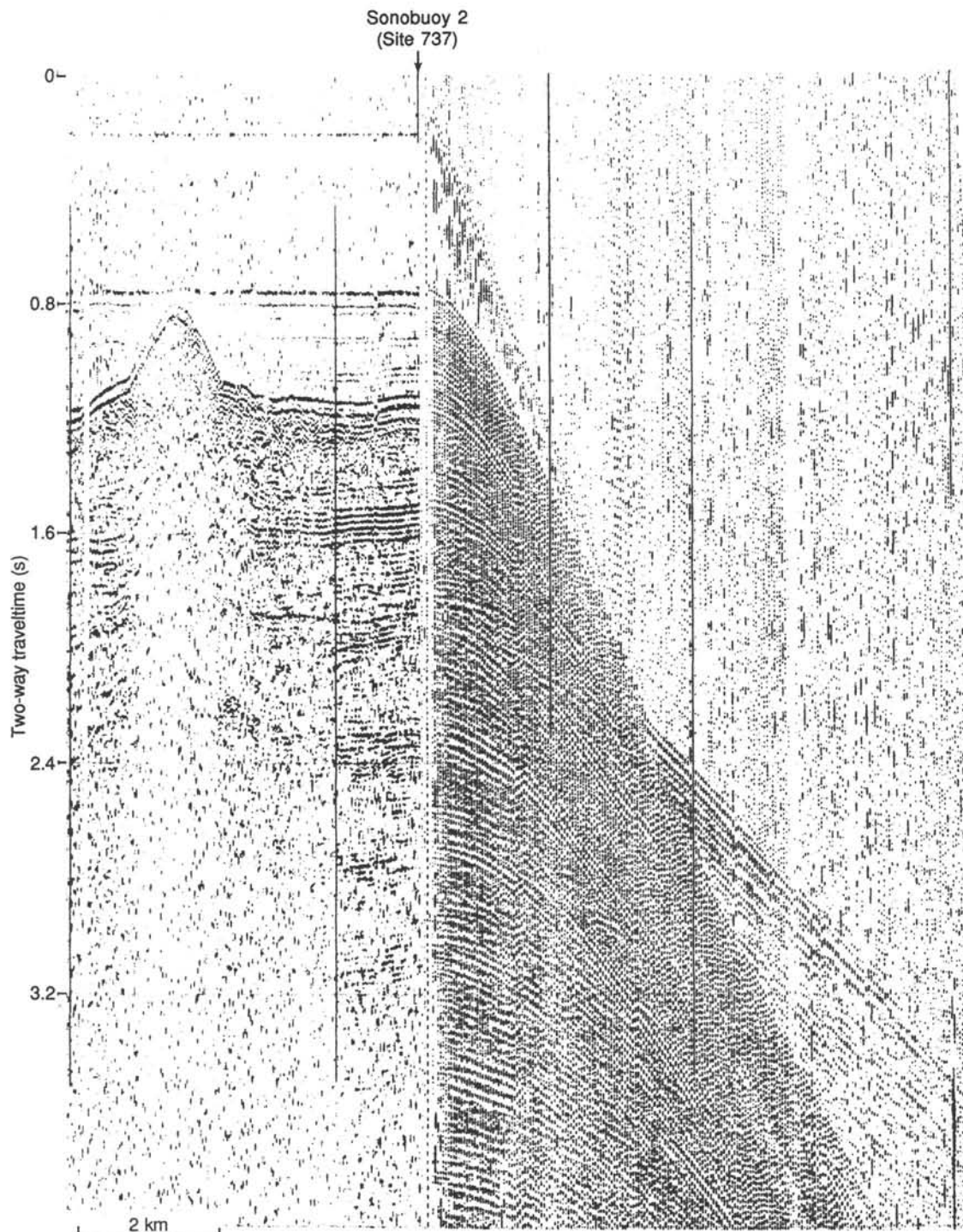


Figure 2. Vertical-incident seismic and sonobuoy seismic record for sonobuoy station 2. Site 737 is directly beneath where the sonobuoy was deployed. See Figure 1 for location.

EE are high-amplitude returns that show a velocity gradient from the top (3.7 km/s) to the bottom (3.91 km/s) of layer EE-FF. The interval velocity for layer EE-FF (3.87 km/s) concurs with the refraction velocities, but is about 10%–15% higher than velocities measured for the deepest unit in Hole 737B (see “Logging” section, this chapter). The sonobuoy velocities are similar to those measured elsewhere on Kerguelen Plateau for acoustic basement, suggesting that volcanic igneous basement

lies at greater depth. At Site 737, horizon FF, which has a refraction velocity of 4.51 km/s, is likely volcanic basement. The total depth to presumed volcanic basement beneath Site 737 is about 2029 m, and the thickness of overlying sedimentary strata is about 1465 m.

The interval velocities determined from the sonobuoy data are similar to those computed from routine stacking velocities for multichannel seismic-reflection data about 3 km from Site

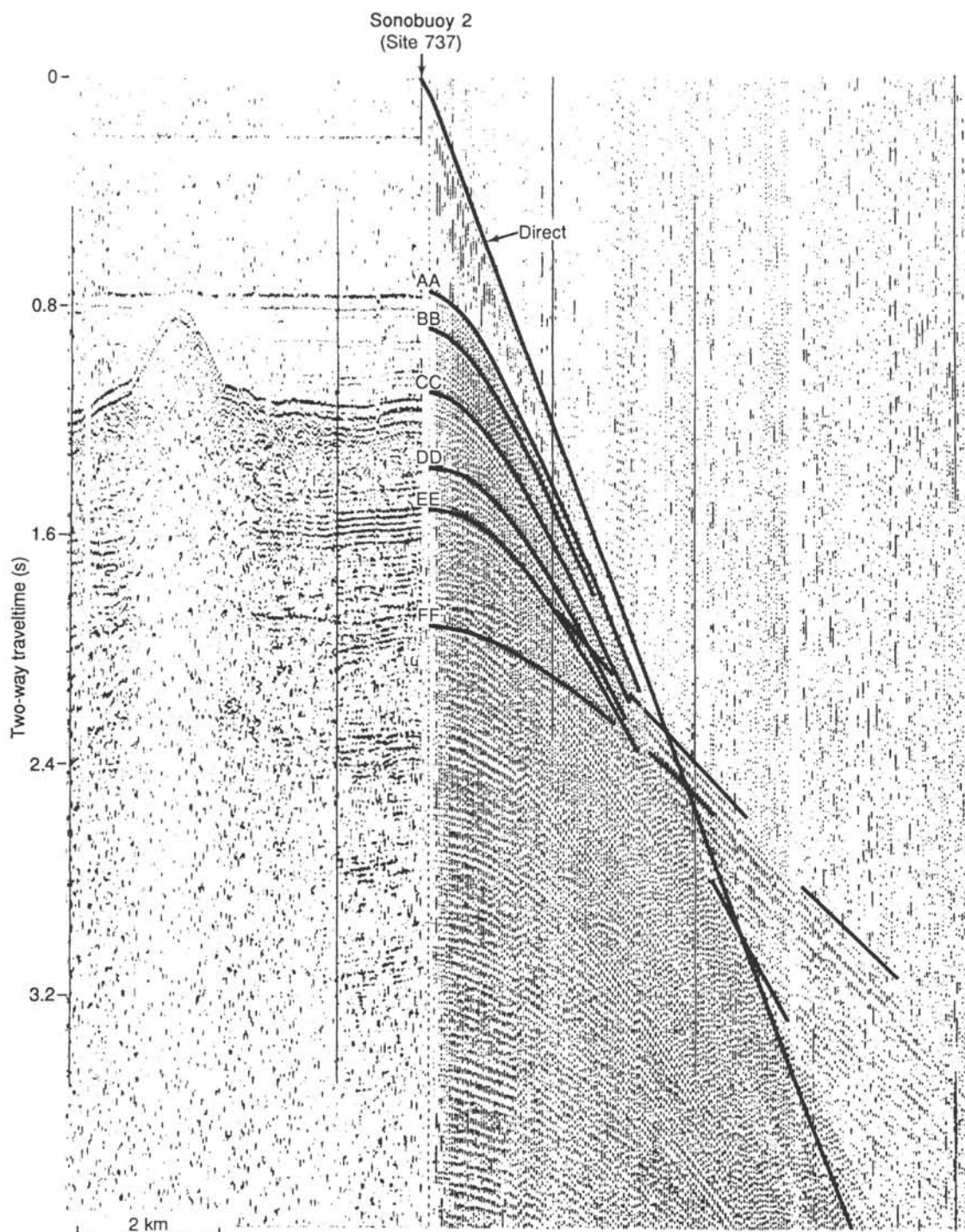


Figure 3. Vertical-incident seismic and sonobuoy seismic record for Site 737 showing wide-angle reflection and refraction interpretations. Letters denote layers in Table 1. See Figure 1 for location.

737. A comparison of sonobuoy velocities with those determined from Hamilton Frame and downhole logging measurements is given in the "Logging" section.

In summary, the sedimentary section at Site 737 is characterized by about 276 m of low-velocity strata (1.49–1.64 km/s) that is separated by a velocity discontinuity from a 395-m-thick underlying unit with velocities of 1.89 to 2.14 km/s. This discontinuity appears to coincide with the geologic hiatus between overlying mid-Miocene and younger diatomaceous oozes and underlying late Oligocene age and older calcareous ooze and

volcanic debris. A deeper layer with a thickness of about 794 m and velocity of 3.70–3.91 km/s is composed of indurated sedimentary rocks that overlie the volcanic basement of the plateau. The presumed volcanic basement is about 1465 mbsf at Site 737 and has a velocity of 4.51 km/s.

OPERATIONS

Site 737 is situated just 100 km southeast of Site 736. The vessel got under way on a reciprocal course and surveyed back across the site location, continuing on course to the new site. A

Table 1. Preliminary results for sonobuoy 2, Site 737.

Horizon ^a	Vrms (km/s)	Vint (km/s)	Ti (s)	Zi (km)	Vrfr (km/s)	To (s)
AA	1.470	1.49	0.75	0.564	nr	—
BB	1.474	1.64	0.90	0.676	nr	—
CC	1.506	1.89	1.10	0.840	1.67	0.43
DD	1.582	2.14	1.36	1.085	2.52	1.25
EE	1.634	3.87	1.50	1.235	3.70-3.91	1.39-1.44
FF	2.378	—	1.91	2.029	4.51	1.68

Note: Vrms = rms velocity for horizon; Vint = interval velocity computed using Vrms, Ti, and Dix equation (e.g., Vint between horizons AA and BB is 1.49 km/s); Ti = vertical-incidence reflection time (two-way) to horizon; Zi = total depth from sea level to horizon computed from Vint and Ti (water depth = 564 m); Vrfr = refraction velocity associated with horizon (e.g., Vrfr at top of layer CC-DD is 1.67 km/s); To = intercept time for refractor associated with horizon; nr = no refractor observed.

^a Letters of horizons do not correlate between drill sites and do not correspond to prior stratigraphic analyses.

sonobuoy was launched about 1 km before the proposed geographic coordinates were reached. The recoverable positioning beacon was dropped on the first pass over the site using GPS navigation. Immediately following the beacon launch, the 3.5-kHz profile showed an unacceptable disruption in the upper sediment section (the multichannel reference profile did not show detail in the upper 0.2 s). After a 2-nmi extension to the southeast, the ship turned, headed back toward the beacon, and retrieved the seismic gear. An offset was then made 1 nmi back along the approach track to a location with a more desirable sediment section, and a second positioning beacon was dropped.

Site 737: North Kerguelen Plateau

Hole 737A

Coring operations began with an APC core to recover the mud line at 574.5 m (drill-pipe measurement). Swells to 8 m again complicated operations, but the experienced crew was able to compensate for much of the motion with the coring line. As at Site 736, motion conditions neutralized efforts for oriented coring and heatflow measurements. Core recovery was quite good (Table 2), but Core 119-737A-14H was lost when a sub in the APC corer failed at the rig floor. An overpull of 90,000 lb prompted the switch to XCB mode at 167 mbsf.

Recovery of the next 107 m of diatom ooze with the XCB was only 21%. The presence of calcareous nannofossil ooze in the last two cores prompted the decision to return to the APC in an attempt to improve core recovery. Core 119-737A-29X was "shot" and apparently fully stroked, but a sub failed at the top of the core barrel and parted with an overpull of only about 25,000 lb. Attempts were made to fish the barrel with a wireline-deployed spear, but without success—at least partly because of a vessel heave of up to 3 m.

Hole 737A operations were then terminated, and a round trip was made for the RCB bottom-hole assembly (BHA) in anticipation of the stratigraphically deeper limestone and chert.

Hole 737B

Following the pipe trip, Hole 737B was spudded at 1930 hr, 31 December. The hole was drilled to 114 mbsf before the wash barrel was recovered. Two cores were then taken to recover the missed interval of Core 119-737A-14H. After another drilled interval to 253 mbsf, continuous RCB coring began. Core recovery began to improve below 300 mbsf (from about 40% to about 60%) and continued to improve slightly with depth. The diatom ooze gave way to chalk at about 465 mbsf. The chalk became more indurated with depth and graded to limestone. Below about 690 mbsf, there were scattered chert nodules, but not

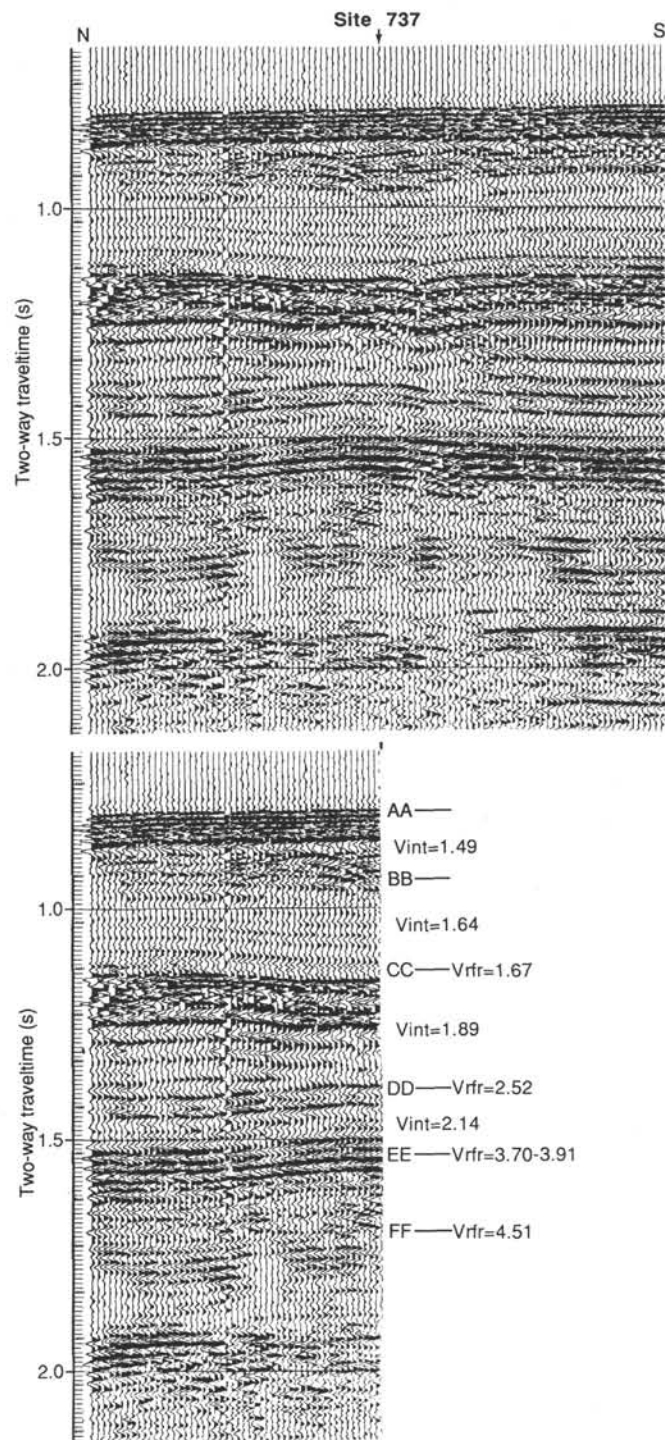


Figure 4. Vertical-incidence seismic data showing sonobuoy interval and refraction velocities at Site 737.

enough to affect drilling operations. At 715.5 mbsf the scientific drilling objective was reached, and coring was stopped.

Because hole stability was perfect for the duration of drilling/coring operations, only a 60-bbl mud flush was circulated in preparation for logging operations. No wiper trip was made. A wireline trip was made to actuate the mechanical bit release (MBR), and the end of the drill string was pulled to logging depth at 125 mbsf.

The first logging run, the seismic stratigraphic combination, was stopped by an obstruction at 260 mbsf. A good-quality log

Table 2. Coring summary, Site 737.

Core no.	Date (1987-1988)	Time	Depth		Length		Recovery (%)
			top (mbsf)	bottom (mbsf)	cored (m)	recovered (m)	
119-737A-							
1H	Dec. 30	0820	0.0	5.0	5.0	4.97	99.4
2H	30	0900	5.0	14.5	9.5	9.78	103.0
3H	30	1000	14.5	24.0	9.5	9.96	105.0
4H	30	1035	24.0	33.5	9.5	10.09	106.2
5H	30	1110	33.5	43.0	9.5	8.21	86.4
6H	30	1210	43.0	52.5	9.5	8.94	94.1
7H	30	1245	52.5	62.0	9.5	9.84	103.0
8H	30	1325	62.0	71.5	9.5	10.06	105.9
9H	30	1355	71.5	81.0	9.5	9.87	104.0
10H	30	1540	81.0	90.5	9.5	9.20	96.8
11H	30	1610	90.5	100.0	9.5	9.69	102.0
12H	30	1645	100.0	109.5	9.5	9.98	105.0
13H	30	1725	109.5	119.0	9.5	9.72	102.0
14H	30	1845	119.0	128.5	9.5	0.00	0.0
15H	30	2030	128.5	138.0	9.5	9.73	102.0
16H	30	2100	138.0	147.5	9.5	9.77	103.0
17H	30	2145	147.5	157.0	9.5	9.75	102.0
18H	30	2230	157.0	166.5	9.5	9.72	102.0
19X	30	2330	166.5	176.2	9.7	1.52	15.7
20X	31	0010	176.2	185.9	9.7	0.32	3.3
21X	31	0035	185.9	195.6	9.7	2.26	23.3
22X	31	0105	195.6	205.3	9.7	0.00	0.0
23X	31	0210	205.3	215.0	9.7	2.59	26.7
24X	31	0245	215.0	224.7	9.7	0.00	0.0
25X	31	0410	224.7	234.4	9.7	5.80	59.8
26X	31	0435	234.4	244.1	9.7	2.20	22.7
27X	31	0505	244.1	253.8	9.7	5.68	58.5
28X	31	0835	253.8	263.5	9.7	1.99	20.5
29X	31	0915	263.5	273.2	9.7	0.00	0.0
					273.2	181.64	
119-737B-							
1W	31	2230	0.0	114.5	114.5	0.00	
2R	31	2315	114.5	124.2	9.7	0.94	9.7
3R	31	2350	124.2	133.8	9.6	4.21	43.8
4W	Jan. 01	0245	133.8	253.5	119.7	0.00	
5R	01	0310	253.5	263.2	9.7	4.98	51.3
6R	01	0350	263.2	272.9	9.7	6.26	64.5
7R	01	0420	272.9	282.5	9.6	1.18	12.3
8R	01	0450	282.5	292.2	9.7	3.72	38.3
9R	01	0505	292.2	301.8	9.6	2.34	24.4
10R	01	0610	301.8	311.5	9.7	5.49	56.6
11R	01	0700	311.5	321.1	9.6	4.42	46.0
12R	01	0725	321.1	330.8	9.7	8.92	91.9
13R	01	0750	330.8	340.4	9.6	5.41	56.3
14R	01	0820	340.4	350.1	9.7	7.79	80.3
15R	01	0845	350.1	359.8	9.7	6.86	70.7
16R	01	0910	359.8	369.4	9.6	5.28	55.0
17R	01	0945	369.4	379.1	9.7	5.39	55.5
18R	01	1035	379.1	388.7	9.6	3.75	39.0
19R	01	1110	388.7	398.4	9.7	4.85	50.0
20R	01	1140	398.4	408.1	9.7	8.06	83.1
21R	01	1230	408.1	417.7	9.6	4.58	47.7
22R	01	1315	417.7	427.4	9.7	9.84	101.0
23R	01	1400	427.4	437.0	9.6	3.09	32.2
24R	01	1445	437.0	446.7	9.7	6.28	64.7
25R	01	1530	446.7	456.4	9.7	5.55	57.2
26R	01	1615	456.4	466.0	9.6	8.27	86.1
27R	01	1655	466.0	475.7	9.7	9.80	101.0
28R	01	1735	475.7	485.4	9.7	6.50	67.0
29R	01	1815	485.4	495.0	9.6	9.85	102.0
30R	01	1905	495.0	504.7	9.7	7.09	73.1
31R	01	2000	504.7	514.4	9.7	9.95	102.0
32R	01	2045	514.4	524.0	9.6	0.00	0.0
33R	01	2130	524.0	533.6	9.6	3.43	35.7
34R	01	2220	533.6	543.3	9.7	9.32	96.1
35R	01	2300	543.3	552.9	9.6	8.91	92.8
36R	01	2340	552.9	562.5	9.6	4.36	45.4
37R	02	0100	562.5	572.2	9.7	9.23	95.1
38R	02	0200	572.2	581.8	9.6	8.48	88.3
39R	02	0300	581.8	591.5	9.7	9.77	101.0
40R	02	0415	591.5	601.1	9.6	2.01	20.9
41R	02	0520	601.1	610.7	9.6	9.34	97.3
42R	02	0630	610.7	620.3	9.6	7.11	74.0
43R	02	0735	620.3	630.0	9.7	7.96	82.0
44R	02	0840	630.0	639.6	9.6	7.49	78.0
45R	02	0945	639.6	649.3	9.7	0.61	6.3
46R	02	1115	649.3	658.6	9.3	2.81	30.2
47R	02	1250	658.6	667.9	9.3	4.07	43.7

Table 2 (continued).

Core no.	Date (1987-1988)	Time	Depth		Length		Recovery (%)
			top (mbsf)	bottom (mbsf)	cored (m)	recovered (m)	
119-737A- (Cont.)							
48R	02	1415	667.9	677.6	9.7	4.04	41.6
49R	02	1615	677.6	686.5	8.9	8.42	94.6
50R	02	1730	686.5	696.2	9.7	9.39	96.8
51R	02	1900	696.2	705.9	9.7	5.57	57.4
52R	02	2115	705.9	715.5	9.6	5.38	56.0
						481.3	298.35
(Wash core)						234.2	0.00
						715.5	298.35

was recorded from there to the end of the pipe, the logging tools were recovered, and the drill pipe was run to clear the bridge from the hole. Circulation was not enough to open the hole, and the top drive was picked up to rotate the pipe through the tight spot. A second try with the same logging tool was then made, and open hole was found down to another ledge or bridge about 100 m above total depth. The interval from 615 to 298 mbsf was then logged successfully. As the most valuable part of the hole was near the bottom, a "clean-out" trip was made to open the hole to total depth (TD = 715.5 mbsf). With the bit released, the open-ended MBR top connector made a poor drill bit. Nevertheless, a stubborn ledge or bridge was "drilled" out after about 15 min of rotation and circulation about 42 m off TD. Torque and weight indicated hole fill about 12 m off TD, and further cleaning attempts were abandoned. The hole was then flushed with bentonite mud and filled with weighted barite/bentonite mud before the pipe was pulled back to 327 mbsf, below the upper bridge. The subsequent logging run, with the lithoporosity combination, was successful from 702 to 296 mbsf.

On completion of logging, the drill string was recovered. Because of the long transit to Antarctica and anticipated rough weather, the BHA was broken down and racked. During that process, the support vessel *Maersk Master*, which had arrived on location a few hours before, came alongside and transferred supplies that had missed the drill ship at the Mauritius port call. *Maersk Master* then retrieved the recallable beacon that had been released acoustically. *JOIDES Resolution* departed for the Prydz Bay operating area at 1015 hr, 4 January 1988.

LITHOSTRATIGRAPHY AND SEDIMENTOLOGY

The sedimentary sequence cored at Site 737 ranges in age from Quaternary to middle Eocene, but contains some major hiatuses. The sequence was sampled with two holes that overlap around 260-270 mbsf and has been divided into six lithologic units (Table 3). Uppermost Unit I consists of 1.5 m of a black, volcanic, and glauconitic sand-rich diatom ooze of Quaternary age; Unit II is an olive diatom ooze of early Pliocene to late Miocene age; Unit III is a middle and late Miocene age white or light gray diatom nannofossil ooze; Unit IV is of middle Miocene age and consists of a black sandy siltstone and a white to olive gray nannofossil ooze with a significant volcanic component; Unit V is an Eocene to late Oligocene age calcareous claystone; and Unit VI is a clayey limestone with a wide range of colors and striking bioturbation features and is late middle Eocene in age. The lithologic units are summarized in Table 3 and described in the barrel sheets. Figure 5 illustrates the compositional data taken from smear slides; further details are on the barrel sheets. Special problems concerning smear slide preparation were faced for the indurated sediments, which did not allow a full disaggregation of the individual sediment components.

Table 3. Summary of lithologic units, Site 737.

Age	Unit	Depth (mbsf)	Thickness (m)	Core (interval in cm)	Dominant lithologies
Quaternary	I	0-1.5	1.5	737A-1H-1	Mixed glauconitic sand and diatom ooze, black
-----Actual contact not recovered-----					
early Pliocene-late Miocene	II	1.5-240.1 114.5-133.8	238.6 > 19.3	737A-2H to -26X 737B-2R-1 to -3R-CC	Diatom ooze, olive to olive gray
-----Actual contact not recovered-----					
late Miocene-middle Miocene	III	240.1-255.1 253.5-306.6	66.5	737A-27X to -28X 737B-5R-1 to -10R-4, 33	Diatom calcareous nannofossil ooze, white to light gray
-----Sharp contact-----					
middle Miocene	IV	306.6-321.1	14.5	737B-10R-4, 33, to -11R-CC	Sandy siltstone (black) and calcareous nannofossil ooze with volcanic sand (white to olive gray)
-----Actual contact not recovered-----					
late Oligocene-middle Eocene	V	321.1-667.9	346.8	737B-12R-1, 5, to -47R-CC	Calcareous claystone, white-gray, green, black; interstratified with clayey limestone at base
-----Actual contact not recovered-----					
middle Eocene	VI	677.9-711.2	43.3	737B-48R-1 to -52R-4, 83	Clayey limestone, light greenish gray to dark greenish gray

Calcium carbonate and organic carbon percentages were determined from core-catcher samples, and a number of X-ray-diffraction analyses were also made. Particle-size data on the finer sediments were obtained using the Lasentec Lab-Tec 100 analyzer (see "Explanatory Notes" chapter).

Drilling Disturbance

The drilling disturbance features in most of the Site 737 cores were those normally encountered in ODP recovery. In soft sediments (Units I through III) the top part of Section 1 of each core is soupy with minor to moderate deformation below (especially in the core-catcher section). In the lithified units (IV through V) recovery took the form of blocks separated by fractures, especially at less lithified levels. Rotary coring usually produced total disruption of soft sediments.

APC coring at a depth of 150 mbsf in the diatom ooze of Unit II produced strong "suction" disturbance in concert with high pullout pressures. As at Site 736, near-surface sands and gravels were encountered as downhole drilling contaminants throughout the diatom ooze section (Cores 119-737A-1H, 119-737A-4H to 119-737A-12H, 119-737A-15H, 119-737A-16H, 119-737A-18H, 119-737A-19X to 119-737A-21X, 119-737A-23X, 119-737A-25X to 119-737A-26X, 119-737B-2R, 119-737B-3R, 119-737B-5R to 119-737B-7R, and 119-737B-9R). At this site, basaltic gravel and sand combined with the glauconitic peloid of Unit I to comprise the downhole contamination. Details on the contamination process are given in the "Explanatory Notes" chapter.

Lithostratigraphy

Unit I

Mixed glauconitic sand and diatom ooze
Section 119-737A-1H-1; depth, 1.5 mbsf.
Age: Quaternary.

Unit I consists of black (5Y 2.5/1) sand intermixed with a very dark gray (5Y 3/1) diatom ooze (Fig. 6). It has an indistinct inhomogeneous appearance that is attributed to bioturbation and drilling disturbance. No obvious sedimentary structures are preserved. The sand is composed of (1) glauconitic peloids; (2) large, subhedral to rounded, clear or cloudy (altered and with dark inclusions) and poorly twinned feldspar; (3) pumice in rounded grains with some alteration (birefringent) and with interstices infilled with glauconite and opaque glass-alteration phases; (4) pale palagonite shard forms; (5) foraminifer, diatom, and radiolarian tests; and (5) clear, green subhedral and elongate pyroxene. Unit I also contains minor gravel composed mainly of subangular to well-rounded pumice granules and pebbles up to 25 mm size.

Glauconitic peloids consisting of green clay mixed with mineral and biogenic, detrital particles compose most of the sand fraction by weight. Most of the peloids have a distinctive, lobed shape as a result of deep fissuring (Fig. 7A); others are aggregates based on whole foraminifer, diatom, or radiolarian tests or pumice grains (Fig. 7B). Identification of the green clay as "glauconite" is pending further geochemical analyses, but is based on the mineral's optical, chemical, and grain-morphological characteristics given in Ehlmann (1978), McCrae (1972), and Scholle (1978). Scanning electron microscope (SEM) images demonstrate authigenic, smectitelike structures between the clay layers (see Welton, 1984).

The boundary with Unit II is placed somewhat arbitrarily at the base of Section 119-737A-1H-1 at 1.5 mbsf. The actual contact with the diatom ooze of Unit II was not recovered, but was probably complicated by burrowing. Thus, in Section 119-737-1H-2 the black sand of Unit I occurs in distinctive burrowlike structures within the homogeneous olive (5Y 4/3) diatom ooze of Unit II. Contacts between these structures and the ooze are sharp. It is possible that drilling disturbance may have affected these structures because they occur mainly in contact with the core liner.

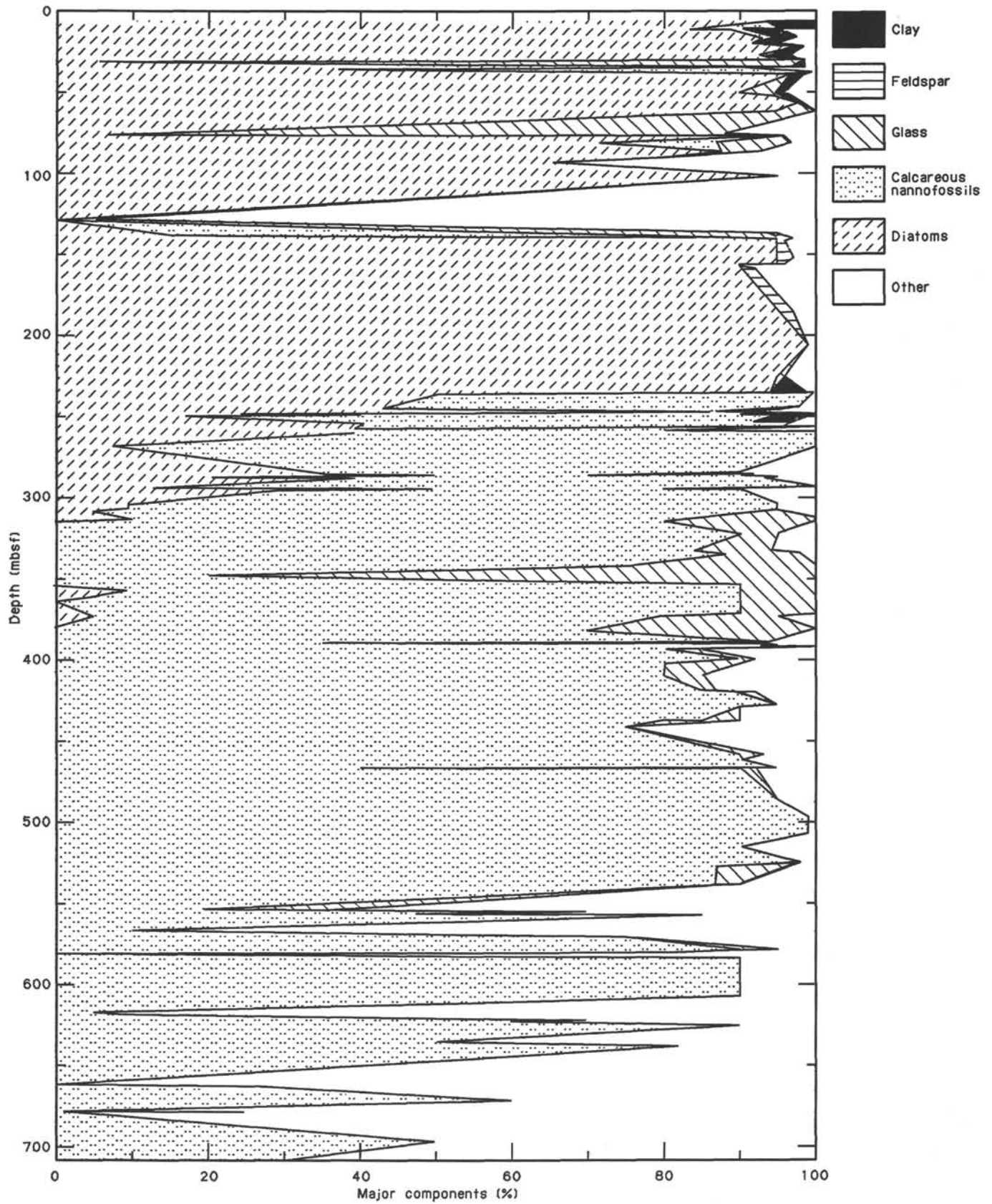


Figure 5. Smear slide compositional data for Site 737. The irregularly spaced data in Hole 737A give undue prominence to some minor lithologies.

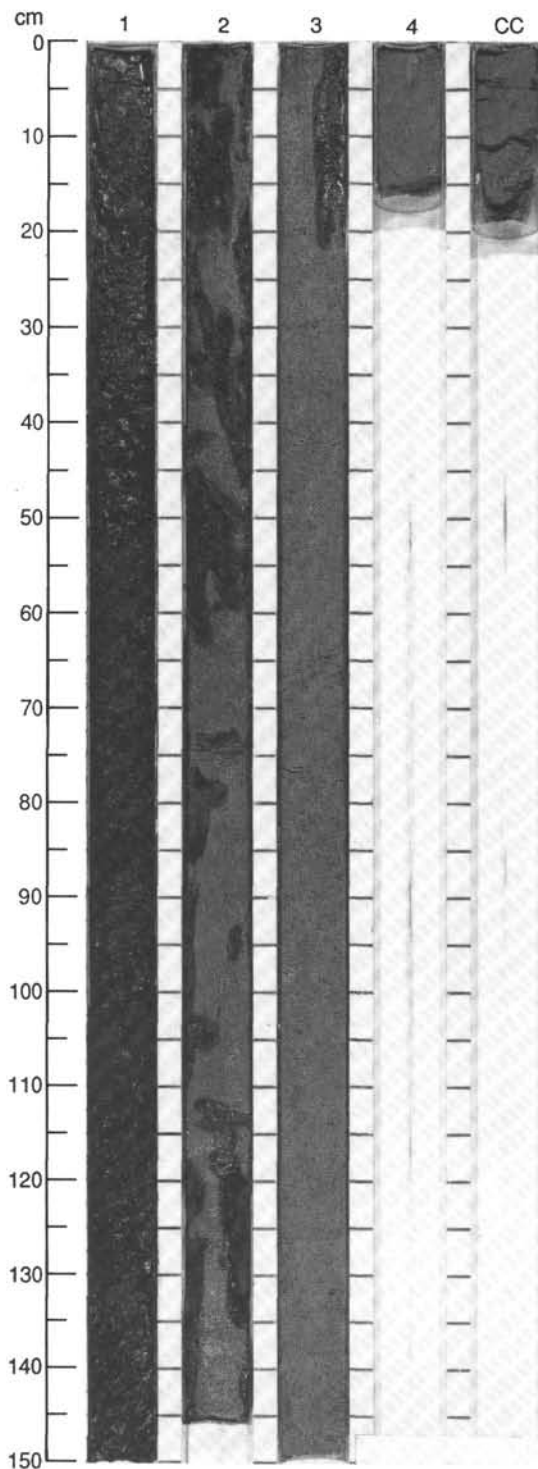


Figure 6. Contact of the Pleistocene black sand and diatom ooze of Unit I and lower Pliocene olive diatom ooze of Unit II. The boundary is drawn at 150 cm between Sections 119-737A-1H-1 and 119-737A-1H-2, but note the burrowing (disturbed by drilling?) in Section 119-737A-1H-2.

Unit II

Diatom ooze

Section 119-737A-1H-2 through Sample 119-737A-26X-1, 123 cm; depth, 1.5–240.1 mbsf.

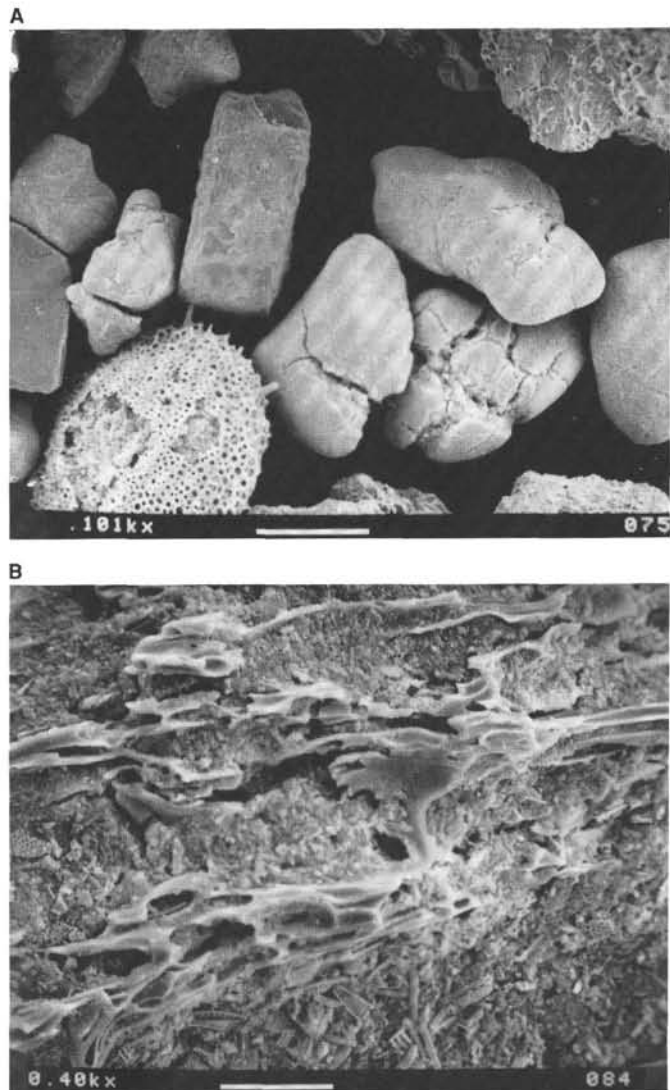


Figure 7. SEM photomicrographs of Unit I glauconite grains; Sample 119-737A-1H-1, 60–61 cm. **A.** Glauconite peloid, radiolarian, feldspar, and pumice grains. **B.** Surface of a palagonitized pumice sand grain, showing proportions of glauconite and biogenic/volcanogenic silt/clay debris in the open bubble cavities.

Sections 119-737B-2R-1 through 119-737B-3R-CC; depth, 114.5–133.8 mbsf.

Age: late Miocene to early Pliocene.

This unit is dominated by olive (5Y 4/3 and 5Y 4/4), homogeneous diatom ooze, but subtle and gradational changes of color to light olive (5Y 5/3 and 5Y 6/3) and olive gray (5Y 4/2) are common. The variations from light olive to gray reflect increasing proportions of volcanic ash and basaltic sand. Bioturbation, including well-defined burrows, is common in several cores, especially 119-737A-1H, 119-737A-4H, and 119-737A-7H to 119-737A-10H. Less obvious bioturbation is suggested by faint mottling. Many burrows show a concentration of ash and basaltic sand, and thus tend to be darker, such as dark gray (5Y 4/1) or black (5Y 2.5/1).

Smear slide and Lasentec analyzer data indicate the following textural ranges for the diatom ooze: 0%–10% sand fraction, 80%–96% silt fraction, and 1%–10% clay fraction. The ooze is composed of 65%–99% (typically >85%) diatoms, 0%–15%

nannofossils, 0%–2% radiolarians, 0%–3% silicoflagellates, 1%–5% clay, and traces of spicules. Small amounts of pyroxene, feldspar, and volcanic glass were also noted in smear slides. Calcium carbonate percentages are generally low (<1%), but a 10-cm-thick olive gray (5Y 5/2) indurated micrite layer is in Core 119-737A-6H (45.3 mbsf). Light olive gray (5Y 6/2) micrite concretions occur in Core 119-737A-8H (67.5 mbsf), and there is a 4-cm-thick carbonate-rich zone in Core 119-737A-13H (110.8 mbsf).

Volcanic ash layers of early Pliocene age are the most important of the minor lithologies (Sections 119-737A-4H-5, 119-737A-5H-5, 119-737A-6H-4, and 119-737A-9H-4). The uppermost part of these layers consists of silt-sized grains, 99% of which is volcanic glass. They range in thickness from 0.5 to 4 cm and are dark gray (5Y 4/1). Two 5-cm-thick diatom ooze layers rich in volcanic sand also occur in Sections 119-737A-25X-3 and 119-737A-4H at 228–230 mbsf and are probably of late Miocene age.

The detrital mineralogy is characterized by minor amounts of dispersed, silt-sized volcanic glass and minerals, augmented at certain levels by influxes of the following sandy volcanic and authigenic materials: (1) detrital glauconite in the form of peloids or silt-sized flakes; (2) a suite of volcanic components consisting of blocky, sand-sized, usually fresh—but with some altered—subhedral plagioclase, altered brown palagonite volcanic glass, some fresh glass, and small quantities of yellow-green, elongate, subhedral pyroxene; and (3) sand-fraction, rounded pumice particles. The primary influxes are identified in Sections 119-737A-15H-1 (129 mbsf; glauconite and pumice), 119-737A-10H-1, 119-737A-11H-1, and 119-737A-13H-2 (82–112 mbsf; glauconite and volcanic suite), and 119-737A-9H-4 (77 mbsf; pumice and volcanic suite). In contrast to other levels, the influx at Section 119-737A-9H-4 contains essentially unaltered feldspar and pumice glass.

Unit III

White to light gray diatom nannofossil ooze
Sections 119-737A-27X-1 through 119-737A-28X-CC; depth,
240.1–255.1 mbsf.
Section 119-737B-5R-1 through Sample 119-737B-10R-4, 33 cm;
depth, 253.5–306.6 mbsf.
Age: middle to late Miocene.

The boundary between Units II and III is not observed because it occurs in an unrecovered interval between Cores 119-737A-26X and 119-737A-27X. Unit III is a diatom nannofossil ooze ranging from white (5Y 8/1) to light gray (5Y 7/1, 5Y 7/2) and less commonly pale yellow (5Y 7/3), gray (5Y 7/2, 5Y 6/1), olive gray (5Y 5/2), and greenish gray (10Y 7/1) are in evidence. The darker varieties contain more diatoms. Clay-fraction nannofossil components account for 50%–80% of the sediment. Interbedded on a decimeter to centimeter scale with the preceding are nannofossil diatom ooze with >50% diatoms (light olive gray, 5Y 6/2) and diatom ooze (dark olive gray, 5Y 3/2, 5Y 4/2) containing <5% calcareous nannofossils and terrigenous material. Smear slide data from both types of ooze show a wide range in grain sizes: 1%–5% sand fraction, 40%–80% silt fraction, and 18%–80% clay fraction. Internally, the beds may be homogeneous, discontinuously or weakly stratified on a centimeter scale, or bioturbated to give darker mottling (gray, 5Y 5/1).

Unit III contains a small amount of volcanic material, including volcanic sand in a 5-cm-thick, very dark gray (5Y 3/1) layer at 19 cm in Section 119-737B-6R-2 and forming an irregular lens a few centimeters across in Core 119-737A-27X. These horizons are not to be confused with downhole contamination. Smear slide analyses of the detrital mineralogy show a very mi-

nor (<1%) component of disseminated, silt-sized feldspar, volcanic glass, palagonite, and glauconite throughout the entire unit. At some levels this is supplemented by coarser influxes of the same types of materials: (1) clear, untwinned, subhedral and blocky feldspar, pale green needles of euhedral (?) pyroxene, a second pyroxene with elongate green euhedral form, deep brown palagonite in shard form, plus clear, fibrous pumice incorporating clays and glauconite in the open interstices and (2) glauconitic peloids. The principal influxes are identified in Sections 119-737B-5R-1 (255 mbsf), 119-737A-6R-1 (263 mbsf), and 119-737A-8R-2 (285 mbsf), where all the preceding components occur in abundance; advanced states of alteration on the plagioclase and glasses imply, however, that these are not primary volcanic influxes.

Calcium carbonate analyses reflect compositional changes in the diatom and nannofossil oozes, with the latter becoming more dominant downhole. The percentage of calcium carbonate ranges from 1% near the top to >70% at the base. There is a continuous range in composition between diatom-rich and nannofossil-rich oozes, although each occurs in discrete beds.

Unit IV

Sandy siltstone and diatom, nannofossil ooze
Sample 119-737B-10R-4, 33 cm, through Section 119-737B-11R-CC; depth, 306.3–321.1 mbsf.
Age: middle Miocene.

The contact between the diatom nannofossil ooze of lithologic Unit III and Unit IV (34 cm in Section 119-737B-10R-4; Fig. 8) is sharply marked by a hard, possibly cherty, black (5Y 2.5/1, 5Y 2.5/2) sandy siltstone. This siltstone has a thickness of 53 cm and continues to the base of the recovered sequence at 87 cm in Section 119-737B-10R-4. It has a turbiditic character and contains dark, olive gray (5Y 3/2), glassy, sand-sized grains of volcanic origin. In the uppermost 25 cm the siltstone shows normally graded, parallel laminations on a millimeter scale; the remainder is moderately bioturbated. In the top 15 cm of the siltstone, burrows are filled with sediment from the overlying Unit III (Fig. 8).

Below the siltstone, the sediments of Core 119-737B-11R may be regarded as a transition from soft calcareous ooze to indurated calcareous claystone. The transition zone is characterized by mostly light olive gray (5Y 6/2) to light gray (5Y 7/1) diatom nannofossil ooze (Fig. 9). It contains about 10% disseminated black (5Y 2.5/1) basaltic fragments and sand, which tend to be concentrated in burrows. Bioturbation is present in various degrees throughout the ooze and is similar to that in the bounding units. It results in a mottled sediment appearance with various grayish and greenish colors. As a minor lithology, there are gray (5Y 5/1) chert fragments at 70–75, 124, and 130 cm in Section 119-737A-11R-1. The detrital content of Unit VI is minor, amounting to background deposition of silty volcanic materials and glauconite.

Unit V

Calcareous claystone
Sample 119-737B-12R-1, 5 cm, through Section 119-737B-47R-CC; depth, 321.1–677.9 mbsf.
Age: late Oligocene to middle Eocene.

Unit V is a calcareous claystone. Carbonate analyses on core-catcher samples show a range in carbonate content from 25% to 60%, but more than 70% of the unit has less than 50% carbonate. The carbonate content shows a cyclic alternation with an overall increase down through the unit. The calcareous claystone lithology generally consists of 75%–90% nannofossils, 1%–5% foraminifers, 0%–3% radiolarians, 5%–30% vol-

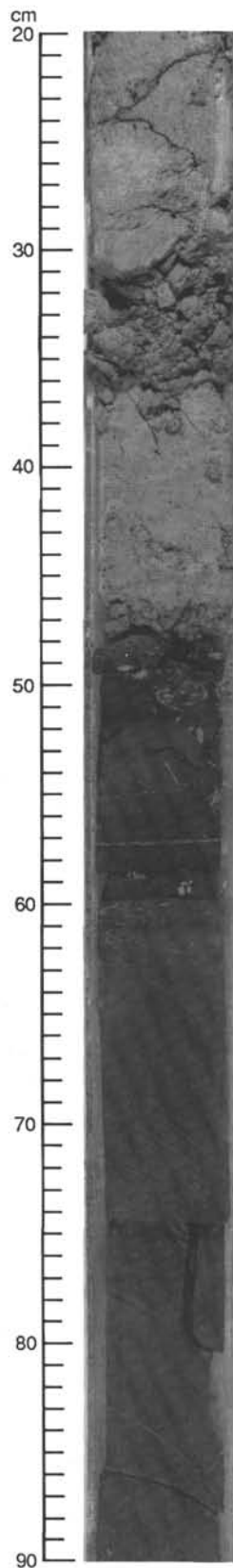


Figure 8. Dark gray, lithified, sandy siltstone and silty claystone of Unit IV and the contact with the overlying Unit III at 48 cm in Section 119-737A-10R-4, 20-90 cm (306.6 mbsf). The dark siltstone is well lithified and shows a multiple-graded, upward-thinning sequence. The burrows are filled mainly with nannofossil chalk.

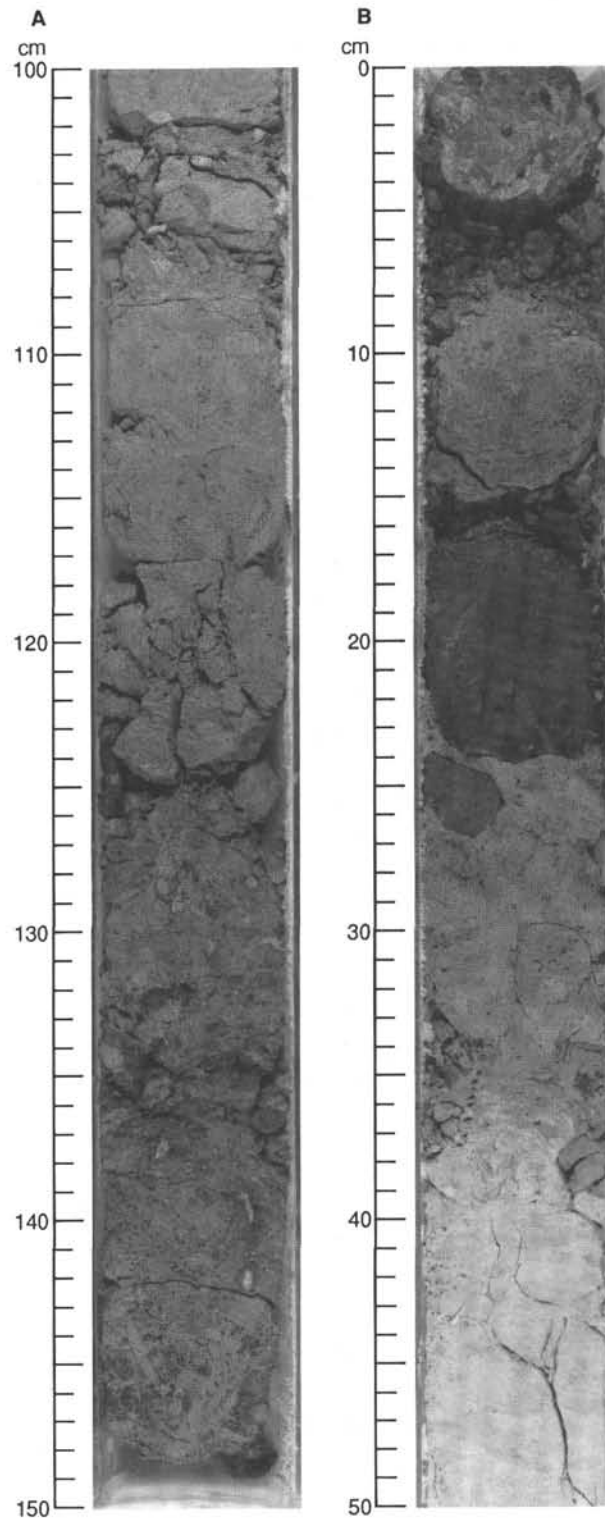


Figure 9. Lithologic expression of the middle Miocene to upper Oligocene hiatus in Units IV and V; Sections 119-737-11R-1, 100-150 cm, and 119-737A-11R-2, 0-50 cm (311.5-314.2 mbsf). **A.** Lower glauconite-rich chalk of Unit III. **B.** Drilling-disrupted firm-ground chalks associated with loose gravels of angular chalk and glauconite. The sharp, top surface of the second firm-ground lump is glauconite mineralized.

canic glass, 5%–10% palagonite, 1%–85% glauconite, 0%–5% feldspar, 0%–1% quartz with 0%–10% opal, and 10%–88% micrite in the lower part of the unit.

Repeated alternations of light and dark layers occur on two scales: (1) apparent primary layering expressed as large-scale horizontal color banding ranging from 5 to 150 cm in thickness and (2) secondary diagenetic, much finer-scale (1–5 mm) color banding in 2–20-cm-thick zones (e.g., Fig. 10). Within the former, color boundaries may be irregular, locally subvertical, and/or diffuse. Color changes within light and dark layers are generally gradational. Dominant colors in the light layers include whitish green (5Y 8/1), light gray green (5GY 7/1), pale green (5Y 5/2, 5Y 7/2, and 5Y 6/2), and greenish gray (5GY 6/1 and 5Y 5/1). Colors in the darker layers include dark greenish gray (5G 4/1), grayish green (5G 4/2), gray (5GY 5/1), dark gray (5GY 4/1), and black (5Y 2.5/1). This large-scale color banding provides the most significant indication of repeated cycles of sedimentation in the unit and is inversely related to carbonate content. Where the average carbonate content is 25% the core colors are dark; where it exceeds 50% lighter colors prevail.

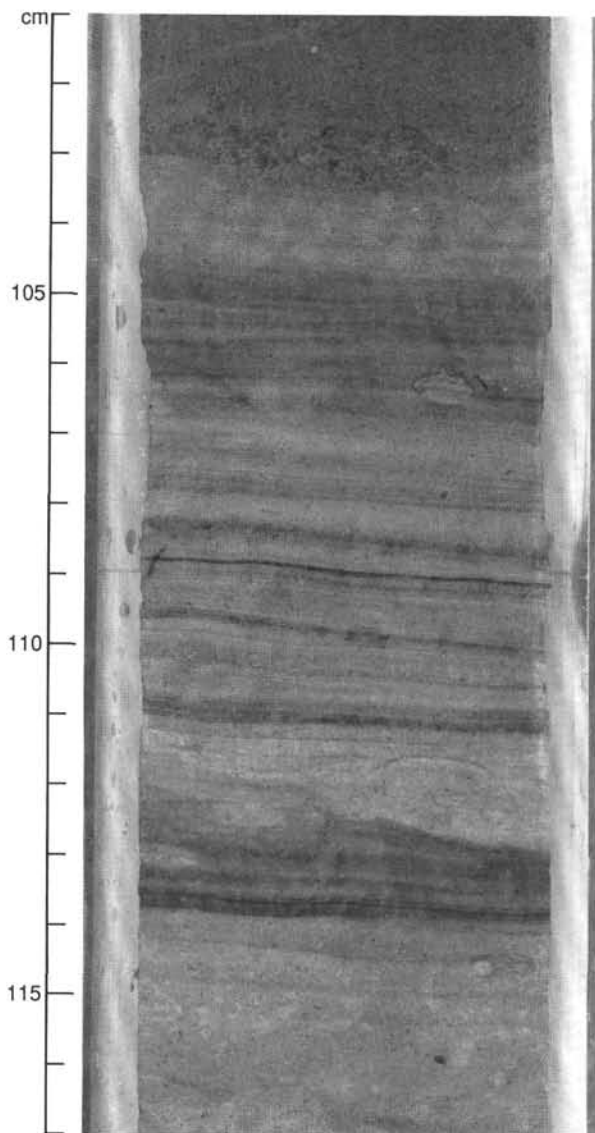


Figure 10. Diagenetic greenish laminations in varicolored calcareous claystone, Unit V; Section 119-737B-28R-4, 101–117 cm (481.5 mbsf). Note that the laminations overprint the burrows.

The small-scale color banding is horizontal to subhorizontal, and it is distinctive by virtue of its deep green (10Y 4/3) color, alternating with shades of gray and gray green (5G 4/1). It overprints depositional structures such as burrows and is therefore interpreted as diagenetic, possibly recording shifts in the levels of early diagenetic chemical fronts. It occurs throughout Unit V.

Unit V is generally weakly to moderately bioturbated, with a few small zones of more intense bioturbation (Fig. 11). Bioturbation is also evidenced in the consistent color mottling of the rock. Burrow types include *Chondrites*, *Planolites*, *Zoophycos*, and *Thalassinoides*. Successive generations of burrowing can be recognized in most areas. A crude upward succession from *Zoophycos* to *Chondrites/Thalassinoides* and *Planolites* occurs above the tops of the pale-colored layers. Most burrows are filled with sediment identical to the host sediment in which they occur and have dark interiors and lighter margins, or vice versa. A few burrows are filled with white sparite or black pyrite grains. Large *Thalassinoides* burrows are commonly concentrated along the contact between the light- and dark-colored calcareous claystone layers. The *Thalassinoides*-burrowed, paler calcareous claystone is sharply overlain by the darker base of the overlying layer. The lower limit of burrowing beneath this surface extends to 8–10 cm and is commonly diffuse.

Within Unit V are minor layers of volcanic-rich nannofossil calcareous claystone, black calcareous siltstone, silty claystone, black tuff, and chert/porcellanite. Through the bulk of the unit, detrital particles were incorporated only at very low levels (<1%). Detected occurrences are chiefly of silt-sized feldspar, volcanic glass (clear and palagonitized), and glauconite, although the glauconite generally appears to be authigenic to the unit. The sole significant detrital influx occurs in Section 119-737B-17R-3 (373 mbsf; upper Oligocene) with the introduction of copious amounts of rich brown palagonitized shards and pumice of bubbly and tubular form. Progressing into younger sediments, this material becomes steadily diluted and virtually disappears by Section 119-737B-12R-1 (321 mbsf).

Some occurrences of clastic dikes composed of indurated black calcareous claystone are emplaced along fractures (Fig. 12). Such fractures also occur elsewhere, locally displacing bedding by up to 5 mm. Unit V becomes more indurated and carbonate-rich toward the bottom, apparently grading into Unit VI at about 667.9 mbsf. The transition coincides with major changes in the physical properties of the sediments.

Unit VI

Clayey limestone

Section 119-737B-48R-1 through Sample 119-737B-52R-4, 83 cm; depth, 677.9–711.2 mbsf.

Age: middle Eocene.

Unit VI consists of a clayey limestone with minor chert layers, nodules, and black claystone. Superficially, it resembles Unit V. However, carbonate content averages 60% and remains consistently high throughout the unit. The clayey limestone consists of 5%–50% clay, 12%–50% nannofossils, 35%–70% micrite, and 3%–20% volcanic glass. Color banding exists on three scales: (1) large-scale alternating, 3–120-cm-thick dark and light layers that dominate the unit; (2) sets of parallel laminae across and along which burrows are developed; and (3) locally developed diagenetic color banding in bands 1–12 cm thick that are internally structured with fine, colored laminae spaced at 1–5 mm. Because it frequently overprints burrowing, the small-scale banding of type (3) is diagenetic. The boundaries between the large-scale colored type (1) bands are irregular and vary from sharp to diffuse in character. The pale-colored layers are light greenish gray (5GY 7/1), greenish gray (5G 5/1), and greenish light gray (5GY 6/1), whereas within the darker layers

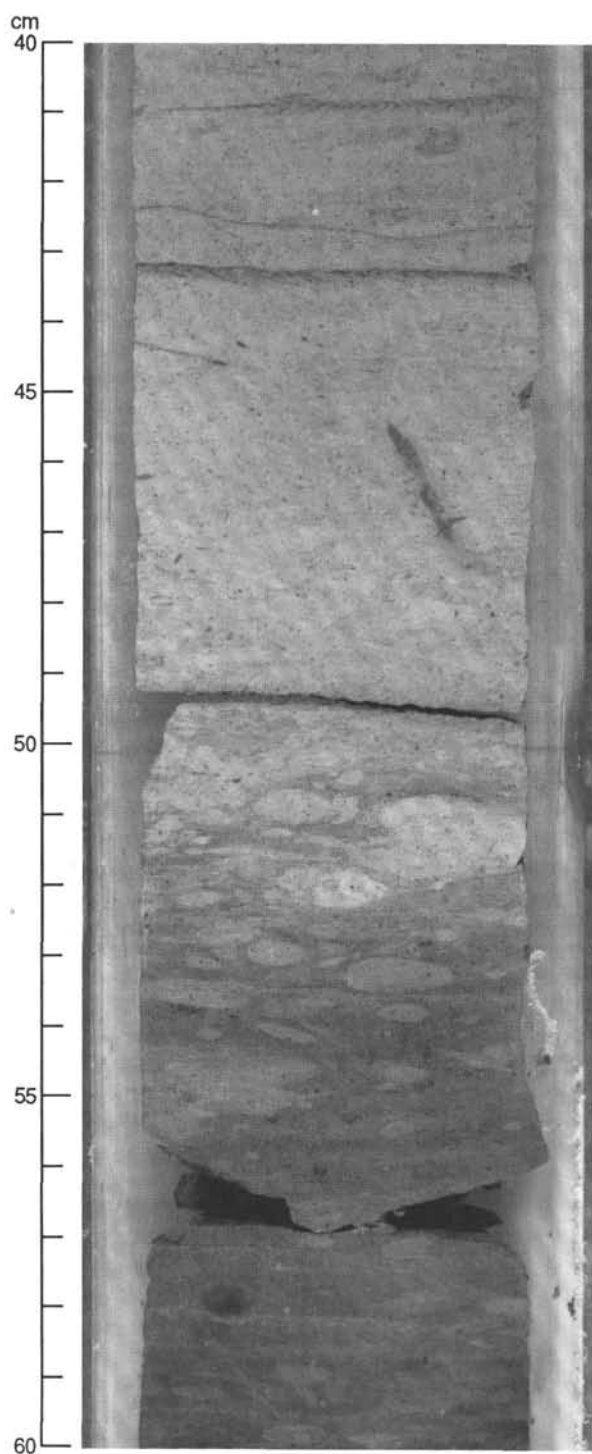


Figure 11. *Zoophycos*, *Planolites*, *Chondrites*, and *Thalassinoides* burrows in the calcareous claystone of Unit VI; Section 119-737B-43R-4, 40–60 cm (625 mbsf).

the principal colors are dark greenish gray (5BG 4/1 and 5G 4/1), green gray (5BY 5/1), and grayish green (5G 3/1). Chert zones within the limestone show complex colors, including dark reddish gray (5R 4/1) and reddish gray (5R 5/1). Most bedded examples were badly brecciated by drilling. The nodules commonly have diffuse extensions into the surrounding sediment.

Weak to moderate bioturbation and mottling give rise to complex color relationships. Burrow types include *Planolites*,

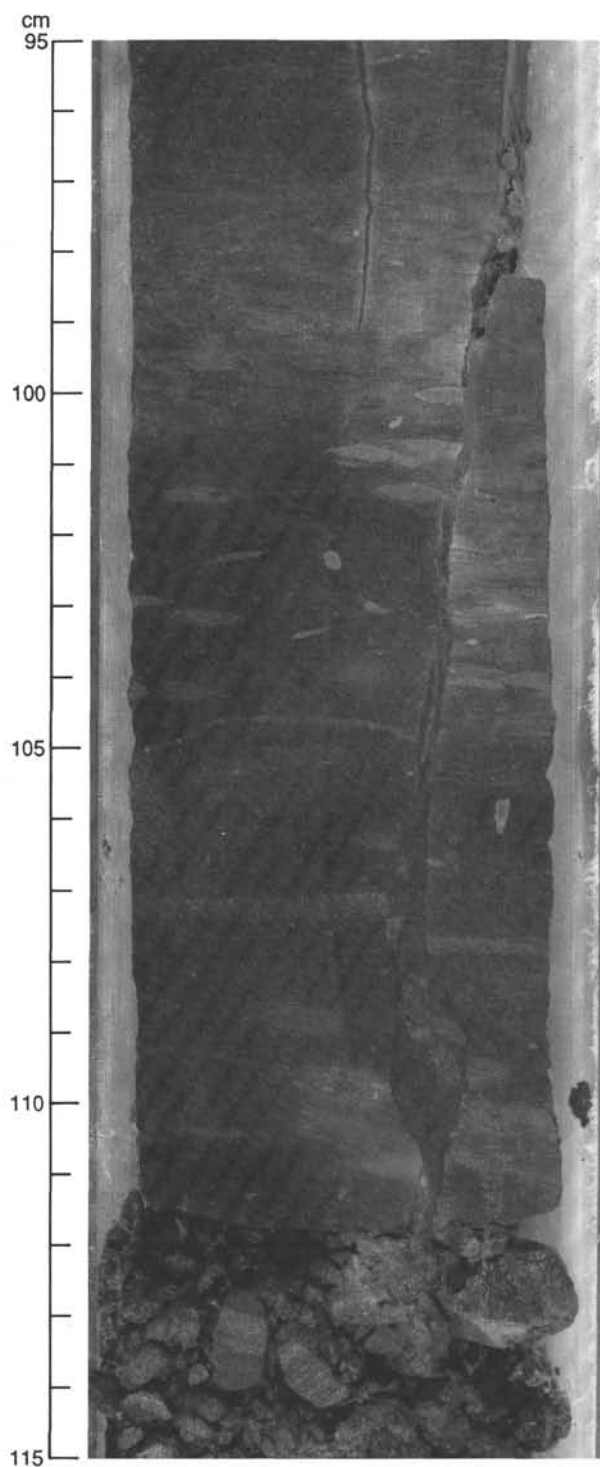


Figure 12. Microfaults and a clastic dike cutting and intruding burrowed calcareous claystone in Unit V; Section 119-737B-42R-4, 95–115 cm (616.2 mbsf). Sparry calcite fills some cavities at the microfaults. The clastic dike material is dark gray clayey limestone.

Chondrites, *Zoophycos*, and *Thalassinoides* (Figs. 11 and 13). Other structural features are deformational microfractures displacing the banding by up to 3 mm and lenticular bedding characters that are probably due to compactional flattening (and elongation) of the burrow structures.

Detrital components are rarely detected in smear slides and consist of silt-fraction feldspar and possibly quartz.

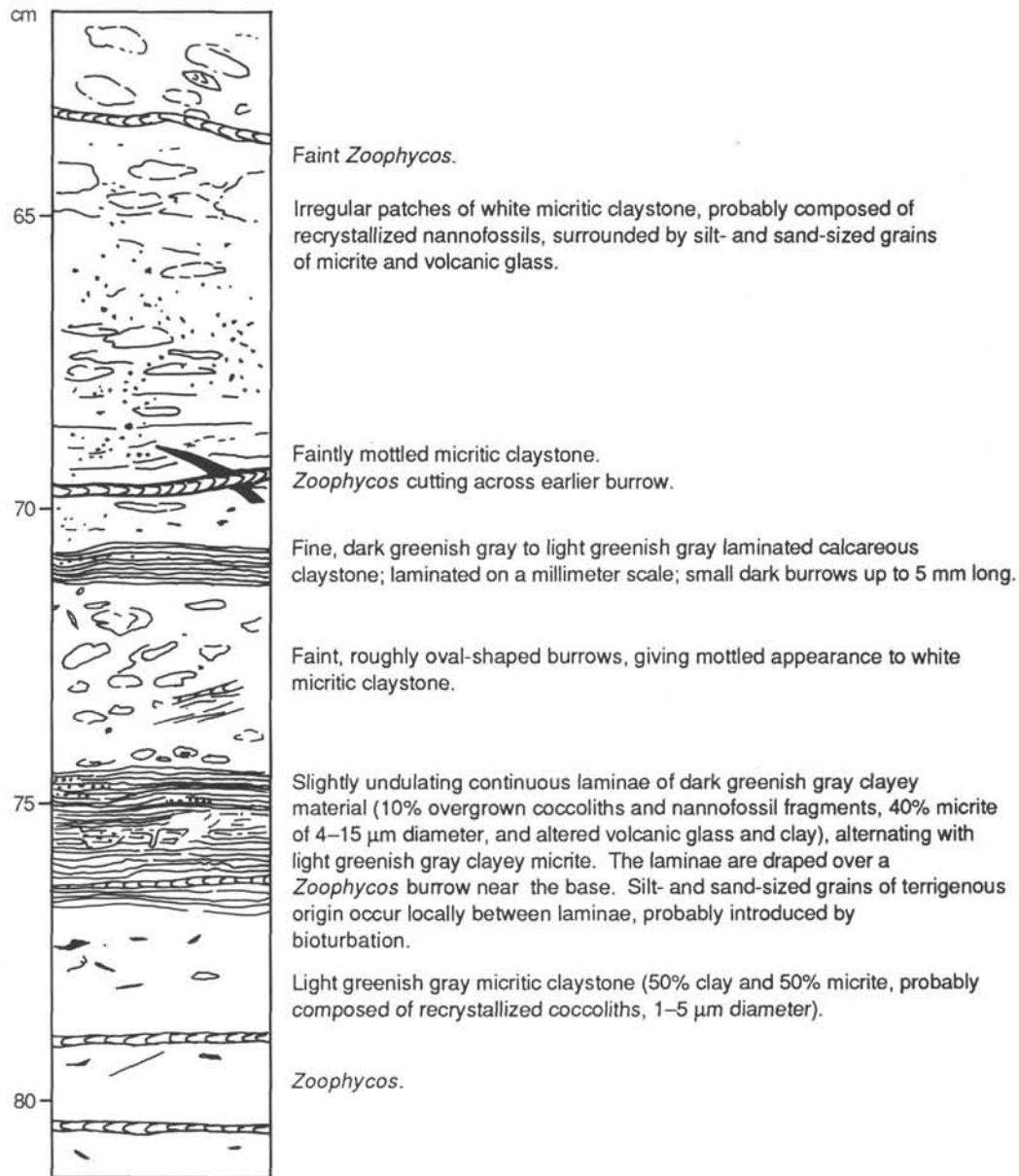


Figure 13. Illustration of sedimentary structures in a section of clayey limestone, Unit VI; Section 119-737B-49R-1 (678.3 mbsf).

Interpretation of Sedimentary Environments

The late Eocene to Quaternary record at Site 737 is characterized by an early phase (middle Eocene to early Oligocene) of carbonate and clay deposition, a middle phase (late Oligocene to middle Miocene) of nannofossil ooze production with minor inputs of volcanic detritus, and a late phase (late Miocene to early Pliocene) of diatom ooze accumulation. The Quaternary record is scanty, amounting to only 1.5 m of mixed diatom ooze and volcanic and glauconitic sand.

Hiatuses are recorded on biostratigraphic evidence for the Pleistocene, late to middle Miocene, late Oligocene to middle Miocene, middle Oligocene and late to middle Eocene (see "Biostratigraphy" section, this chapter), but only the upper Oligocene to middle Miocene hiatus is discernible as a lithologic contact in the core material (Fig. 9).

Possible ice-rafted pebbles were observed near the base and top of Unit II (Miocene and Pliocene, respectively). The pebbles

are basalt, but they are too weathered to reveal any fine surface details such as striations. Small concentrations of similar pebbles resulting from drilling disturbance have been observed as low as the base of Unit III at 300 mbsf (the lowermost soft sediment), but they are most likely derived from an unknown higher level.

Significant influxes of detrital volcanic products are also evident in the stratigraphy and may be important evidence for tectonic/volcanic/oceanographic changes in the region. Coarse brown, palagonitized glass and pumice at 373 mbsf in Unit V (upper Oligocene), suites of igneous minerals plus pumice in Units III (285, 262, and 255 mbsf; middle Miocene) and II (129, 82-112, and 77 mbsf; upper Miocene to lower Pliocene), and the high volcanogenic sand content throughout Unit I are inferred to be due to turbid and traction current supply from seafloor areas undergoing erosion, direct ash fall, ice rafting, and pumice attrition. Silt fractions may also have entered through nepheloid or eolian processes. Intervals of fresh mineral and glass supply occur in

the lower Pliocene, implying new volcanic activity in the region at the time of deposition, but most of the detritus is reworked in nature. In some layers volcanogenic detritus may account for >10% of the sediment; such layers have significant mesoscopic expression. Discrete volcanic ash or sand layers occur at 346.9 (upper Oligocene), 315.31 (upper Oligocene), 264.87 (middle Miocene), 254.78 (upper Miocene), and 76.75, 48.60, 39.95, and 31.06 mbsf (lower Pliocene).

Glaucinite occurs in the form of authigenic growths and as reworked grains, such as sand-sized accretionary peloids of mixed bioclastic/glaucinite composition and silt-sized flakes. Influxes of coarse, reworked glauconite may coincide with periods of local or even regional seafloor erosion resulting from tectonic or oceanographic readjustments. These periods are identified in the Pleistocene to Quaternary (Unit I, 0–1.5 mbsf), lower Pliocene to upper Miocene (Unit II, 78–130 mbsf), middle Miocene (Unit III, 285–254 mbsf), and lower Oligocene (Unit V, 441–469 mbsf). For the most part, they correspond with influxes of reworked, coarse volcanic detritus.

Depositional environments for Units I through VI are inferred as follows:

Units V and VI contain many indicators of depositional environment that signify fairly constant conditions of sedimentation throughout the late Oligocene to late Eocene. The major hiatus in the middle to late Eocene is evidenced only by a change in sediment color from light gray to green to black. The calcareous claystone and clayey limestone lithologies were probably deposited in an oceanic environment of middle bathyal depth. *Zoophycos* is generally regarded as indicative of bathyal depth and fairly continuous sediment accumulation without major changes in texture or environment (Wetzel, 1984). *Chondrites* and *Planolites* are not depth significant (Wetzel, 1984; Ekdale et al., 1984). Sedimentation was dominated by the supply and preservation of pelagic biogenic carbonate, with lesser amounts of biogenic silica in the upper part of Unit V. Carbonate content gradually increases through Units VI and V; biogenic silica is most prominent in the upper part of Unit V. Other than a slight and fluctuating supply of reworked volcanic materials terrigenous input was limited. The origin of the important clay components is unknown. Abundant bioturbation, the well-preserved burrows, and the association of *Chondrites*, *Planolites*, *Zoophycos*, and *Thalassinoides* suggest a relatively firm, stable substrate and oxygenated bottom-water conditions. The lack of organic carbon (see "Organic Geochemistry" section, this chapter) probably resulted from metabolism by organisms (burrowing and otherwise) and destruction by oxidation. The association of large *Thalassinoides* burrows with sharp, distinctive color changes in the chalk may indicate the development of omission surfaces and periods of interrupted deposition (Ekdale et al., 1984). Green chemical halos seen around some burrows are early diagenetic oxidation-reduction effects similar to the fine-scale diagenetic laminations. A small number of burrows contain pyrite or sparry calcite infills, with voids remaining in at least one, suggesting that firm ground early cementation may have occurred. One associated set of dark graded-bedded calcareous siltstones and claystones indicates that turbidite emplacement did occur at some levels.

The 14.5-m-thick middle Miocene Unit IV represents a transitional depositional phase. Sedimentation occurred at deep bathyal levels; biogenic accumulations of nannofossil ooze (soft chalk) were supplemented by minor sand-silt turbidites composed of mixed volcanic (vitric) and biogenic carbonate materials. A hiatus marks the contact with Unit III. Bioturbation is extensive.

Unit III is a middle to upper Miocene pelagic unit composed of calcareous nannofossils and diatoms in widely varying proportions. The sediments appear only slightly bioturbated and

may have accumulated in a middle slope setting. There are no signs of reworking by currents or slumping.

Unit II, a pelagic diatom ooze (upper Miocene to lower Pliocene), is similar in character to Unit II of the Site 736 sequence. Except for minor burrowing features, few sedimentary structures are preserved, and the sediments are homogeneous. Depths of seafloor deposition were probably similar to those for Unit III.

Unit I represents the only evidence of Quaternary sedimentation: a distinctive dark green, black, glauconitic and volcanoclastic sand mixed with diatom ooze. Detrital volcanic materials such as feldspar, palagonite, unaltered glass, pumice, and pyroxene occur in states of alteration varying from fresh to advanced. The sediments may have been heavily reworked and may represent a lag deposit after current erosion. The glauconite peloids may have formed in areas of reducing conditions under the seafloor, only to be exposed later by currents at the surface.

Diagenesis

A detailed consideration of sediment diagenesis requires data from physical properties and interstitial-water geochemistry (see respective sections, this chapter). The discussion here reports only special mineralizations observed in smear slides. It is important to note that the measurements of interstitial-water geochemistry have a sensitivity that is well beyond the resolution of smear slide samples. No particular diagenetic phenomena were noted in the diatom and nannofossil ooze Units I–IV, and observations are restricted to the chalk Units V and VI.

Neomorphic carbonate was detected in the form of 7–25- μm microspar in Sections 119-737B-42R-1, 119-737B-5R-1, and 119-737A-13H-1 (617, 256, and 110 mbsf, respectively). Crystal shapes are euhedral and rhombic, and twinning lamellae are observed. Silica spherulites composed of microquartz were encountered in Sections 119-737B-38R-1, 119-737B-37R-5, 119-737B-34R-5, and 119-737B-14R-1 (573, 569, 540, and 331 mbsf, respectively). These attain sizes of 10 to 80 μm , have a highly pitted (etched-looking) exterior, and at some levels are coated with a 2.5- μm thickness of green material, which is probably glauconite. Silica infilling of foraminifer chambers has occurred in Section 119-737B-24R-3 (441 mbsf).

Diagenetic effects on the volcanic constituents have not been examined in any detail. In the sediments of Units V and VI, the micrite, nannofossils, and clay exist in cloudy aggregations that are difficult to probe using smear slides. These aggregations appear to be manifestations of the chalk lithification. Bathurst (1975) refers to similar "clotted" micrite structures in carbonate diagenesis.

The clastic dikes common in Unit V signify post-depositional brittle fracture of the sediments in conjunction with the interstratal migration of water-rich sediment phases.

BIOSTRATIGRAPHY

Middle Eocene through upper Quaternary sediments were recovered at Site 737. The biostratigraphic zonation, recovery, lithology, abundance, and preservation of the various fossil groups and a preliminary paleomagnetic scale are summarized in Figure 14. The siliceous microfossils are consistently common to abundant in the upper part (middle Miocene to Quaternary) of the sequence. Abundant, well-preserved, and highly diversified diatom assemblages dominate the biogenous components throughout this interval. They consist of species characteristic of the Southern Ocean as well as species characteristic of the lower latitudes. Radiolarian assemblages are less diversified and consist mainly of Antarctic species. Most Eocene and Oligocene sediments are barren of siliceous microfossils. Calcareous nanno-

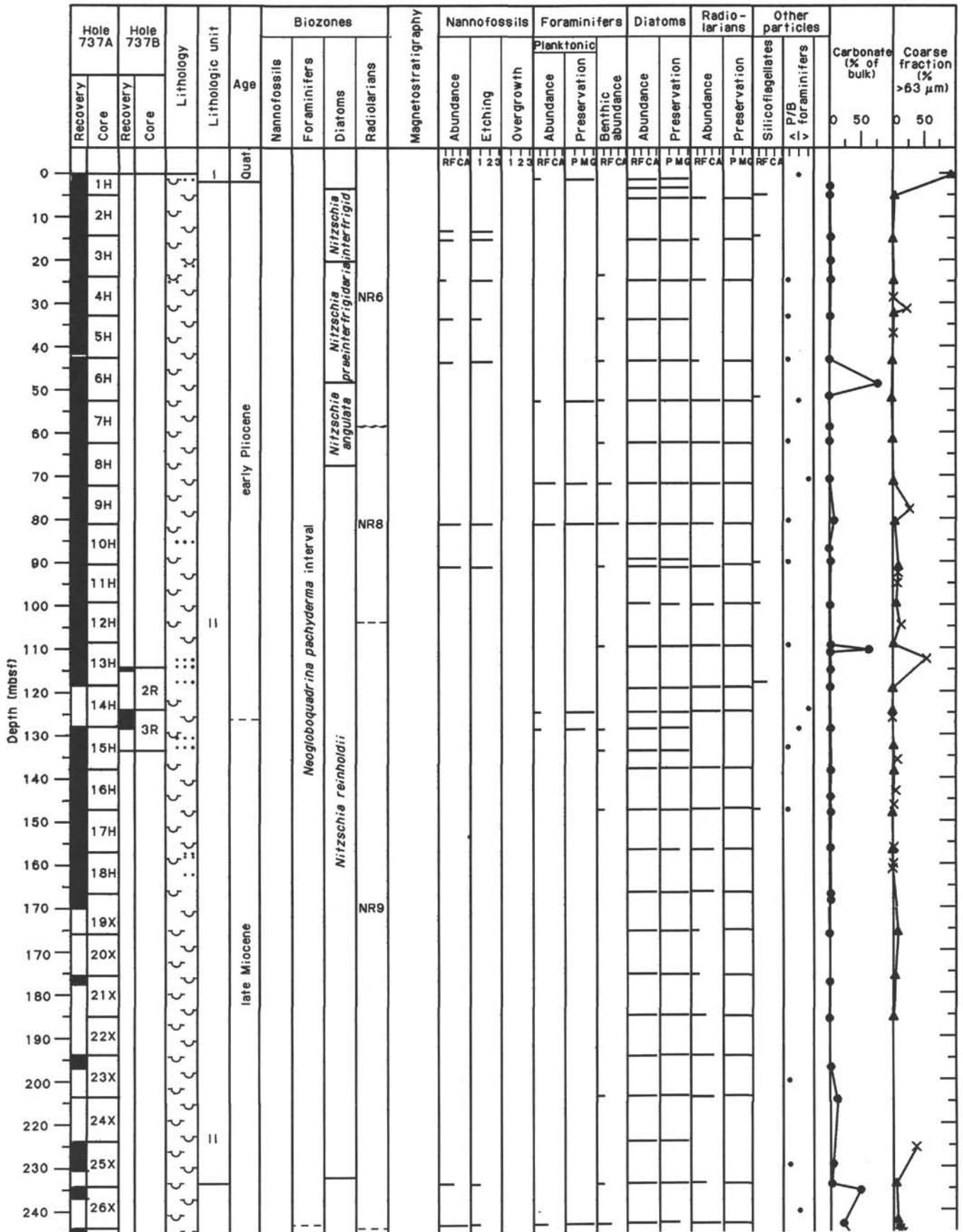
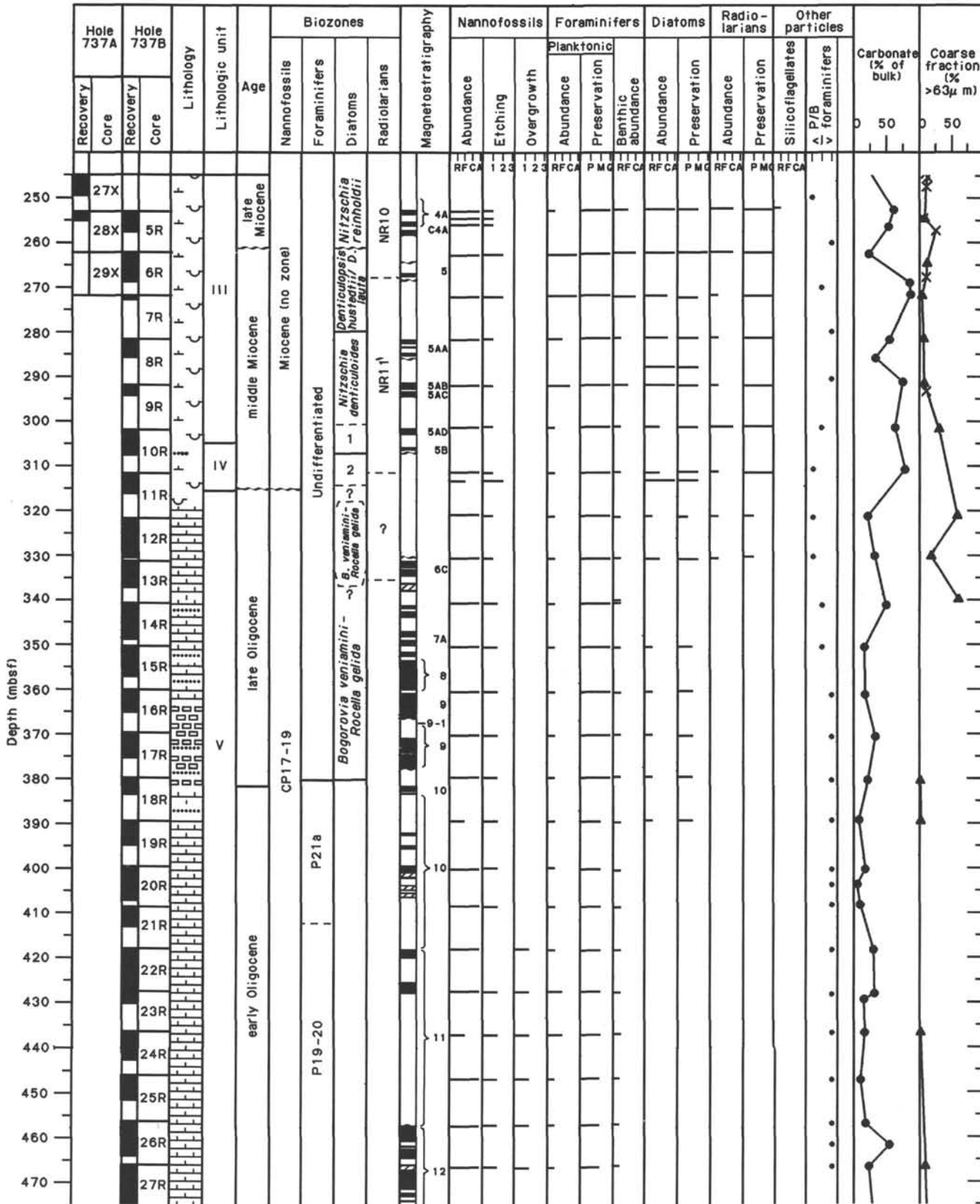


Figure 14. Biostratigraphic summary, Site 737.



Diatom zones: 1 = *Nitzschia grossepunctata* 2 = *Coscinodiscus lewisianus*

Figure 14 (continued).

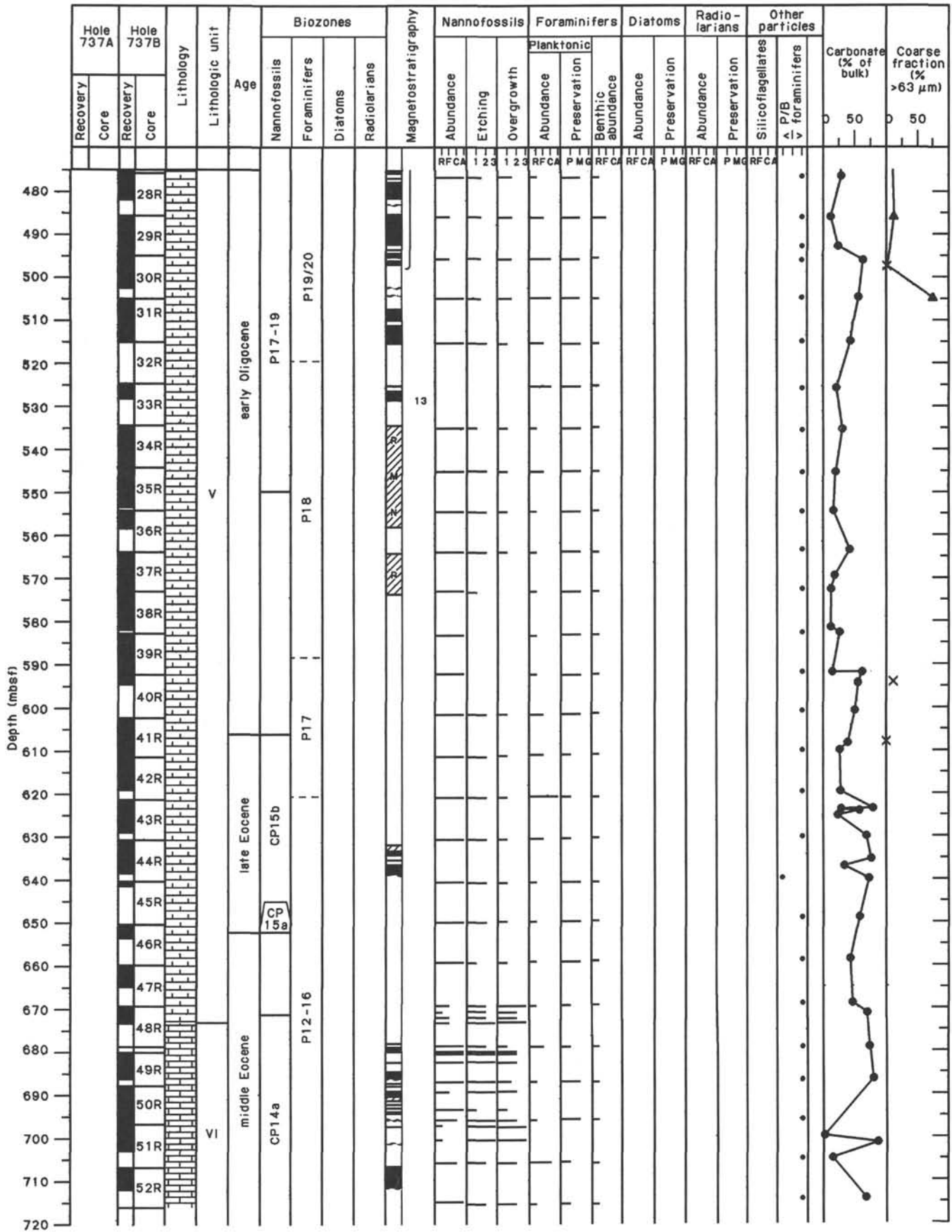


Figure 14 (continued).

fossils are abundant throughout the Eocene-Oligocene sequence. The assemblages are moderately to well preserved. Diversity and assemblage composition are similar to those found in the Falkland Plateau and the Maud Rise.

Calcareous microfossils are generally well preserved in upper Miocene through lower Pliocene sediments. Assemblages are low in diversity, and they occur in discontinuous levels. Foraminifers are rare to absent and very low in diversity within the upper Miocene through Quaternary sediments. Below 245 mbsf all examined core-catcher samples yielded foraminifers. Nearly all samples are dominated by planktonic taxa, but species diversity is low throughout the sequence. Low-diversity silicoflagellates are present throughout the Miocene to Pliocene part of the sequence. No organic-walled microfossils were found at Site 737.

The Eocene/Oligocene boundary occurs in Section 119-737B-41R-4. It is recognized by the extinctions of the calcareous nannofossil *Discoaster saipanensis* and the planktonic foraminifer *Globigerinatheka index*. The nannofossil abundance patterns do not indicate any abrupt environmental change from the late Eocene to early Oligocene. The planktonic foraminifers indicate that the lower/upper Oligocene boundary occurs between Cores 119-737B-17R and 119-737B-18R. The precise position of the upper Miocene/lower Pliocene boundary is tentatively placed in Core 119-737A-15H, based on paleomagnetic data and the first occurrence of the diatom *Thalassiosira praeoestrupii* in Sample 119-737A-13H-CC.

Three hiatuses are recognized in the sediment section at Site 737. An important hiatus is present in the lower part of the Neogene and the top of Oligocene. Based on nannofossil and diatom datums, this hiatus is tentatively estimated to be 8 to 6 m.y. in duration. The second hiatus is in the lower upper Miocene between the top of common *Denticulopsis dimorpha*, at approximately 10.0 Ma, and the bottom of *Thalassiosira burckliana*, at 8.2 Ma. This hiatus corresponds with the interval of combined widespread hiatuses NH4 and NH5 of Barron and Keller (1982). A hiatus spanning the upper Pliocene and most of the Quaternary (about 3.4 m.y.) occurs at the top of Hole 737A (0.2 to 0.8 mbsf).

Calcareous Nannofossils

Hole 737A recovered 29 cores down to a total depth of 273 mbsf. Nannofossils are generally well preserved but low in diversity and occur in discontinuous levels. Species present are long-ranged forms. Cores 119-737B-2R and 119-737B-3R (114.5–133.8 mbsf) are barren of nannofossils. The Miocene interval (253.5–315 mbsf) contains well-preserved nannofossils, although the diversity is low. The Oligocene and upper Eocene interval (315–608 mbsf) yields abundant, moderately preserved to well-preserved, diverse nannofossil assemblages. Nannofossil diversity and assemblage composition at this site are similar to those found in material from the Falkland Plateau and Maud Rise. The expanded Oligocene section (over 300 m) recovered at this site is especially valuable for fine-resolution study of calcareous plankton evolution and its implication for paleoceanography in the Southern Ocean.

Core-catcher samples and several core intervals from Holes 737A and 737B were examined for calcareous nannofossils. The preliminary stratigraphy is presented in Figure 14. Okada and Bukry's (1980) zonation was followed. This zonation is applicable for the middle Eocene to lower Oligocene section at this site but is not applicable for the younger section because of the absence or scarcity of sphenoliths.

Hole 737A

All of the core-catcher samples were examined for nannofossils; only those that contain nannofossils are described in the following. Samples not mentioned are barren of nannofossils.

Samples 119-737A-2H-5, 59 cm, and 119-737A-2H-CC through 119-737A-5H-CC contain rare to few *Reticulofenestra perplexa*, a high-latitude species, and scattered rare *Coccolithus pelagicus*. In Samples 119-737A-9H-CC and 119-737A-10H-CC, two additional species were found: *Calcidiscus leptoporus* and *Reticulofenestra pseudoumbilica*. The former has a range from lower Miocene to Holocene, whereas the latter ranges from middle Miocene to upper Pliocene. Sample 119-737A-25X-CC contains few species of *Reticulofenestra hesslandii*. Rare *C. pelagicus* and very abundant *R. hesslandii* were found in Sample 119-737A-26X-CC. Samples 119-737A-27X-CC and 119-737A-28X-CC both contain abundant *R. perplexa*, common *R. hesslandii*, and a few specimens of *C. pelagicus*.

Hole 737B

The first core was washed down to 114.5 mbsf, and no sediment was recovered. Core-catcher samples from the second and third cores are barren of nannofossils. The fourth core was also a washed core. One specimen of *C. pelagicus* and abundant *Reticulofenestra gelida* were found in Sample 119-737B-5R-1, 122 cm. Sample 119-737B-5R-1, 127 cm, contains common *R. perplexa*, abundant *Reticulofenestra producta* (<3.5 μm), and few *R. gelida*. Core-catcher samples from Cores 119-737B-5R to 119-737B-10R yield *R. perplexa*–*R. hesslandii* assemblages, which have limited stratigraphic value. Abundant, well-preserved, diverse nannofossils were encountered in core-catcher samples from Cores 119-737B-11R to 119-737B-46R. A sharp change was observed between Samples 119-737B-10R-CC and 119-737B-11R-CC, with *Chiasmolithus altus*, *Cyclicargolithus floridanus*, *Reticulofenestra bisecta*, *Reticulofenestra daviesi*, *Reticulofenestra filewiczii*, *Pyrocyclus orangensis*, and *Discoaster deflandrei* occurring in the lower sample but not in the upper sample. An unconformity must be present between the two samples. The hiatus is estimated to be 8 m.y. in duration based on nannofossil and diatom datums. This unconformity also brings the middle Miocene section in contact with the upper Oligocene section. A similar hiatus found in the South Atlantic sector of the Southern Ocean is accounted for by the opening of the Drake Passage.

The boundaries between Zones CP19 through CP17 are defined by sphenolith datums. Because sphenoliths are rare or absent in high latitudes, the differentiation of these zones is difficult. The first-appearance datum (FAD) of *Cyclicargolithus abisectus* was used by previous workers to approximate the FAD of *Sphenolithus ciperensis*, which defines the bottom of CP19 (discussed in Perch-Nielsen, 1985). We initially tried to apply this, but the CP17 through CP18 interval at this site turned out to be extremely condensed (<10 m in 6 m.y.), and we have no reason to believe that a major hiatus is present. Moreover, the FAD of *C. abisectus* has been correlated to the magnetostratigraphy and is estimated to be 34.2 Ma (Wei and Wise, in press), 0.4 m.y. after the last-appearance datum (LAD) of *Reticulofenestra umbilica* and 5.6 m.y. (4.0 m.y. in Berggren et al., 1985) before the FAD of *S. ciperensis*. Apparently, the FAD of *C. abisectus* can not approximate the FAD of *S. ciperensis* either in high latitudes or in midlatitudes. Thus, core-catcher Samples 119-737B-11R through 119-737B-34R are placed in the nondifferentiated Zone CP19–17. The FAD of *C. abisectus* occurs in Sample 119-737B-33R-CC and may be a useful datum level in a high-latitude zonation defined differently from those of Bukry (1973, 1975) or Martini (1971). The LAD of *R. umbilica* was found in Sample 119-737B-35R-CC, and this datum level defines the upper boundary of Zone CP16.

The Eocene/Oligocene boundary is defined, in terms of nannofossil datums, by the LAD of *D. saipanensis* or *Discoaster barbadiensis* (see Berggren et al., 1985). Rare but consistent *D. saipanensis* were found up to Sample 119-737B-41R-4, 40 cm,

but not in Sample 119-737B-41R-3, 132 cm, or higher levels. The Eocene/Oligocene boundary is thus placed between these two samples. The nannofossil abundance patterns at this site do not indicate an abrupt environmental change from late Eocene to early Oligocene.

The LAD of *Ismolithus recurvus*, which was used in Wise's (1983) high-latitude nannofossil zonation, was found in Sample 119-737B-37R-CC. The FAD of *I. recurvus* in Sample 119-737B-47R-CC marks the lower boundary of CP15b. The LAD of *Reticulofenestra reticulata* was recognized in Sample 119-737B-46R-1, 1–2 cm. This datum is recognized as useful in low and high latitudes (Perch-Nielsen, 1985; Martini and Müller, 1986). Correlation of the LAD of *R. reticulata* yields an estimated age of 37.4 Ma (Wei and Wise, in press). The FAD of *Chiasmolithus oamaruensis* found in Sample 119-737B-46R-2, 21–22 cm, is the bottom of CP15A.

The LAD of *Chiasmolithus solitus* in Sample 119-737B-48R-CC marks the top of Subzone CP14a. Rare specimens of *Discaster bifax* were observed in Sample 119-737B-52R-CC, the lowermost sample from this hole. Therefore, the oldest sediment in Hole 737B is assigned to Subzone CP14a.

Foraminifers

Foraminifers are rare to absent and very low in diversity within the dominantly siliceous upper Miocene through Quaternary sediments at Site 737, between 0 and 245 mbsf. Below this interval, all examined core-catcher samples yielded foraminifers. The predominantly low abundance of foraminifers in the >150- μ m size fraction recorded for the middle Eocene through upper Miocene interval (Fig. 14) is due to the dominance of carbonate grain aggregates, which did not break down during sample processing, and scattered intervals of volcanogenic clasts. Foraminifer preservation remains good to a depth of 380 mbsf, below which calcite overgrowth and test infilling become apparent, particularly among the planktonic foraminifers. At this same stratigraphic level, a prominent change occurs in the physical properties of the sediment, including an increase in the seismic velocity and the more common occurrence of siliceous spherules, suggesting a possible hiatus. Preservation further diminishes downcore, below the Eocene/Oligocene boundary, where test infilling by silica and calcite overgrowths obscure apertural and test surface detail.

Nearly all of the samples analyzed are dominated by planktonic taxa, with notable exceptions occurring between Cores 119-737B-8R and 119-737B-14R (290–350 mbsf) and in Core 119-737B-44R (640 mbsf), where benthic foraminifers are equally abundant or dominate the assemblages. Planktonic species diversity is low throughout the sequence, relative to coeval lower latitude assemblages, with a total of 22 species recognized. The total benthic diversity is also quite low.

Planktonic Foraminifers

Neogene to Holocene

The mud-line sample, which is composed mainly of volcanic material with abundant glauconite and a lesser amount of siliceous material, contained only a few specimens of *Neogloboquadrina pachyderma*. No age-diagnostic planktonic foraminifers were found in the Neogene sediments at Site 737. Specimens of *N. pachyderma* and *Globigerina bulloides* occur in low abundance at several sporadic intervals within the upper Miocene to Holocene samples. The oldest occurrence of *N. pachyderma* is in Core 119-737A-26X (upper Miocene), whereas *G. bulloides* ranges down to Core 119-737B-6R (middle Miocene). Kennett and Srinivasan (1983) reported that the range of *N. pachyderma* is no older than late Miocene.

Globorotalids are very rare in the Neogene sequence. Single or few specimens of *Globorotalia scitula* occur in several samples between 80 and 290 mbsf (lower Pliocene to middle Miocene). *Globorotalia scitula gigantea* and *Globorotalia praescitula* are found in Core 119-737B-8R, and the latter species also occurs within Core 119-737B-9R. Both taxa have a reported range of lower to middle Miocene. Rare specimens of *Globigerina falconensis* and *Globigerina praebulloides* also occur in several of the Neogene samples.

Paleogene

The biostratigraphic utility of planktonic foraminifers increases considerably in the mid-Eocene to Oligocene sediments. The following datums were used to define ages for several of the Paleogene intervals in Hole 737B (from Berggren et al., 1985):

Datum	Section	Chron	Age
LAD <i>Chiloguembelina cubensis</i>	18R-CC	C10	early/late Oligocene boundary
LAD <i>Globigerina angiporoides</i>	22R-CC	C11	late early Oligocene
LAD <i>Globigerina ampliapertura</i>	41R-CC	C12	middle early Oligocene
LAD <i>Globigerinatheka index</i>	41R-CC	C13	Eocene/Oligocene boundary

Determination of the Berggren et al. (1985) planktonic foraminifer zonal boundaries (Fig. 14) was based on a calculated minimum sedimentation rate of 31 m/m.y. for the Oligocene. The zonal boundaries occur at the following depths:

Boundary	Depth (mbsf)
P21A/19-20	412
P19-20/18	518
P18/17	588
P17/12-16	621

Other important planktonic species found at Site 737 include *Globorotalia opima nana*, *Globorotalia gemma*, *Globorotalia munda*, *Globigerina linaperta*, and *Catapsydrax dissimilis*. Their ranges at Site 737 and correlated age assignments are listed in the following:

Species	Range (Hole 737B)	Age
<i>G. opima nana</i>	31R to 14R	late early Oligocene to late Oligocene
<i>G. gemma</i>	40R to 34R	early Oligocene
<i>G. munda</i>	38R to 28R	early Oligocene
<i>G. linaperta</i>	51R to 38R	middle Eocene to early Oligocene
<i>C. dissimilis</i>	35R to 13R	early Oligocene to late Oligocene

The ranges of these species at Site 737 are comparable with the ranges established by Jenkins (1985) for midlatitude planktonic species. The occurrence of *G. linaperta* is limited to the middle and upper Eocene (Jenkins, 1985), whereas we find this species ranging into the lower Oligocene.

A few planktonic species occur sporadically throughout the sequence or show some taxonomic problems resulting from lack of preserved characteristic features. *Globigerina woodi connecta* is found in the upper Oligocene (Cores 119-737B-12R to 119-737B-16R). A similar, rather variable form that occurs in moderate to high abundance in several samples from the bottom of this interval to Core 119-737B-42R is designated as *Globigerina cf. connecta*. The identification of *G. praebulloides* is also based on a relatively broad species concept which results in a long range (upper Eocene to middle Miocene). This range is comparable to the range reported by Bolli and Saunders (1985). *Globigerina juvenilis* has a sporadic occurrence in the upper lower Oligocene to upper Oligocene and is found only in low num-

bers. Jenkins (1985) reported the first occurrence of this species in the upper Oligocene.

Several planktonic foraminifer zonal markers for the existing range charts of the southern midlatitude regions are not found in this site. Factors that may account for this include (1) preservation problems, (2) limitation of the study to only core-catcher samples, and (3) biogeographic exclusion resulting from the high-latitude position of Site 737. A detailed shorebased study will afford a better interpretation of the faunal distributions.

Benthic Foraminifers

Benthic foraminifers from Site 737 were studied from the mud-line sample and all core-catcher samples. The abundance of benthic species is low throughout the entire sequence and the total numbers are insufficient for a quantitative study. The sparse Miocene to Holocene foraminiferal fauna is dominated by benthic species except in Samples 119-737A-8H-CC and 119-737B-2R-CC, where planktonic species dominate. The preservation of benthic foraminifers is moderate to good. In many samples the preservation of benthic species is better than that of planktonic species. Species diversity is low throughout the cored interval, and it varies widely from sample to sample. The fauna is dominated by calcareous species; only a few arenaceous taxa, including *Karreriella*, *Eggerella*, and *Cyclamina*, occur randomly in the samples.

The overall scarcity of the benthic component and the sporadic occurrences make it difficult to recognize downcore distribution patterns or faunal assemblage subdivisions related to the geological time scale. Many of the more common species have long ranges without distinct, dominant occurrences. Changes through time occur as fluctuations in diversity and variations in the number of representative species of certain genera. The following observations enabled the benthic fauna to be grouped into four assemblages:

Assemblage 1 (Quaternary to Pliocene)

Assemblage 1 is characterized by a very low species diversity. The mud-line sample contains extremely rare benthic specimens related to *Bulimina aculeata*, *Nonionellina* sp., and *Angulogerina earlandi*. Samples 119-737A-1H-CC and 119-737A-2H-CC are barren of benthic foraminifers. Below this barren interval to 130 mbsf the fauna contains additional species such as *Globobulimina pacifica*, *Melonis barleeanus*, *Pullenia bulloides*, *Sphaeroidina bulloides*, *Uvigerina* spp., and *Cassidulina oblonga*. The species composition corresponds with the Pliocene fauna found at Site 736. A predominantly barren interval in the uppermost Miocene, ranging from 130 to 240 mbsf, yields rare specimens of *Martinotiella antarctica*.

Assemblage 2 (early late to middle Miocene)

Most of the benthic species of assemblage 1 also occur in assemblage 2. The transition from a diatom ooze into a diatom nannofossil ooze and an overall increase in carbonate content are accompanied by an increase in diversity of the benthic fauna. Additional species include *Buliminella elongata*, *Gyroidina orbicularis*, *Gyroidina lamarckiana*, *Cassidulina laevigata*, *Cibicidoides robertsonianus*, *Cibicidoides kullenbergi*, *Stilostomella aculeata*, *Oridorsalis umbonatus*, and *Pullenia simplex*. Several of these species have been described from lower bathyal surface sediments of the southeastern Indian Ocean (Corliss, 1979a, 1979b). An estimation of the Site 737 water paleodepth, however, remains difficult because of the broad bathymetric distribution and equitable abundance of the species occurring at this site. Agglutinated taxa included in assemblage 2 are represented by *M. antarctica*, *Karreriella bradyi*, and *Eggerella bradyi*.

Assemblage 3 (Oligocene)

Assemblage 3 shows an increased number of taxa related to *Stilostomella* and *Cibicidoides*. Other typical species include *Anomalinoidea globulosus*, *Pullenia quinqueloba*, *Anomalinoidea spissiformis*, *Gyroidinoidea globosus*, *Epistominella* sp., *Pleurostomella* spp., *Orthomorphina* sp., *Globocassidulina subglobosa*, and *Laticarinina pauperata*. A distinct increase in diversity of *Cibicidoides*, *Stilostomella*, and *Pleurostomella* was also found in deep-water regions of the equatorial Pacific Ocean below the middle Miocene (Thomas, 1985). The upper boundary of this change at Site 637 was not recovered because of the hiatus between the late Oligocene and middle Miocene.

Assemblage 4 (upper to middle Miocene)

Although no marked change in the benthic fauna occurs at or below the Eocene/Oligocene boundary, preservation quality is generally poor, which probably accounts for a decrease in species diversity. The genus *Stilostomella* is present, although there are fewer species of morphotypes. Long-ranging forms such as *O. umbonatus*, *G. subglobosa*, and *P. bulloides* are represented. *A. spissiformis*, *Lenticulina* sp., *G. globosus*, *Cibicidoides* spp., and *P. quinqueloba* are accessory species.

The composition of benthic species at Site 737 suggests a water paleodepth similar to the present depth of upper to middle bathyal, without a major change throughout the Neogene and upper Paleogene sequence.

Diatoms

Diatoms are consistently present in the middle Miocene through lower Pliocene and Quaternary sediments, sporadically present in the upper Oligocene sediments, and absent in the Eocene and lower Oligocene sediments recovered from Site 737. Preservation is generally good in the Pliocene and Miocene sediments, but deteriorates in the Oligocene sediments. Likewise, the samples examined contain a more abundant and diverse assemblage in the Miocene through Quaternary sediments than in the Oligocene sediments. Reworked specimens are not obvious, except in the upper few meters cored where a thin (less than 40 cm thick), surficial Quaternary unit overlies the lower Pliocene and where burrows are present.

The diatom assemblage present at Site 737 consists of species characteristic of the Southern Ocean as well as species characteristic of the lower latitudes. The abundance of these two components fluctuates from sample to sample, most likely reflecting latitudinal fluctuations in the Antarctic Convergence during the Neogene.

The two components of the diatom assemblage allow the partial usage of the Southern Ocean zonation defined by Ciesielski (1983), the low-latitude zonation of Barron (1985), and the temperate, midlatitude zonation of Barron (1985). Stratigraphic markers are prevalent in the middle Miocene through lower Pliocene and in the Quaternary sediments, but they are extremely rare in the upper Oligocene sequence.

The upper 2 cm of Section 119-737A-1H-1 contains abundant specimens of *Nitzschia kerguelensis* and rare specimens of *Thalassiosira lentiginosa* and *Thalassiosira gracilis*, indicating a Quaternary age for this sample. However, slightly below this sample (Sample 119-737A-1H-1, 40 cm) the diatom assemblage is dominated by specimens of *Thalassionema* sp. and contains *Nitzschia interfrigidaria*, *Nitzschia weaveri*, and *Nitzschia angulata*, allowing the placement of this sample in the lower Pliocene *Nitzschia interfrigidaria* Zone. Thus, a hiatus spanning the upper Pliocene and most of the Quaternary (about 3.4 m.y.) occurs between Samples 119-737A-1H-1, 2 cm, and 119-737A-1H-1, 40 cm (0.2–0.4 mbsf).

Core 119-737A-1H is also of interest in that it is moderately burrowed. Comparing the diatom assemblage from burrowed intervals with that from nonburrowed intervals at the same stratigraphic level indicates that the burrows are dominated by specimens of *N. kerguelensis* and are Quaternary in age whereas the nonburrowed intervals contain numerous specimens of *N. interfrigidaria*, *N. weaveri*, and *N. angulata*, which is suggestive of an early Pliocene age. It should be noted that several burrows were observed to contain a mixed assemblage containing *N. kerguelensis* and *N. interfrigidaria*.

Samples 119-737A-1H-1, 40 cm, through 119-737A-2H-CC are assigned to the *N. interfrigidaria* Zone based on the co-occurrence of *N. interfrigidaria* and *N. weaveri*. The first occurrence of *N. weaveri* is present in Sample 119-737A-3H-2, 57 cm. This interval is characterized by typical Southern Ocean species, including *N. angulata*, *N. interfrigidaria*, and *T. gracilis*.

The first occurrence of *N. interfrigidaria* in Sample 119-737A-5H-CC allows core-catcher Samples 119-737A-3H through 119-737A-5H to be placed in the *N. praeinterfrigidaria* Zone. This interval is dominated by specimens of *N. praeinterfrigidaria*, *Thalassionema nitzschioides*, *Thalassionema* sp., and *Thalassiosira* spp.

N. angulata first occurs in Sample 119-737A-7H-CC, allowing the interval represented by core-catcher Samples 119-737A-6H and 119-737A-7H to be assigned to the *Nitzschia angulata* Zone. *N. angulata* has an abrupt and common first occurrence and appears to be a reliable stratigraphic indicator at this site. R. Gersonde (pers. comm., 1987) believes that this *Nitzschia* species is not a true *N. angulata*. Other species prevalent in this interval include *Thalassionema* sp., *Stephanopyxis turris*, *Thalassiosira eccentrica*, *Eucampia antarctica*, and *T. gracilis*.

Samples 119-737A-8H-CC through 119-737A-26X-1, 57 cm, and Cores 119-737B-2R and 119-737A-3R are assigned to the *Nitzschia reinholdii* Zone based on the first occurrence of *N. angulata* in Sample 119-737A-7H-CC and the last common occurrence of *Denticulopsis hustedtii* in Sample 119-737A-26X-CC. The diatom assemblage observed in this interval is characterized by species typical of the Southern Ocean, but more importantly, also by species characteristic of the warmer, lower latitudes. Representing the latter assemblage are specimens of *Nitzschia miocenica*, *Nitzschia fossilis*, *Nitzschia porteri*, *Thalassiosira nativa*, *Thalassiosira miocenica*, *Thalassiosira convexa* var. *aspinosa*, *Thalassiosira praeconvexa*, and *T. burckliana*.

The occurrence of these species increases the stratigraphic resolution of the diatom biostratigraphy by allowing the partial usage of the low-latitude and temperate diatom zonations of Barron (1985). Although further shorebased analyses are required to determine the isochroneity of most of these markers, a tentative stratigraphy can be employed.

The first occurrence of *T. praeostrupii* (in Samples 119-737A-13H-CC and 119-737B-2H-CC) marks the base of the lower Pliocene (5.3 Ma). The successive first occurrences of tropical species *T. miocenica* (between Samples 119-737A-19X-1, 57 cm, and 119-737A-19X-CC) and *N. miocenica* (between Samples 119-737A-21X-CC and 119-737A-23X-CC) and the last occurrence of *T. burckliana* (between Samples 119-737A-21X-CC and 119-737A-23X-CC) allow placement of the base of the *Thalassiosira convexa* Zone (6.1 Ma), the base of the *Nitzschia miocenica* Zone (6.7 Ma), and the base of Subzone B of the *Nitzschia porteri* Zone, respectively.

The diatom assemblage observed in this interval is characterized by a temperate—rather than Southern Ocean—assemblage. Observed species include *T. nitzschioides*, *T. burckliana*, *Hemidiscus cuneiformis*, *Denticulopsis katayamae*, *T. convexa*, *N. fossilis*, and *T. miocenica*.

The last common occurrence of *D. hustedtii* in Sample 119-737B-26X-1, 57–59 cm, allows placement of the *D. hustedtii/N.*

reinholdii zonal boundary between Samples 119-737A-26X-1, 57–59 cm, and 119-737A-26X-CC. Thus, Cores 119-737A-27X through 119-737A-28X and 119-737B-5R are placed in the *Denticulopsis hustedtii* Zone. All of these samples contain *T. burckliana* and are likely younger than 8.2 Ma (Barron et al., 1985). A probable hiatus is present between Samples 119-737B-5R-CC and 119-737B-6R-1, 16 cm, based on ODP Leg 113 diatom biostratigraphy (R. Gersonde, pers. comm., 1987), the abrupt appearance of calcareous nannofossil-rich chalk in the lower sample, and an abrupt change in sedimentation rates (see “Sedimentation Rates” section, this chapter). Specimens of *Denticulopsis dimorpha* are common in Sample 119-737B-6R-1, 16 cm, along with specimens of *Denticulopsis lauta*, whereas *T. burckliana* and a number of *Thalassiosira* and *Nitzschia* species, which are present in the overlying interval, are no longer present. Sample 119-737B-6R-1, 16 cm, is placed in the *Denticulopsis hustedtii/Denticulopsis lauta* Zone.

Magnetostratigraphy and diatom stratigraphy for ODP Site 689 place the top of common *D. dimorpha* and the top of a calcareous nannofossil-rich interval in the lower part of magnetic polarity anomaly 5, at approximately 10.0 Ma (R. Gersonde, pers. comm., 1987). Consequently, the interval between 8.2 and 10.0 Ma appears to be represented by a hiatus in Hole 737B at about 263 mbsf. Unfortunately, the contact between the chalk and the overlying more diatom-rich unit, the most likely horizon for an unconformity, was not recovered. This hiatus corresponds with the interval of combined widespread hiatuses NH4 and NH5 of Barron and Keller (1982).

The *D. hustedtii/D. lauta* Zone continues downcore to the last occurrence of *Nitzschia denticuloides* between Samples 119-737B-7R-CC and 119-737B-8R-2, 57 cm. Species typically observed in this interval include *D. hustedtii*, *D. dimorpha*, *Rhizosolenia barboi*, *Thalassiosira yabei*, and *Actinocyclus ingens*.

Sample 119-737B-8R-2, 57 cm, is assigned to the *Nitzschia denticuloides* Zone based on the last “common” occurrences of *N. denticuloides* in this sample. The base of the *N. denticuloides* Zone is placed in Sample 119-737B-9R-CC, as *Nitzschia grossepunctata* has its last occurrence in Sample 119-737B-10R-1, 57 cm. Other species observed in this interval include *Denticulopsis praedimorpha*, *Denticulopsis nicobarica*, *Rhizosolenia praebarboi*, *D. lauta*, *A. ingens*, *D. hustedtii*, and *D. dimorpha*.

Samples 119-737B-10R-1, 57 cm, and 119-737B-10R-3, 57 cm, are placed in the *Nitzschia grossepunctata* Zone based on the occurrence of *D. hustedtii* and the nominative species. Samples 119-737B-10R-CC through 119-737B-11R-1, 23 cm, are placed in the *Coscinodiscos lewisianus* Zone above the first occurrence of *Denticulopsis hyalina* (approximately 15.0 Ma). Typical species observed include *D. nicobarica*, *D. hyalina*, *R. praebarboi*, *A. ingens*, *Synedra jouseana*, and *Actinocyclus ingens* cf. *nodus*. Sample 119-737B-11R-1, 123 cm, the lowest sample in Hole 737B containing “good” diatoms, contains *D. hyalina* and is assigned to the *Denticulopsis hyalina* Zone.

With the exception of Sample 119-737B-12R-CC, the remaining core-catcher samples are unzoned. The occurrence of *Bogorovia veniamini* in Sample 119-737B-12R-CC suggests that this sample is equivalent to the uppermost Oligocene to lower Miocene *Bogorovia veniamini*–*Rocella gelida* Zones. With the exception of rare to few and poor to moderately well-preserved diatoms in core-catcher Samples 119-737B-14R through 119-737B-18R, the remaining core-catcher samples from Hole 737B are barren of diatoms.

Radiolarians

Pliocene and Miocene radiolarians are abundant and well preserved throughout all cores recovered at Hole 737A, but diversity is low due to the relatively shallow water depth (<1000 m) of the site. In Hole 737B, Miocene radiolarians were found in

Samples 119-737B-2R-CC through 119-737B-12R-CC. The material recovered in Cores 119-737B-13R through 119-737B-47R is completely barren of radiolarians. Core-catcher samples from Cores 119-737B-48R to 119-737B-52R contain a few recrystallized specimens diagnostic of an Eocene age, but this age determination is quite uncertain because these specimens are very rare and are diagnosed to the genus level only.

Hole 737A

Samples 119-737A-1H-CC through 119-737A-7H-CC contain a well-preserved assemblage dominated by *Pseudocubus vema*, *Prunopyle titan*, and *Clathrocyclas bicornis*. This assemblage is correlated with the Pliocene NR6 Zone. Few temperate species, such as *Anthocyrtdium pliocenica* and *Eucyrtidium teuscheri*, were found in Sample 119-737A-6H-CC, suggesting warmer environments during the late early Pliocene. Sample 119-737A-7H-CC is correlated to the base of the NR6 Zone because it includes one or two specimens of *Helotholus praevema*, the last occurrence of which marks the top of the NR7 Zone. However, sediments deposited within the NR7 Zone are either absent or are highly condensed, because the core catcher of Core 119-737A-8H is correlated with the NR8 Zone. The radiolarian assemblage of this sample contains abundant specimens of *H. praevema*, but not a single specimen of *Desmospyris spongiosa*, the first occurrence of which marks the bottom of the NR7 Zone. Few reworked specimens of *Diartus hughesi* (middle to late Miocene) were found in this same sample, suggesting erosional and transportation processes during the early Pliocene. The occurrence of *Stychocorys peregrina* in Samples 119-737A-12H-CC through 119-737A-26X-CC correlates this interval to the NR9 Zone.

Radiolarians are very abundant and well-preserved. Temperate forms related to warmer conditions were found in Sample 119-737A-13H-CC. Some reworked specimens of *Actinomma tanyacantha* and *Diartus laticonus* were found in Samples 119-737A-17H-CC and 119-737A-21X-CC, suggesting transportation during the late Miocene to early Pliocene. Radiolarian assemblages from Samples 119-737A-27X-CC and 119-737A-28X-CC are assigned to the NR10 Zone because of the abundant occurrence of *Clathrocyclas bicornis spongothorax* and the absence of *Stychocorys peregrina*. Radiolarian abundances are reduced, and deeper-living forms such as *Stylatractus universus*, *Siphocampe arachnea*, and *Stichopodium inflatum* are more abundant. This increase in abundance suggests increased upwelling and high productivity during the latest Miocene at Site 737.

Hole 737B

Samples 119-737B-2R-CC and 119-737B-3R-CC contain the same radiolarian assemblage as Sample 119-737A-26X-CC. They can be assigned to the NR9 Zone. Sample 119-737B-5R-CC is placed within the NR10 Zone and also contains deep-living forms. Few, reworked specimens of *Lithomitrella* sp., which is diagnostic of the Eocene, suggest an increase in the oceanic circulation. This increase of deep circulation was significant enough to create a gap in the sedimentary record, as evidenced by the radiolarian assemblage from Sample 119-737B-6R-CC. This assemblage contains some specimens of *Cyrtocapsella japonica*, for which the last occurrence is from the middle to the basal magnetic Chronozone 10. Other species, such as *Prunopyle hayesi*, *Circodiscus ellipticus*, *Clathrocyclas humerus*, and *A. tanyacantha*, are indicative of the early late Miocene, and thus Sample 119-737B-6R-CC can be assigned to the NR11 Zone.

Radiolarians are rare downhole and well-preserved in Samples 119-737B-7R-CC through 119-737B-9R-CC. All these samples fall within the NR11 Zone because they contain *A. tanyacantha* and have no representatives of *C. bicornis spongothorax*. Radiolarians are rare and poorly preserved in Samples 119-

737B-10R-CC through 119-737B-13R-CC. Only two species, *Stauraxiphos communis* and *P. hayesi*, can be recognized. No assignment to a radiolarian zone can be made. Samples 119-737B-14R-CC through 119-737B-41R-CC are barren of radiolarians. Very rare and recrystallized specimens of *Lithomitrella* species not identifiable to the species level were found in core-catcher samples from Cores 119-737B-47R through 119-737B-51R. One specimen of *Dictyoprora mongolfieri* was found in Sample 119-737B-49R-CC.

Palynology

Hole 737A

Three core-catcher samples (119-737A-9H, 119-737A-26X, and 119-737A-28X) were processed for palynomorphs, but were found to be barren.

Hole 737B

Eighteen core-catcher samples were processed for palynomorphs and, as in the previous hole, were found to be almost entirely barren of organic material. A small amount of wood, leaf cuticle, and a solitary, poorly preserved bisaccate pollen grain contained in Sample 119-737B-7R-CC suggest some minor terrigenous input. All the other samples are characterized by very low amounts of organic carbon. No dinoflagellate cysts were recorded.

PALEOMAGNETICS

Hole 737A

Two hundred twenty-three oriented paleomagnetic samples were collected from Hole 737A by pressing plastic sampling cubes into the soft sediments acquired by APC coring. These samples were then measured in the shipboard laboratory using the Molspin spinner magnetometer. The magnetic declination, inclination, and intensity are shown in Figure 15. In general, the magnetic intensities of the rocks are moderate to strong (0.08 to 80 mA/m). The magnetic intensity is uniform down to 50 mbsf. A sharp decrease in intensity at 50 mbsf corresponds to a polarity reversal. The intensity of the field rises progressively from 50 to 75 mbsf. A peak in the natural remanent magnetization (NRM) intensity at 75 to 88 mbsf corresponds to a short interval of normal polarity. At this point in the core, there is a significant drop in intensity that suggests the presence of a sedimentary hiatus. Intensity declines from 88 to 250 mbsf. Significant intensity changes in this interval, however, can be identified and correlated with polarity boundaries.

The NRM intensity measurements are compared to the bulk susceptibility measurements in Figure 16. In general, there is good agreement between the measurements, except in the intervals from 65 to 85, 120 to 135, and 225 to 235 mbsf. The NRM intensities in the 65–85 mbsf interval are greater than the susceptibility which suggests that there was an actual increase in the geomagnetic field during this interval. In the two remaining intervals, the susceptibility values are anomalously high.

Some samples from Hole 737A were demagnetized. Results from Samples 119-737A-12H-1, 107–109 cm, and 119-737A-9H-5, 32–34 cm, are shown in Figure 17. The alternating field (AF) demagnetization (peak fields of 20 and 50 mT) indicates that the sediments are not stably magnetized. The samples do not display directional stability on demagnetization. Sample 119-737A-12H-1, 107–109 cm, loses 80% of its normalized intensity on demagnetization to only 5 mT. In contrast, Sample 119-737A-9H-5, 32–34 cm, has a higher coercivity, retaining 80% of the normalized intensity after demagnetization at 20 mT. These AF demagnetization experiments show that the primary component of magnetization has been overprinted by a significant sec-

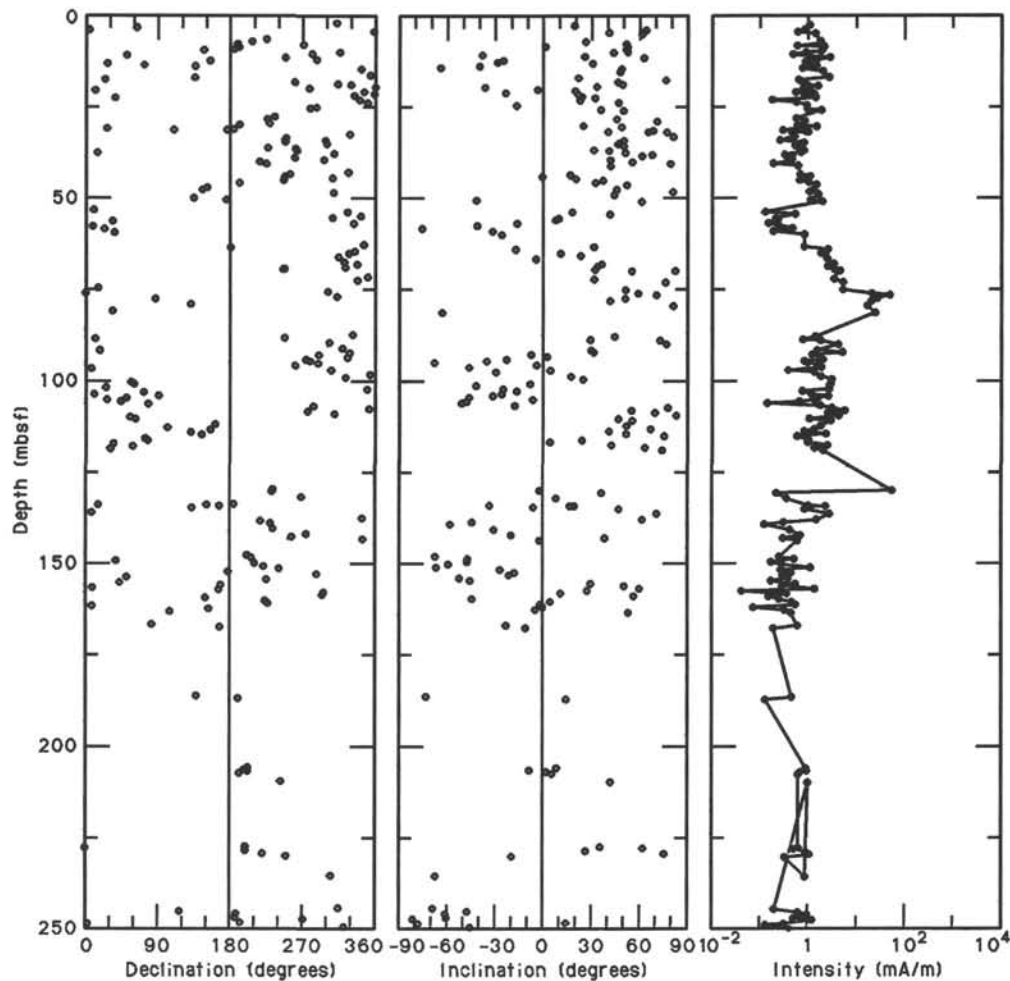


Figure 15. Stratigraphic plot of NRM sample declination, inclination, and intensity sequence for samples from Hole 737A.

ondary component of magnetization. The secondary component of magnetization in most cases acts to shallow the magnetic inclinations so that many of the NRM inclinations are scattered at intermediate values instead of clustered around the expected field values of approximately $\pm 70^\circ$. Further demagnetization of all samples from this site would be extremely valuable. A reliable paleomagnetic polarity sequence will probably only be possible after demagnetization of these samples.

A preliminary interpretation of the magnetic polarity sequence is shown in Figure 18. Clear shifts in inclination and declination can be seen in the stratigraphic plots of data; however, where the single-point polarity inversions occur it is impossible to verify the reliability of the polarity. Large gaps in the sampling add to the likelihood that polarity reversals were missed in the stratigraphic sequence.

Hole 737B

Three hundred forty-six oriented paleomagnetic samples were collected from the sedimentary sequence cored in Hole 737B. Roughly 40% of these samples was collected by pressing plastic sampling boxes into the soft sediments from the upper part of the hole. Another 30% of the samples, beginning at Core 119-737B-26R, was collected by using a rock saw to cut cubes from the lithified sediments, which were placed in plastic sampling cubes. The remaining samples were collected from the lithified sediment cores by using a drill press to cut 2.5-cm-diameter cy-

lindrical samples that were trimmed to a length of 2.5 cm. The samples were then measured on the shipboard Molspin spinner magnetometer. The results of the measurements are plotted stratigraphically in Figure 19.

Because Hole 737B was cored with the RCB, the cores are not azimuthally oriented. Thus, only inclination was used for polarity determinations. The stratigraphic plot of inclination shows clear shifts of inclination from values of roughly 80° through 0 to roughly 80° of opposite sign. The magnetic intensity appears to increase gradually downhole between 250 and 450 mbsf. Between 450 and 550 mbsf, there is an interesting oscillation in magnetic intensity, first decreasing and then increasing back to the peak intensity prior to the oscillation. The oscillation appears to correspond to a flip from normal to reversed polarity, which is closely followed by a second reversal back to normal polarity at approximately 500 mbsf. The NRM intensities can be directly compared with bulk susceptibility measurements in Figure 20. In general, there is good agreement between the two measurements in the stratigraphic sequence except at magnetic polarity boundaries. At polarity changes the NRM intensity drops significantly, for example, at depths of 350, 500, 540, and 580 mbsf. The bulk magnetic susceptibility measurements indicate that the magnetic minerals in the sedimentary sequence either remain reasonably constant or increase in a systematic fashion in these parts of the core. Thus, the decrease in magnetization is probably not due to variation in the influx of

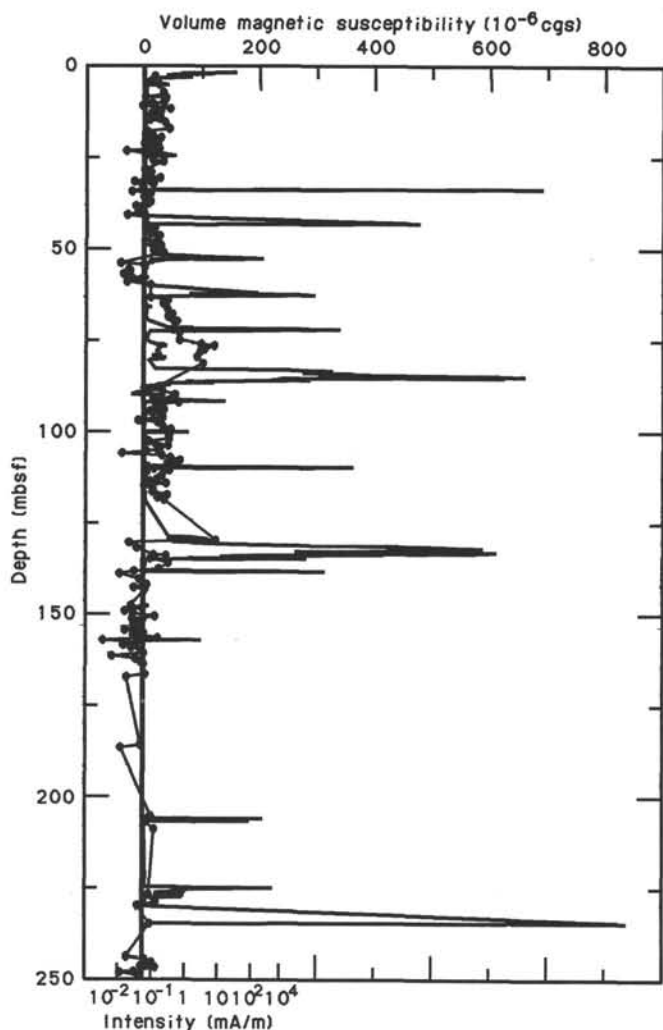


Figure 16. Stratigraphic plot of Hole 737A magnetic susceptibility (plotted as line trend) with NRM discrete sample intensity measurements (solid circles) superimposed.

magnetic minerals but instead reflects a real loss in the intensity of the Earth's magnetic field during these geomagnetic polarity changes.

A pilot demagnetization study was conducted on samples from the lithified part of this hole. Examples of the magnetic behavior upon AF demagnetization in peak fields of 50 mT are shown in Figure 21. Each of the samples studied is directionally stable after AF demagnetization. Initial directional changes at low fields correspond to only a few percent of the normalized intensity. Samples 119-737B-41R-4, 59-61 cm, and 119-737B-20R-3, 28-30 cm, show increases in intensity upon demagnetization in fields of 5-20 mT, indicating that a normally magnetized component of secondary magnetization was removed from samples for which the primary component of magnetization is of reversed polarity. This observation is consistent with the reversal stratigraphy found within the hole. The magnetic chronology, polarity, inclination, and intensity of discrete samples from Hole 737B are shown in Figure 22. The numerous identified single-point polarity changes are marked by hatched intervals. It is difficult to interpret this particular magnetic polarity sequence because of the relatively low sampling density and the relatively large number of single-point reversals that cannot be verified as reliable determinations. In order to better resolve the polarity

sequence further paleomagnetic studies using the cryogenic magnetometer were desirable.

Magnetostratigraphy

A successful at-sea transfer of liquid helium dewars was made during Leg 119, which allowed us to cool the cryogenic magnetometer and conduct shipboard whole-core magnetic stratigraphy studies. The cryogenic coolant was transferred to the magnetometer while the ship was underway. However, a large (5000-mT) magnetic field was trapped within the machine during cooling. Cores from Hole 737B were thus measured in the presence of this strong magnetic field.

In conducting the magnetic measurements, however, numerous problems were identified with the computer programs and electronics interface for the cryogenic magnetometer. These problems were of a technical nature and involved inaccurate measurement of flux jumps, transposition of the background magnetic moment measurements on the X, Y, and Z axes, transient background noise jumps (which exceeded the maximum measurement range of the cryogenic system), and incorrect calculation of moments on the extended measurement range. Many of these problems were corrected, and the magnetization of samples was subsequently recalculated.

In the case of the inaccurate measurement of flux jumps, the basic data on the number of flux jumps were not stored in the computer as backup data. Thus, much of the data, particularly for core sections that were strongly magnetized, were irretrievably lost. Data that are obviously incorrect for those sections have been marked by a hatched pattern in the magnetostratigraphic analysis and should be considered unreliable.

Using only the core sections that appear to be reliably measured, we have developed a magnetic polarity stratigraphy for parts of Hole 737B. These intervals of reliably determined polarity range from 260 to 310, 320 to 400, 400 to 500, 630 to 650, and 670 to 700 mbsf. The biozones defined on the basis of calcareous nannofossils, diatoms, and radiolarians (discussed in the "Biostratigraphy" section) were used to correlate the observed polarity sequences to the approximate epochs and chrons based upon reference polarity sequences (Berggren et al., 1985). Specific correlations of the anomalies were then accomplished by comparing the length and frequency of polarity intervals. The correlation of the polarity sequences identified in Hole 737B and those of Berggren et al. (1985) is shown in Figure 23.

The youngest identified sequence of reversals is late Miocene in age. The sequence from the upper part (Core 119-737B-5R) correlates to polarity Chrons 4A to 5, and the lower part (Core 119-737B-8R to 119-737B-10R) correlates to Chrons 5AA to 5AD. A second sequence of early to late Oligocene reversals correlates to polarity Chrons 6C to 11. The next older sequence of reversals occurs at depths of 400 to 500 mbsf. In the upper part of the hole, two normal polarity sections correlate to Chron 13. The oldest sequence of anomalies identified in Hole 737B occurs between 630 and 700 mbsf. These cores are assigned ages of late Eocene and middle Eocene based on calcareous nannofossil and planktonic foraminifer biozones. The sequence of the reversals from 670 to 710 mbsf correlates to Chrons 17 to 19 (early and middle Eocene) using the Berggren et al. (1985) polarity sequence.

SEDIMENTATION RATES

Biostratigraphic and magnetostratigraphic control at Site 737 are documented in the preceding "Biostratigraphy" and "Paleomagnetism" sections of this chapter. Diatoms are the dominant biomarkers in the upper 310 m of diatom oozes and calcareous nannofossils, and planktonic foraminifers are significant in the chalk and limestone sequences at 310-700 mbsf.

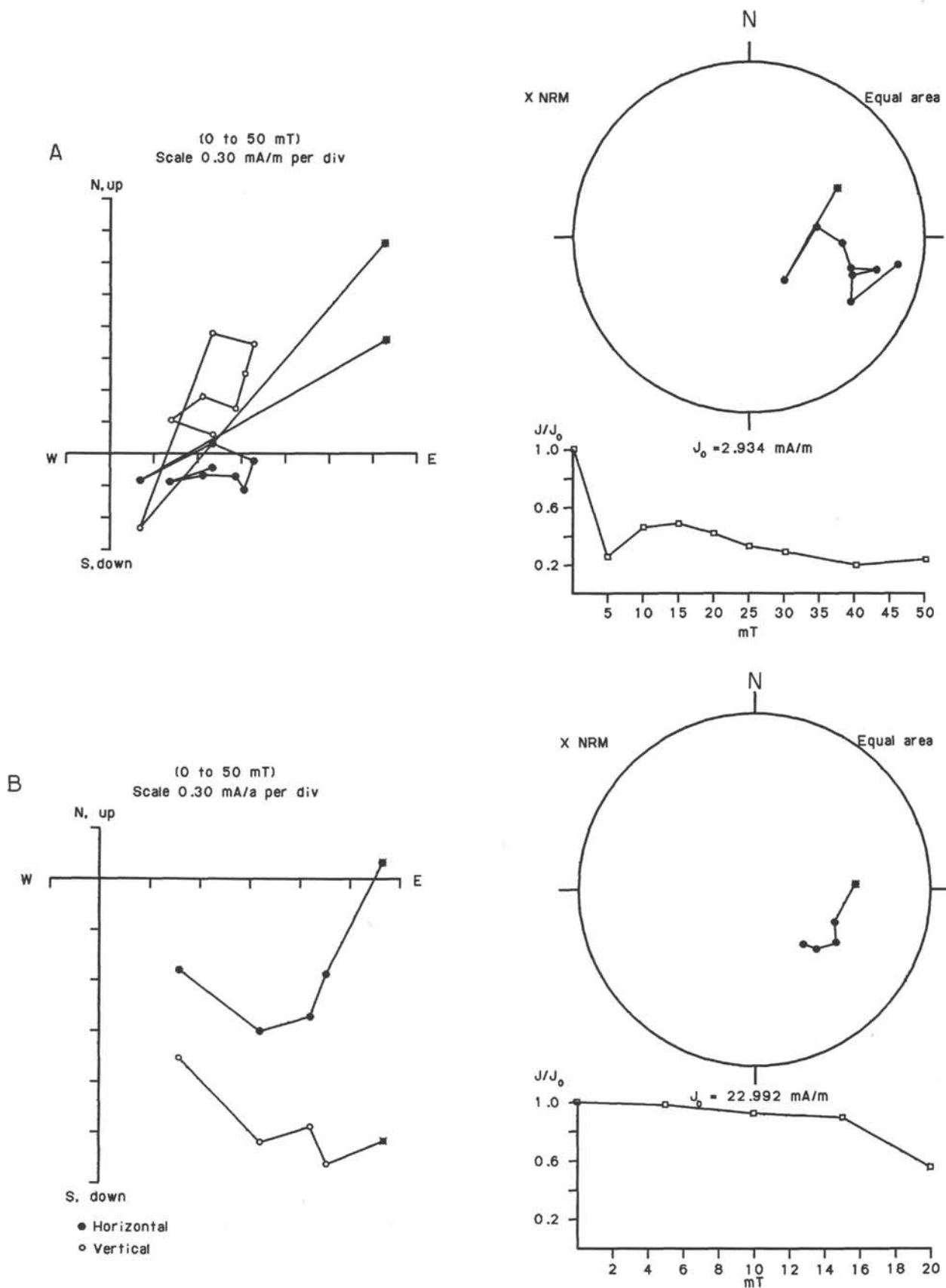


Figure 17. Orthogonal plots of sample demagnetization vectors for samples from Hole 737A. A. Sample 119-737A-12H-1, 107-109 cm. B. Sample 119-737A-9H-5, 32-34 cm.

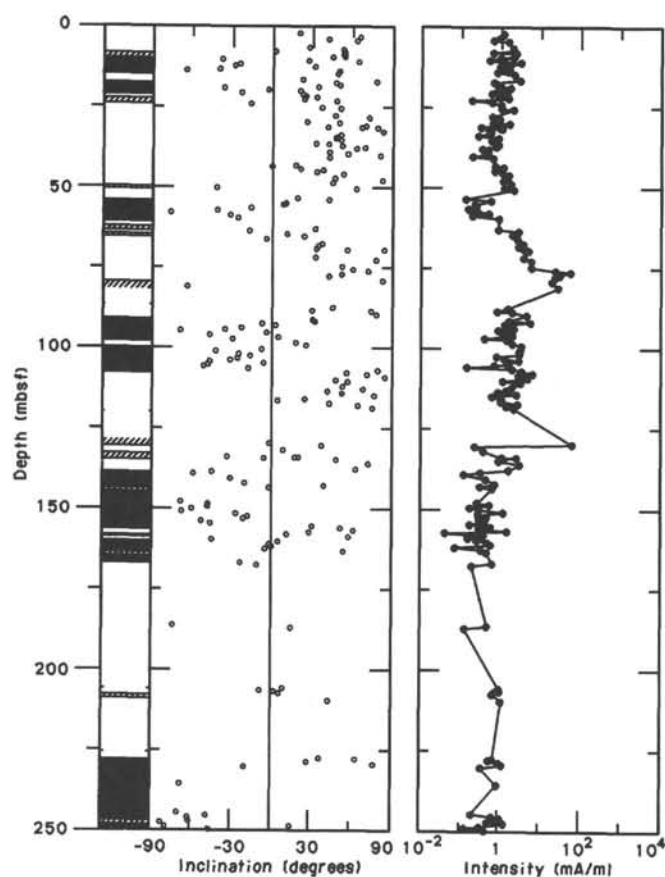


Figure 18. Stratigraphic plot of NRM sample inclination, intensity, and polarity sequence for samples from Hole 737A.

The biostratigraphic marker horizons used for the calculation of average sedimentation rates and their age estimates are given in Table 4. These data and the resulting sedimentation rates are shown in Figure 24.

The sediment sequence recovered at Site 737 is topped by a pebbly lag deposit of a few decimeters thickness and containing Quaternary diatoms. The lag deposit overlies 260 m of upper Miocene to lower Pliocene diatom oozes that were deposited at an average sedimentation rate of 56 m/m.y. (using the FAD of *Nitzschia interfrigidaria* and the FAD of *Thalassiosira burckliana*). A hiatus of about 2.7-m.y. duration separates this unit from the underlying 48-m-thick middle Miocene nannofossiliferous diatom ooze, which was deposited at an average rate of only 11.8 m/m.y. A further hiatus of about 13.3 m.y. is inferred at about 311 mbsf. This duration is arrived at by using the LAD of *Chiloguembelina cubensis* to calculate a sedimentation rate and extrapolating to the top of the upper Oligocene section at 311 mbsf. A stratigraphically complete 353-m-thick upper Eocene (FAD *Isthmolithus recurvus*) to upper Oligocene (LAD *C. cubensis*) sequence of volcanic glass-rich nannofossil chalk was deposited at an average rate of 28.1 m/m.y. No calculation of a sedimentation rate was made for the underlying 60 m of sediment because of the lack of reliable datums.

INORGANIC GEOCHEMISTRY

Two holes were cored in a water depth of 564 m at Site 737, approximately 100 km south of Site 736 on the Kerguelen-Heard Plateau. The sediments cored at Site 737 range from Pliocene to Eocene in age. Twenty whole-round minicores 5 to 10 cm in length were taken from Holes 737A and 737B for the purpose of

interstitial-water chemical studies. The maximum depth sampled was 608.5 mbsf.

Interstitial-water samples were squeezed from a variety of sediment types at Site 737. Most of the samples from Hole 737A were taken from diatom oozes. Sediment minicores from Hole 737B contained much higher percentages of calcium carbonate. Volcanic debris occurs throughout the sampled section. All of the sediments sampled for interstitial waters contained less than 0.6% organic carbon (see "Organic Geochemistry" section). The water content and porosity of the samples decreased with depth, and we were unable to obtain interstitial waters below 608.5 mbsf (see "Physical Properties" section, this chapter).

Methods

All of the samples were analyzed for pH, alkalinity, salinity, chloride, calcium, magnesium, sulfate, ammonium, phosphate, and silica. The analytical methods employed are discussed in the "Explanatory Notes" chapter. Because of the high concentrations of dissolved alkaline earth elements in Site 737 interstitial waters and the desire to duplicate analyses, 100- and 200-mL samples were used instead of the usual 500-mL samples for the calcium and total alkaline earth titrations, respectively. All of the analyses were completed within two days of the final day of drilling.

Results

Interstitial-water geochemical data for Site 737 are shown in Table 5. All of the data are reported to the appropriate level of precision for each type of analysis. Figure 25 represents a composite of data from both of the holes drilled at Site 737.

Salinity and Chloride

Both the salinity (total dissolved solids) and the chloride concentration of Site 737 interstitial waters exhibit an overall increase as a function of depth (Fig. 25). Downhole increases in these pore-water parameters may be relic signatures of more saline ocean bottom waters that were trapped in the sediments during a past glacial event. Uptake of water during the alteration of volcanic debris and basement rocks and the concomitant release of large amounts of calcium may also be responsible for these trends.

Calcium and Magnesium

The concentration of dissolved calcium steadily increases from values similar to average seawater at 3 mbsf (11.5 mmol/L in Section 119-737A-1H-2) to extremely high values, greater than 100 mmol/L, below 348 mbsf (Fig. 25). From 404 to 608 mbsf in Hole 737B there is little variation in the interstitial-water calcium concentrations. Magnesium concentrations mirror the dissolved calcium concentrations, decreasing from values similar to average seawater at 3 mbsf (52.0 mmol/L in Section 119-737A-1H-2) to values near 2 mmol/L below 348 mbsf (Fig. 25). There is also little variation in dissolved magnesium concentrations between 404 and 608 mbsf. The magnesium to calcium ratio decreases rapidly in the first 100 mbsf and approaches zero asymptotically with increasing depth.

A plot of dissolved calcium concentration vs. dissolved magnesium concentration (Fig. 26) displays two distinct chemical zones within the Site 737 interstitial waters. The interstitial waters between 3 and 372 mbsf show a linear relationship between the concentrations of calcium and magnesium. A regression line through these data points has a slope of -1.82 and a correlation coefficient of -0.9979 . McDuff and Gieskes (1976), McDuff (1978), and Gieskes (1983) have shown that a linear correlation between ΔCa and ΔMg implies conservative behavior for both of these elements. Thus, the behavior of dissolved calcium

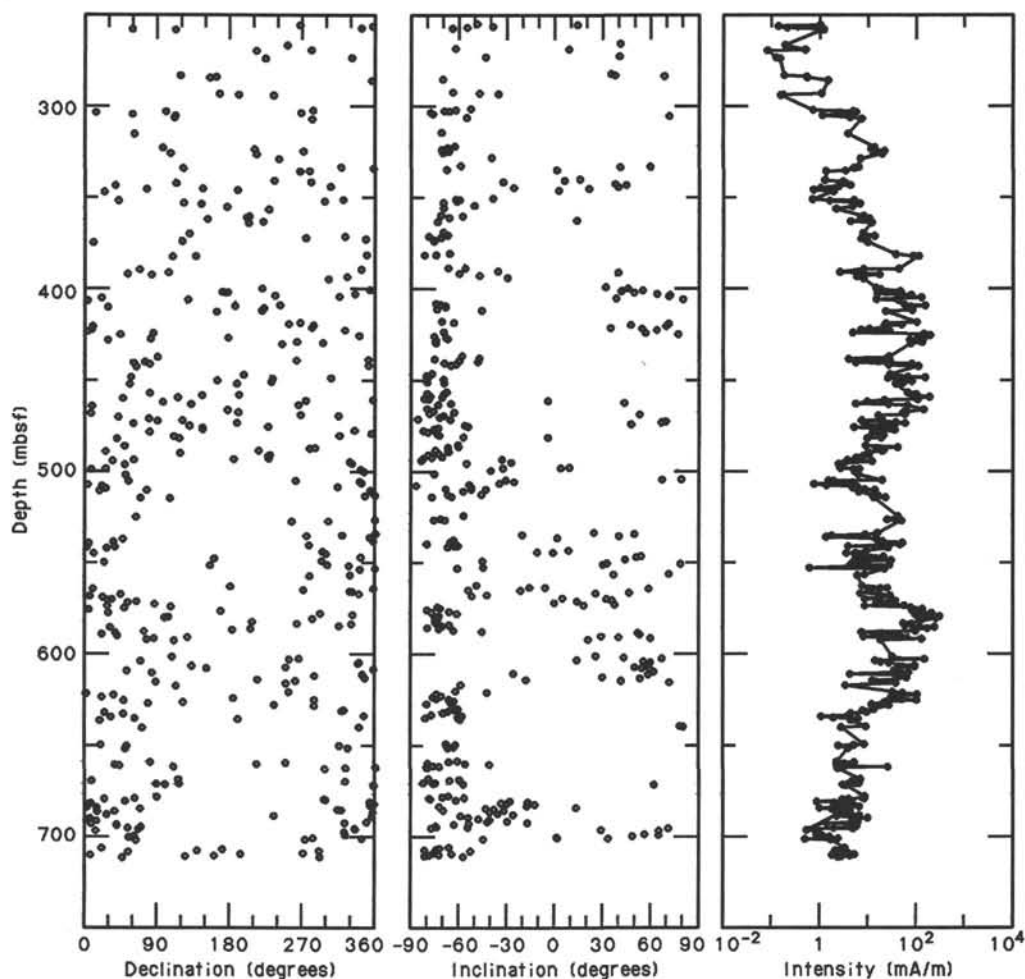


Figure 19. Stratigraphic plot of NRM sample declination, inclination, and intensity sequence for samples from Hole 737B.

and dissolved magnesium is probably controlled by diffusive processes in the upper 372 m of the sediment column at Site 737. Below this level the correlation between ΔCa and ΔMg is less linear ($r = -0.5238$), and it seems likely that dissolved calcium and dissolved magnesium are participating in reactions between the interstitial waters and their host rocks.

Silica

Dissolved silica concentrations sharply increase from 576 $\mu\text{mol/L}$ at 3 mbsf to 1240 $\mu\text{mol/L}$ at 144 mbsf (Fig. 25). This large increase takes place within the biosiliceous oozes of Hole 737A and is due to the continual dissolution of diatom frustules. Interstitial-water silica concentrations at Site 737 remain at high levels between 144 and 285 mbsf, becoming quite variable between 285 and 372 mbsf. Below 372 mbsf there is a sharp decrease in dissolved silica concentrations to values of around 300 $\mu\text{mol/L}$. Interstitial-water silica concentrations remain at low levels between 372 and 608 mbsf.

The dramatic drop in dissolved silica concentrations takes place in the same part of the sedimentary section in which the discontinuity in the behavior of magnesium and calcium occurs. These three chemical species may be reacting in this part of the section to form authigenic silicates. Thus, the silicification front that may be present at this level could create an effective barrier to the diffusion of these species between the upper and lower parts of the sediment column.

pH, Alkalinity, and Sulfate

The pH of interstitial waters at Site 737 shows little variation from a value of about 7.5 in the upper 285 m in the sediment column, increases sharply to values greater than 8 between 285 and 404 mbsf, and remains at consistently high levels down to 608 mbsf (Fig. 25). The pH increase coincides with the zones in which dissolved silica concentrations drop sharply and in which there is a discontinuity in the behavior of dissolved calcium and dissolved magnesium. The high pH values in the interstitial waters below 404 mbsf may be due to the increased abundance of, and buffering by, calcium carbonate in the sediments.

Alkalinity decreases to extremely low values in the upper 314 m of the sediment column and remains at low levels to 608 mbsf (Fig. 25). The rapid increase in dissolved calcium concentrations as a function of depth may result in the precipitation of calcium carbonate, thus decreasing the alkalinity of the interstitial waters. In addition, a lack of microbial production of bicarbonate by means of organic matter degradation may be a limiting factor in the consumption of alkalinity in Site 737 interstitial waters.

Sulfate concentrations in the interstitial waters gradually decrease as a function of depth throughout Holes 737A and 737B (Fig. 25). The quantity of organic matter is quite low in all of the sediments analyzed at Site 737; below 400 mbsf the percent organic carbon in all of the samples analyzed at Site 737 is close

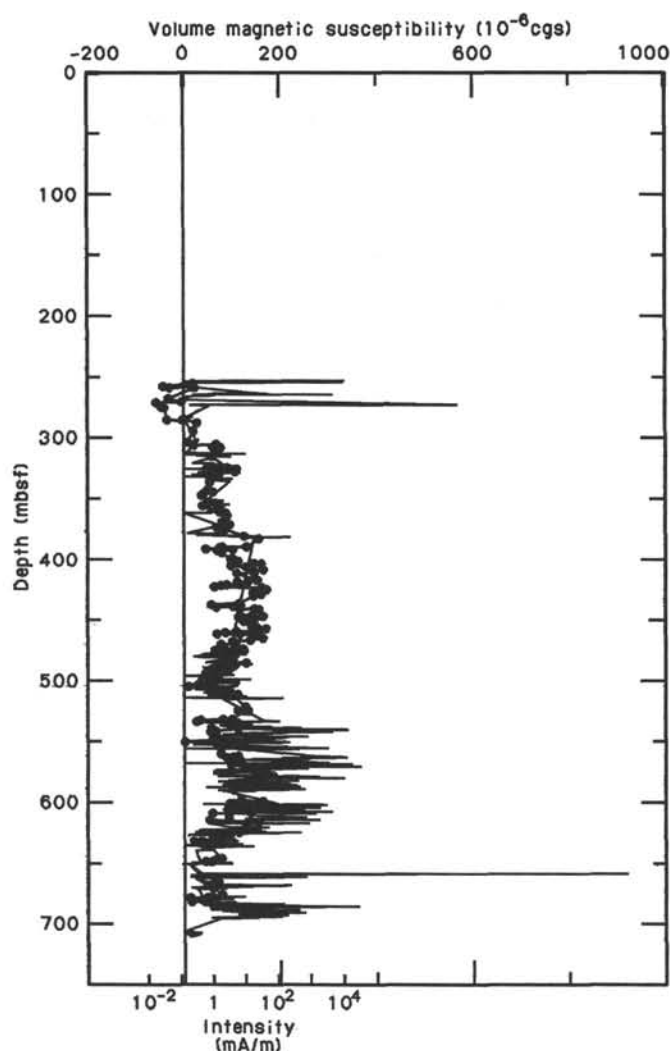


Figure 20. Stratigraphic plot of Hole 737B magnetic susceptibility (plotted as line trend) with NRM discrete sample intensity measurements (solid circles) superimposed.

to zero (see "Organic Geochemistry" section). The continual decrease in interstitial-water sulfate concentrations suggests that sulfate reduction is taking place over a large depth range at Site 737. Thus, the amount of reactable organic matter incorporated into the sediments at Site 737 was large enough to produce anaerobic conditions, but too small to exhaust the available sulfate supply above 608.5 mbsf.

Ammonium and Phosphate

Interstitial-water ammonium concentrations exhibit a broad maximum between 150 and 400 mbsf at Site 737 (Fig. 25). The increase in ammonium concentrations in the top 150 m of the sediment column is undoubtedly tied to microbial degradation of organic matter. At depth, the most probable sink for ammonium is the interlayer sites of clay minerals produced during the alteration of volcanic debris.

Only two of the Site 737 interstitial-water samples contained measurable amounts of phosphate. The shallowest sample contained $3 \mu\text{mol/L}$, which is similar to average seawater concentrations. Below this level phosphate concentrations were not measurable.

Summary

The low organic matter content of the sediments cored at Site 737 appears to control the behavior of several chemical species in the interstitial waters. Phosphate concentrations are quite low and decrease to levels below the detection limit of the spectrophotometer within 20 m of the sediment/water interface. Ammonium concentrations are also low and exhibit a maximum between 150 and 400 mbsf. This maximum may indicate that most of the ammonium is produced by microbial activity within this zone and that abundant clay minerals in the lower part of the sediment column provide a sink for removal of ammonium from the interstitial waters. Sulfate decreases gradually with increasing depth throughout the sediment column, indicating that sulfate reduction occurs locally to depths of several hundred meters below the seafloor at Site 737. The amount of reactable organic matter in the sediments has limited the degree of sulfate depletion in the interstitial waters at Site 737.

The production of phosphate, ammonium, and sulfate is intimately linked to microbial metabolic processes that involve the degradation of organic matter. The absence of large changes in the concentrations of these chemical species in the interstitial waters at Site 737 indicates that the type and/or the abundance of organic matter present in these sediments places strict limits on the intensity of microbial metabolic activity. The decrease in alkalinity of the interstitial waters with increasing depth supports this possibility. Sites 737 and 736 are similarly enigmatic in that large quantities of biogenic sediments were rapidly deposited at both sites, yet there is little evidence for large supplies of reactive organic matter in the interstitial-water chemistry of either site.

Sharp discontinuities are present in the interstitial-water concentration profiles of calcium, magnesium, silica, and pH at Site 737 (Fig. 25). Dissolved calcium concentrations increase to extremely high levels with increasing depth in the upper 404 m of the sediment column and remain consistently high down to 608 mbsf. The concentration of magnesium in the interstitial waters mirrors calcium concentrations, decreasing with increasing depth through 404 mbsf and remaining at consistently low levels to 608 mbsf. The correlation between dissolved calcium concentrations and dissolved magnesium concentrations changes significantly at around 400 mbsf. In the upper part of the sediment column at Site 737, interstitial-water calcium and magnesium concentrations are linearly correlated, implying that both cations behave conservatively in this region. Below 404 mbsf this relationship changes sharply, and it is likely that both cations are involved in reactions with the sediments in this lower part of the section. The dissolved silica profile also shows a sharp discontinuity near 400 mbsf at Site 737. Interstitial-water silica concentrations increase with increasing depth in the first 144 m of the sediment column and remain at high levels (around $1200 \mu\text{mol/L}$) between 144 and 285 mbsf. Below this level dissolved silica concentrations become quite variable with a dramatic decrease to approximately $300 \mu\text{mol/L}$ around 380 mbsf. The pH of the interstitial waters also increases abruptly between 285 and 404 mbsf.

The discontinuities discovered in the concentration profiles of calcium, magnesium, silica, and pH indicate that there is a distinct change in the chemical environment near 400 mbsf at Site 737. It seems likely that the alteration of volcanic debris and basement rocks near and at the bottom of the sedimentary section provides the source for the high dissolved calcium concentrations and the sink for dissolved magnesium. The reason for the sharp discontinuity in the behavior of these two cations is less clear, but it may be tied to the rapid decrease in dissolved silica concentrations at the same level. These three aqueous spe-

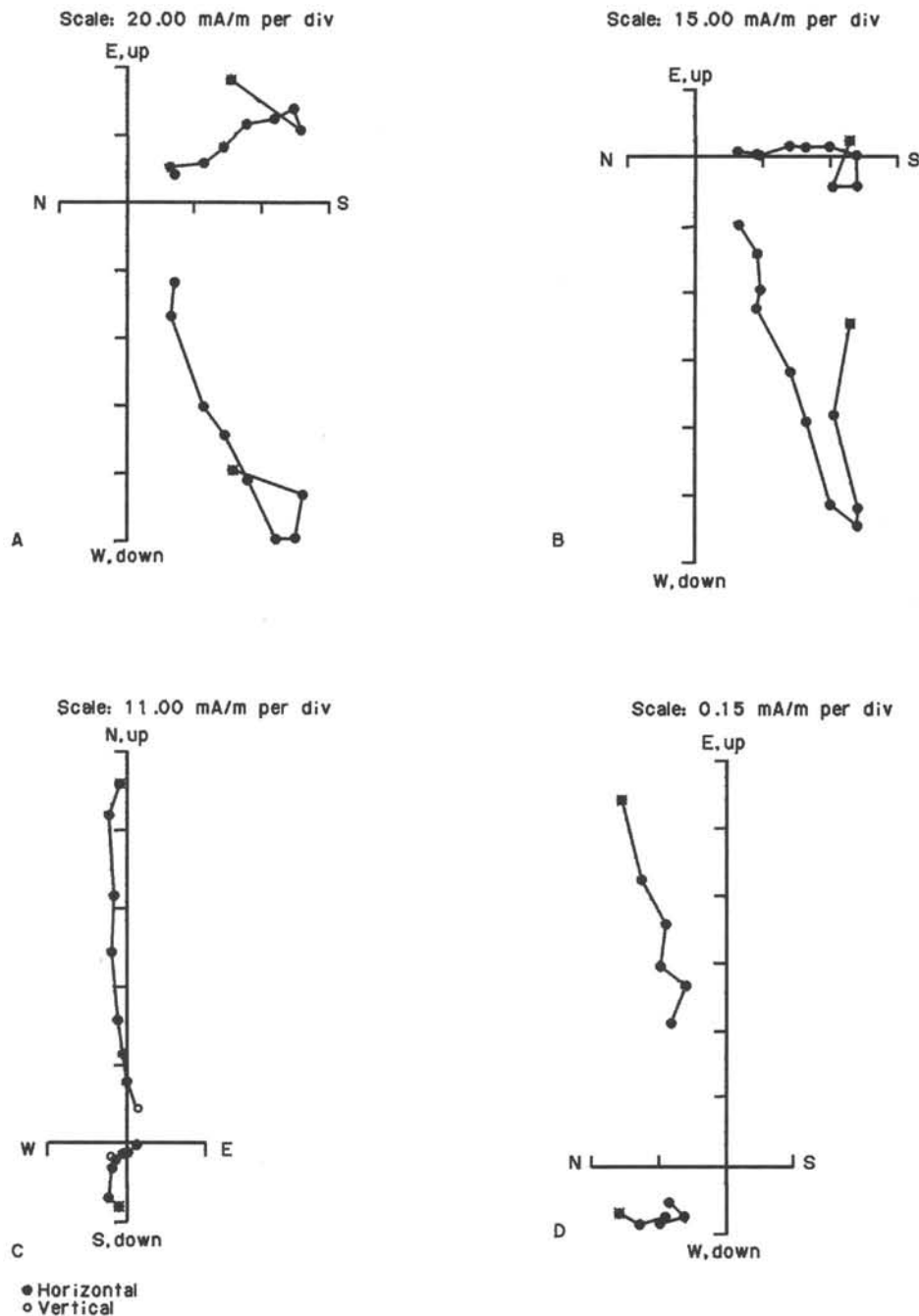


Figure 21. Orthogonal plots of sample demagnetization vectors for samples from Hole 737B. A. Sample 119-737B-41R-4, 59-61 cm. B. Sample 119-737B-20R-3, 28-30 cm. C. Sample 119-737B-25R-4, 35-37 cm. D. Sample 119-737B-8R-3, 68-70 cm.

cies may be involved in the formation of authigenic silicates (e.g., silica phases and clay minerals), creating a zone of silicification that provides a barrier to diffusion near 400 mbsf. A lithologic change from siliceous to calcareous sediments occurs near this boundary and may be the ultimate cause of the chemical discontinuities. The interstitial-water chemical data suggest that the sedimentary section from around 350 mbsf to the bottom of Hole 737B should be extensively resampled for more detailed post-cruise mineralogical and chemical studies to determine the geochemical processes responsible for the distinct discontinuities identified during on-site investigations.

ORGANIC GEOCHEMISTRY

Organic geochemistry was studied with squeeze-cake samples from interstitial-water studies of Holes 737A (0-273.2 mbsf) and 737B (253.5-715.5 mbsf). Below Core 119-737B-44R, routine geochemistry sampling was terminated because the sediments were lithified to the extent that no interstitial water was obtained at a squeezing pressure of 40,000 psi. In addition, the levels of organic carbon had also dropped below 0.1%. Dark-colored Samples 119-737B-48R-1, 22-23 cm, 119-737B-51R-1, 37-38 cm, and 119-737B-52R-1, 23-24 cm, were suspected to contain high

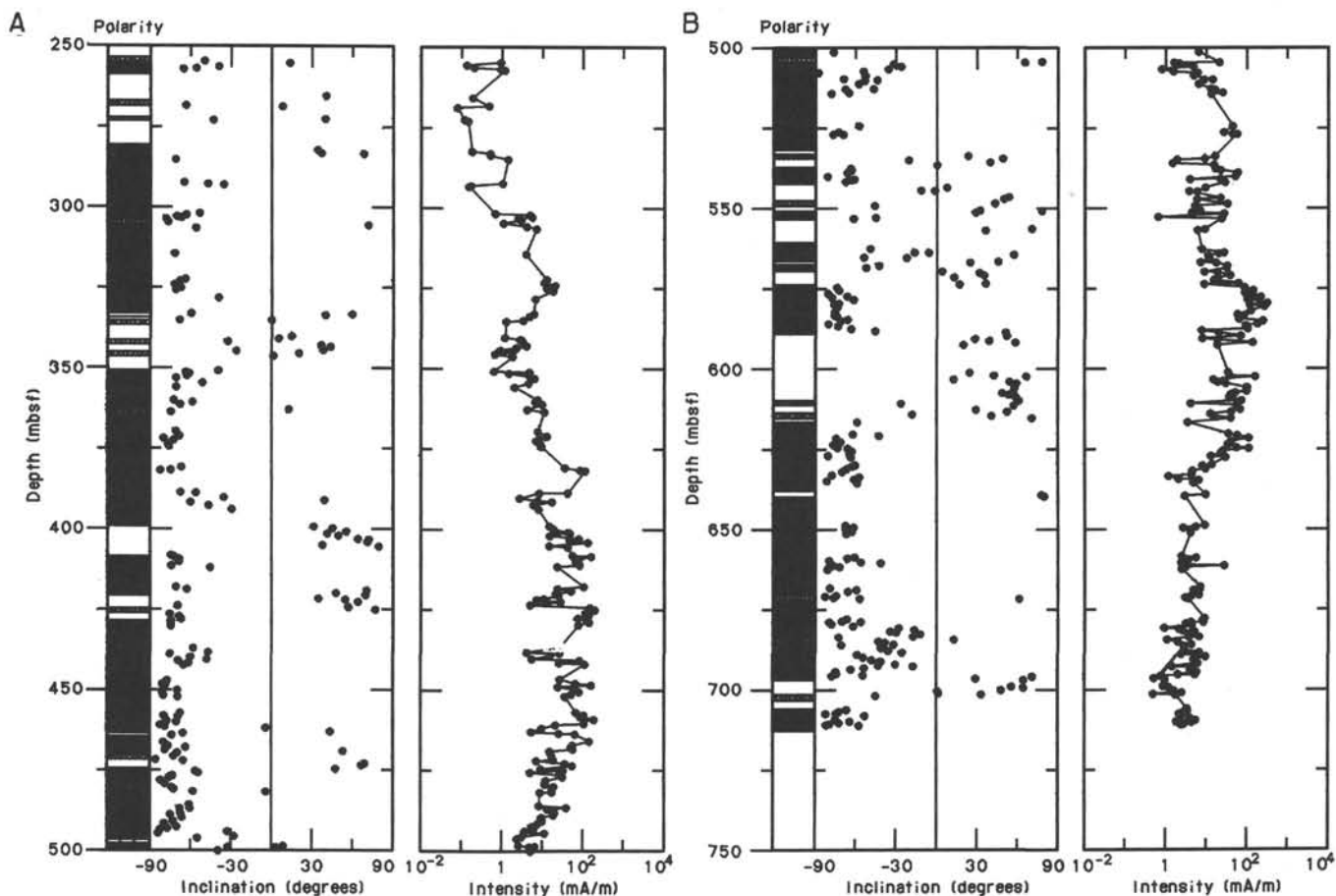


Figure 22. Stratigraphic plot of NRM sample inclination, intensity, and polarity sequence from 250 to 750 mbsf in Hole 737B.

organics, but analysis of these samples found that they contained less than 0.1% total organic carbon (TOC).

Hydrocarbon Gases

No gas pockets were encountered in any of the cores at Site 737. The headspace procedure (see "Explanatory Notes" chapter) was used approximately every 30 m to determine hydrocarbon gases. That all of the samples from Site 737 were at or near the 3-ppm mean level for laboratory air, along with the lithification of the sediments, warranted termination of headspace studies following Core 119-737B-23R. The cores were still monitored for the presence of gas pockets.

As at Site 736, the absence of gas at Site 737 suggests that methanogenic bacteria had been inactive since sedimentation at this site. Furthermore, methanogens are anaerobes that are inhibited by the sulfate ion (Claypool and Kvenvolden, 1983), and analysis of interstitial waters showed that the sulfate ion concentration steadily decreased downhole to approximately half the seawater concentration of 28.9 mmol/L (see "Inorganic Geochemistry" section).

Carbon Analysis

Inorganic carbon was measured on most core-catcher samples and all of the interstitial-water squeeze-cake samples. Total carbon was measured on all of the interstitial-water squeeze cakes and on dark layers. TOC was calculated for all samples measured for total carbon. See Table 6 for the tabular data and Figures 27 and 28 for graphic representation of the data. Inorganic carbon values are low to approximately 200 mbsf, except

for two spikes at 49.0 and 110.8 mbsf. Below 250 mbsf, the values fluctuate in a complex manner.

Organic carbon decreases downhole, as expected. TOC values are 0.5%–0.3% in the upper 225 m and <0.1% below 225 mbsf. The organic content was moderate in the upper 225 mbsf and low downhole from that level. Generally, <0.3% TOC is considered low for pelagic oozes (Tissot and Welte, 1984). The generation of petroleum is dependant on many other parameters, so TOC has only a small roll in determining if petroleum will be produced.

Rock-Eval Pyrolysis

Rock-Eval pyrolysis was performed on the squeeze cakes left over from interstitial-water studies. The parameters measured and calculated are listed in Table 7 and shown graphically in Figures 29 through 32.

These results show that sediments at Site 737 are generally moderate to low in TOC (less than 0.1% below about 300 mbsf) (Fig. 29). Most of the samples exhibit T_{max} values below 435°C, which is characteristic of immature organic matter (Tissot and Welte, 1984). Six samples have T_{max} values over 500°C, indicating redeposition of mature organic matter. Doubled S2 peaks also indicate more than one source of organic input. Results similar to these were found by Deroo et al. (1978, 1979) on Deep Sea Drilling Project Legs 44 in the Blake-Bahama Basin and 48 in the Bay of Biscay.

Most of the samples below 225 mbsf have S2 values that are at or near zero, corresponding to their low organic carbon contents. Many of these have high S3 values, however. High S3 is a

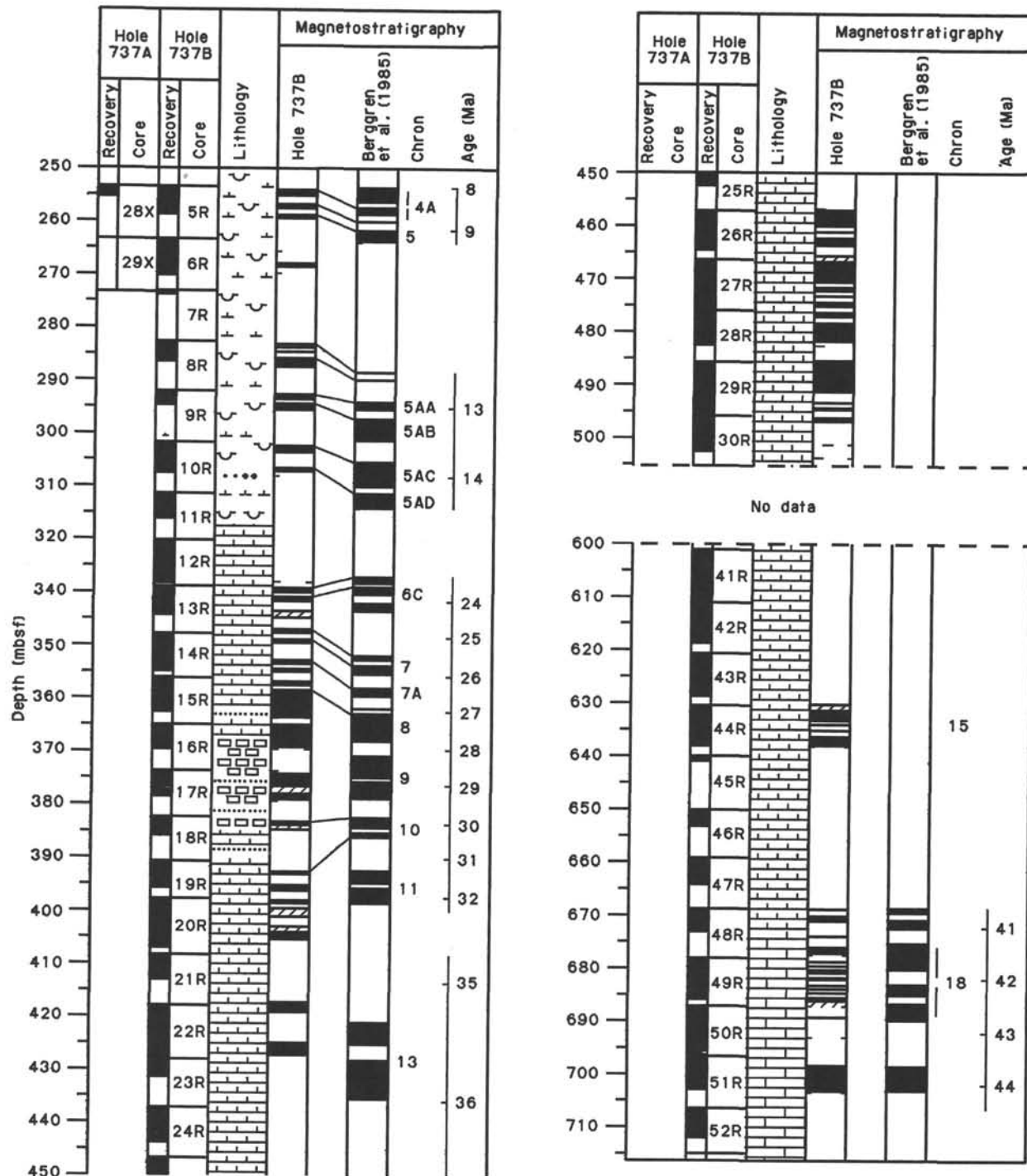


Figure 23. Magnetostratigraphic correlations for Hole 737B that summarize the polarity time scale and chron identifications of Berggren et al. (1985) and the magnetostratigraphy and lithostratigraphy results of shipboard studies.

measure of CO₂ from kerogen pyrolyzed after it has cracked and released its potential hydrocarbons. Because TOC is low in these samples, the anomalously high S3 values could be due to carbonates that break down below 390°C. Another possible explanation is contamination, which could be fresh (in which case there should be a correspondingly high S2 value) or residual in the instrument. Low blank levels indicate that the instrument was fairly clean and there were no S2 peaks; therefore, some of the carbonate material was probably pyrolyzed below 390°C. High S3 levels make the corresponding oxygen indices (Fig. 31)

anomalously high. These samples are not included on the van Krevelen-like diagram (Fig. 32).

Pelagic oozes generally show type II kerogen when aerobic bacterial inhibition occurs because lipids from the contributing organisms are preserved. The kerogen is mainly type II with some type III at Site 737 (type III-like kerogen can also be produced from intense oxidation of marine/type II material). Site 737 has been oxic (as supported by the high sulfate concentrations, "Inorganic Geochemistry" section); therefore, marine organisms may be a major contributor to the TOC. Oxidation of

Table 4. Bioevents identified at Site 737.

Biostratigraphic event ^a	Depth (mbsf)	Age (Ma)
FAD <i>Nitzschia interfrigidaria</i>	43.0–52.5	3.7–3.8
FAD <i>Nitzschia "angulata"</i>	62.0–71.5	4.2
FAD <i>Pseudocubus vema</i>	62.0–71.5	3.9
FAD <i>Thalassiosira gracilis</i>	81.0–90.5	4.6–4.7
LAD <i>Stichocorys peregrina</i>	100.0–109.5	4.4–4.6
LAD <i>Thalassiosira miocenica</i>	109.5–119.0	5.1
FAD <i>Thalassiosira miocenica</i>	167.1–176.2	6.1
LAD Common <i>Denticulopsis hustedtii</i>	235.0–244.1	7.1–7.2
LAD <i>Actinomma tanyacantha</i>	253.8–263.5	9.5–9.8
FAD <i>Thalassiosira burckliana</i>	263.5–263.6	8.2
LAD Common <i>Denticulopsis dimorpha</i>	263.2–263.4	10.0
LAD <i>Cyrtocapsella japonica</i>	263.2–272.9	10.5–11.2
LAD <i>Nitzschia denticuloides</i>	282.5–284.5	11.0–11.1
FAD <i>Denticulopsis dimorpha</i>	284.6–284.6	11.1–11.2
FAD Common <i>Denticulopsis hustedtii</i>	305.4–311.5	13.8
FAD <i>Denticulopsis hyalina</i>	<311.7	15.0
LAD <i>Reticulofenestra bisecta</i>	311.5–321.1	25.4
LAD <i>Chiloguembelina cubensis</i>	369.4–379.1	30.0
LAD <i>Globigerina angiorporoides</i>	417.7–427.4	32.0
LAD <i>Globigerina ampliapertura</i>	437.0–446.7	32.8
FAD <i>Cyclicargolithus abisectus</i>	528.0–543.3	34.2
LAD <i>Reticulofenestra umbilica</i>	543.3–552.9	34.6
LAD <i>Isthmolithus recurvus</i>	557.0–572.2	35.8
LAD <i>Discoaster saipanensis</i>	605.3–605.9	36.7
LAD <i>Globigerinatheka index</i>	601.1–610.7	36.8
LAD <i>Reticulofenestra reticulata</i>	649.3–658.6	37.4
FAD <i>Isthmolithus recurvus</i>	652.0–653.0	38.7

^a FAD = first-appearance datum; LAD = last-appearance datum.

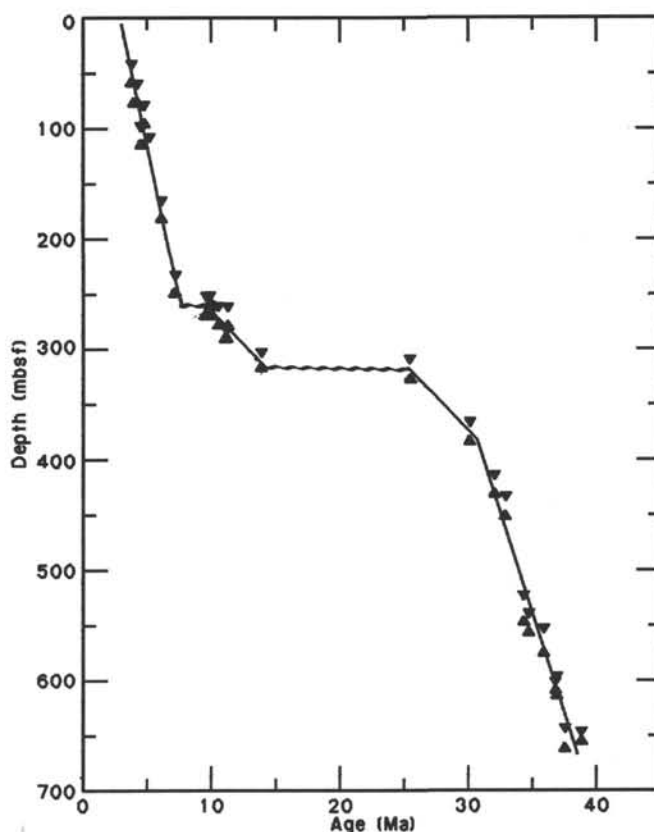


Figure 24. Sedimentation rates at Site 737, based on bioevents of Table 4.

Table 5. Interstitial-water geochemical data, Site 737.

Core, section, interval (cm)	Depth (mbsf)	Volume (mL)	Salinity (g/kg)	Chloride (mmol/L)	Calcium (mmol/L)	Magnesium (mmol/L)	Mg ²⁺ /Ca ²⁺	Silica (μmol/L)	pH	Alkalinity (mmol/L)	Sulfate (mmol/L)	Ammonium (mmol/L)	Phosphate (μmol/L)
119-737A-													
1H-2, 145-150	2.95	70	35.5	554	11.5	52.0	4.5	576	7.5	2.74	27.42	0.07	3
3H-4, 145-150	20.45	70	36.5	558	17.1	49.8	2.9	717	7.4	2.29	27.05	0.11	0
7H-4, 145-150	58.45	60	37.5	564	26.6	44.1	1.6	856	7.4	1.87	24.07	0.17	0
10H-4, 145-150	86.95	50	37.5	556	32.4	38.8	1.2	1012	7.4	1.38	22.95	0.22	0
13H-4, 145-150	115.45	70	36.5	564	38.8	35.8	0.9	939	7.3	1.17	21.46	0.26	0
16H-4, 145-150	143.95	75	37.0	569	44.8	32.4	0.7	1240	7.4	1.17	20.71	0.30	1
21X-1, 145-150	187.35	45	36.5	567	49.7	29.3	0.6	1230	7.5	1.17	20.17	0.26	0
25X-3, 145-150	229.15	65	37.5	574	64.3	21.5	0.3	1269	7.3	0.92	19.22	0.28	0
119-737B-													
5R-2, 145-150	256.45	50	37.5	574	68.9	18.6	0.3	1205	7.3	0.74	18.85	0.33	0
8R-2, 145-150	285.45	42	38.0	585	79.4	14.4	0.2	1209	7.3	0.63	18.10	0.25	0
11R-2, 145-150	314.45	20	38.0	580	88.1	8.6	0.1	810	7.7	0.37	16.98	0.27	0
14R-5, 145-150	347.80	60	38.5	579	96.6	5.64	0.0	1053	8.1	0.38	16.61	0.24	0
17R-2, 145-150	372.30	60	39.0	589	104.8	1.97	0.0	1099	8.2	0.28	11.78	0.25	0
20R-4, 145-150	404.30	30	39.5	581	127.5	1.49	0.0	293	8.9	0.53	16.62	0.25	0
23R-1, 145-150	428.80	40	39.0	577	125.6	2.38	0.0	322	8.9	0.51	15.50	0.21	0
26R-4, 145-150	462.30	30	39.0	577	125.6	3.45	0.0	389	8.6	0.38	15.87	0.18	0
29R-4, 145-150	491.30	14	38.5	576	116.9	6.19	0.0	268	8.3	0.30	16.25	0.15	0
34R-5, 145-150	541.00	15	39.0	579	128.4	5.80	0.0	278	8.5	0.22	17.36	0.16	0
37R-4, 145-150	568.40	20	39.5	586	141.5	1.80	0.0	291	8.8	0.31	15.87	0.14	0
41R-5, 145-150	608.50	15	39.5	582	135.6	3.81	0.0	252	8.6	0.40	15.87	0.14	0

organic material can be accompanied by CO₂ formation, but none was detected here. The permeability of this sediment sequence is such that gases formed by the breakdown of organic material can easily escape.

BIOLOGY AND OCEANOGRAPHY

Phytoplankton: Living, Holocene, and Pleistocene Diatoms

As at Site 736, phytoplankton samples were collected daily for a six-day period (30 December 1987 to 4 January 1988) at

Site 737 for comparison with near-surface sediments. Surface water temperatures were 3.5°, 3.2°, 3.1°, 3.1°, 3.0°, and 3.1°C at winds of 28, 31, 4, 22, 30, and 12 kt, respectively. Wind direction changed from northwest to southeast on 31 December with the passage of a low-pressure area (Table 8). A marked change in the abundance and health of the phytoplankton community began on 31 December, with the amount collected in 5 min greatly reduced, reminiscent of the "striking paucity" of diatoms north of 52°S in the open Pacific Ocean (Fenner et al., 1976). In addition, chains were shorter and often principally composed of empty cells. Dinoflagellate abundance and diver-

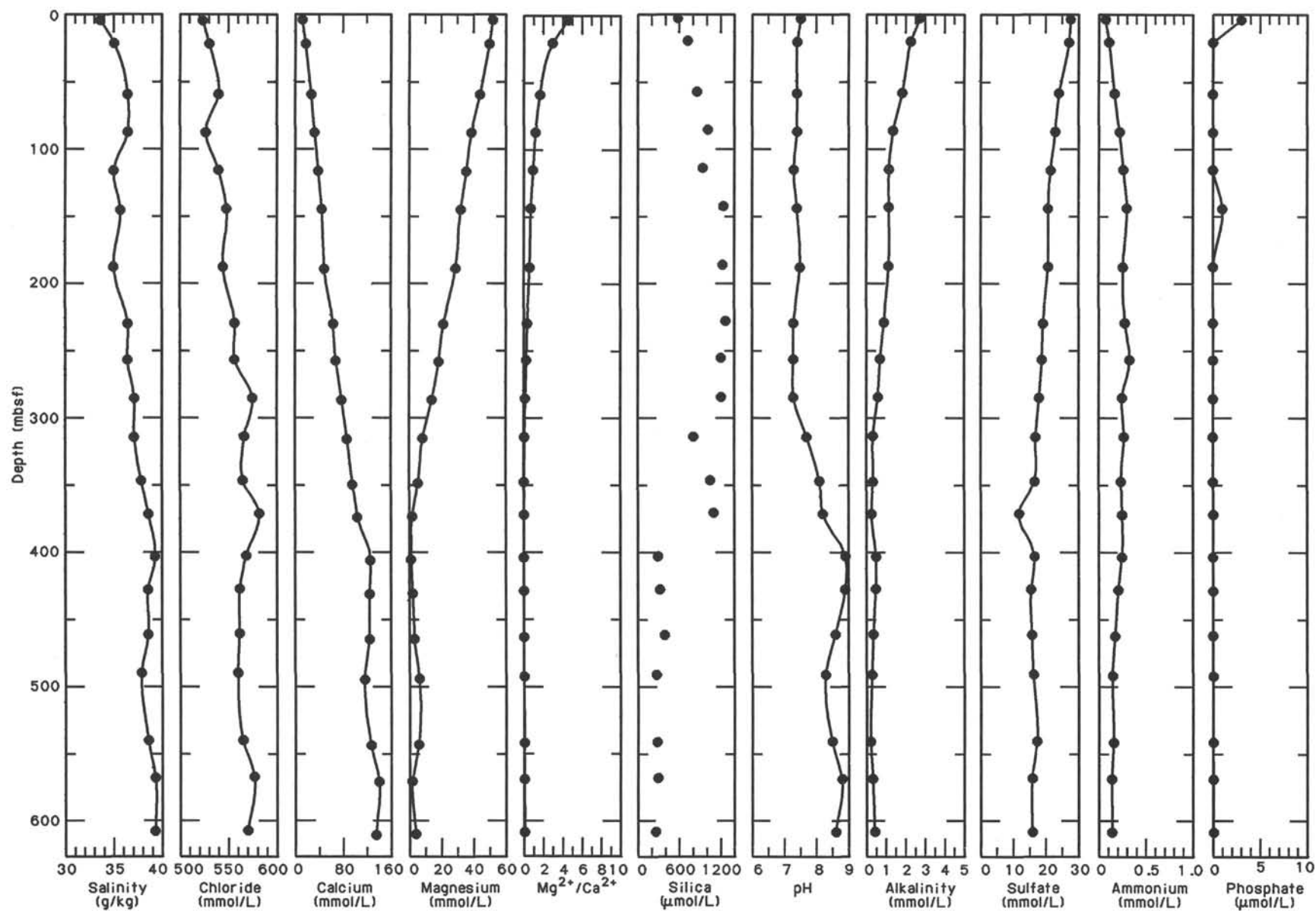


Figure 25. Salinity, chloride, calcium, magnesium, Mg²⁺/Ca²⁺ ratio, silica, pH, alkalinity, sulfate, ammonium, and phosphate interstitial-water profiles, Site 737.

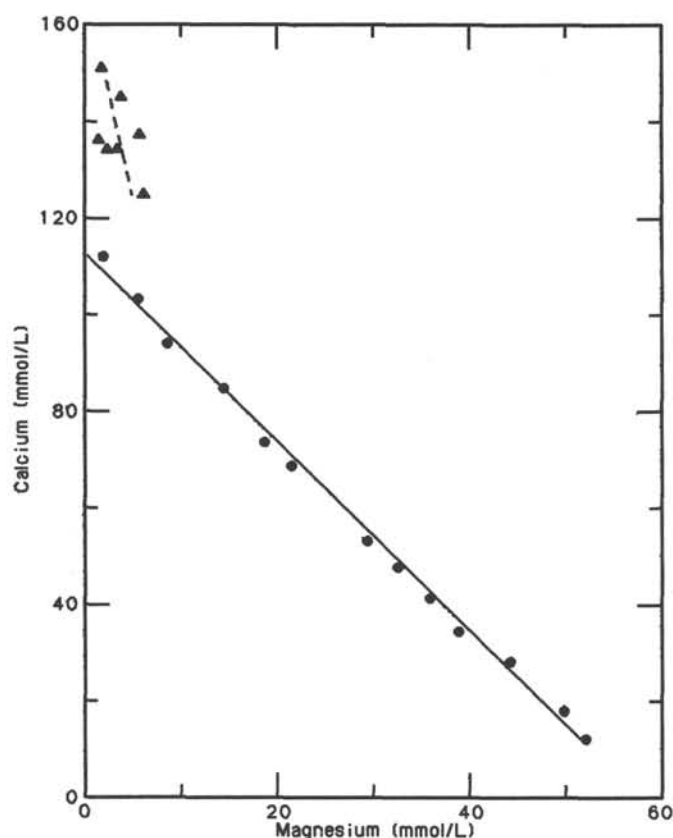


Figure 26. Calcium concentration vs. magnesium concentration for Site 737 interstitial waters. The solid regression line passes through data points representing interstitial-water samples in the upper 372 mbsf and has a slope of -1.82 ($r = -0.9979$). The dashed regression line passes through data points representing interstitial-water samples from 404 to 608 mbsf and has a slope of -2.21 ($r = -0.5238$).

sity increased, and fecal pellets changed from containing mainly pennate diatoms (many of them reproducing) to pellets containing both centrics and pennate diatoms with little evidence of growth inside the pellets. Several krill-like pellet strings were seen with frustules fragmented. By the last sampling date, the number of empty cells observed in a hand-thrown net sample was greatly reduced, and many cells were dividing. Small gelatinous colonies of *Thalassiosira gravida* (previously noted in Weddell Sea spring flora) were seen.

Diatom species seen in the Site 737 phytoplankton samples that were not noted at the previous station are listed in Table 9. Only *Chaetoceros pendulus* was seen at Site 736 but not at Site 737.

The needle-shaped *Nitzschia* species totally dominated the samples collected off the stern of the ship in the effluent of the thrusters. Many chains of *Nitzschia kerguelensis* were also present, containing both empty and full cells. A periodicity of about every fourth cell alive was noted on several occasions and documented. In later samples, groups of four living cells were seen separated by empty cells in long chains. Long chains of living cells were again seen in the final net sample.

The flora appeared to be in transition between the abundance of the spring phytoplankton increase and the photoinhibited summer surface flora (Rivkin and Putt, 1987). From the presence of *Azpeitia tabularis*, common in the Subantarctic Zone and the Antarctic Convergence Zone (Fenner et al., 1976), the cosmopolitan (but not polar) *Thalassionema nitzschioides* (loc. cit.; G. Fryxell, pers. comm., 1987), and the dinoflagellate

Table 6. Total carbon, inorganic carbon, organic carbon, and percent calcium carbonate, Site 737.

Core, section, interval (cm)	Depth (mbsf)	Total carbon (%)	Inorganic carbon (%)	Organic carbon (%)	CaCO ₃ (%)
119-737A-					
1H-1, 0-1	0.00		0.05		0.4
1H-2, 145-150	2.95	0.54	0.01	0.53	0.1
1H-CC, 0-1	4.77		0.01		0.1
2H-5, 70-71	11.70	0.66	0.18	0.48	1.5
2H-CC, 0-1	14.60		0.29		2.4
3H-4, 145-150	20.45	0.55	0.06	0.49	0.5
3H-CC, 0-1	24.22		0.11		0.9
4H-CC, 0-1	33.92		0.22		1.8
6H-5, 0-1	49.00		9.08		75.6
6H-CC, 0-1	51.74		0.06		0.5
7H-4, 145-150	58.45	0.43	0.01	0.42	0.1
7H-CC, 0-1	62.12		0.02		0.2
8H-CC, 0-1	71.93		0.04		0.3
9H-CC, 0-1	81.17		0.86		7.2
10H-4, 145-150	86.95	0.30	0.06	0.24	0.5
10H-CC, 0-1	90.13		0.20		1.7
11H-CC, 0-1	100.04		0.01		0.1
12H-CC, 0-1	109.75		0.01		0.1
13H-1, 119-120	110.69		0.01		0.1
13H-1, 130-131	110.80		7.26		60.5
13H-2, 9-10	111.09		0.09		0.8
13H-4, 145-150	115.45	0.46	0.00	0.46	0.0
13H-CC, 0-1	118.96		0.01		0.1
15H-CC, 0-1	138.13		0.01		0.1
16H-4, 145-150	143.95	0.58	0.01	0.57	0.1
16H-CC, 0-1	147.60		0.01		0.1
17H-CC, 0-1	157.06		0.01		0.1
18H-CC, 0-1	166.50		0.00		0.0
19X-CC, 0-1	167.80		0.01		0.1
20X-CC, 0-1	176.20		0.01		0.1
21X-1, 145-150	187.35	0.59	0.02	0.57	0.2
21X-CC, 0-1	187.85		0.01		0.1
23X-CC, 0-1	207.59		0.06		0.5
25X-3, 145-150	229.15	2.03	1.64	0.39	13.7
25X-CC, 0-1	230.20		0.21		1.8
26X-CC, 0-1	236.13		0.01		0.1
26X-CC, 2-3	236.15		5.52		46.0
27X-CC, 0-1	249.40		2.17		18.1
28X-CC, 0-1	255.59		6.76		56.3
119-737B-					
2R-CC, 0-1	115.40		0.08		0.7
3R-CC, 0-1	128.32		0.03		0.3
5R-2, 145-150	256.45	6.50	6.28	0.22	52.3
5R-CC, 0-1	258.32		2.74		22.8
6R-CC, 0-1	269.40		10.30		85.8
7R-CC, 0-1	273.98		10.60		88.3
8R-2, 145-150	285.45	6.80	6.51	0.29	54.2
8R-CC, 0-1	286.09		4.05		33.7
9R-CC, 0-1	294.37		9.19		76.6
10R-CC, 0-1	307.19		7.38		61.5
11R-2, 145-150	314.45	9.41	9.33	0.08	77.7
11R-CC, 0-1	315.78		3.98		33.2
12R-CC, 0-1	329.87		2.48		20.7
13R-CC, 0-1	336.06		3.40		28.3
14R-5, 140-150	347.80	5.85	5.73	0.12	47.7
15R-CC, 0-1	356.78		1.60		13.3
16R-CC, 0-1	364.91		1.82		15.2
17R-2, 140-150	372.30	4.06	3.95	0.11	32.9
17R-CC, 0-1	374.69		2.60		21.7
18R-CC, 0-1	382.62		0.92		7.7
19R-CC, 0-1	393.48		2.09		17.4
20R-4, 140-150	404.30	0.81	0.76	0.05	6.3
20R-CC, 0-1	406.30		1.20		10.0
21R-CC, 0-1	412.51		3.56		29.7
22R-CC, 0-1	427.38		3.93		32.7
23R-1, 140-150	428.80	2.20	2.20	0.00	18.3
23R-CC, 0-1	430.30		2.15		17.9
24R-CC, 0-1	443.15		1.25		10.4
25R-CC, 0-1	452.10		2.12		17.7
26R-4, 140-150	462.30	6.28	6.27	0.01	52.2
26R-CC, 0-1	464.62		2.77		23.1
27R-CC, 0-1	475.68		3.25		27.1
28R-CC, 0-1	482.15		1.42		11.8

Table 6 (continued).

Core, section, interval (cm)	Depth (mbsf)	Total carbon (%)	Inorganic carbon (%)	Organic carbon (%)	CaCO ₃ (%)
119-737B- (Cont.)					
29R-4, 140-150	491.30	2.72	2.68	0.04	22.3
29R-CC, 0-1	495.08		7.53		62.7
30R-CC, 0-1	501.97		6.52		54.3
31R-CC, 0-1	514.38		5.07		42.2
33R-CC, 0-1	527.31		2.41		20.1
34R-3, 140-150	538.00	3.45	3.38	0.07	28.2
34R-CC, 0-1	542.82		2.16		18.0
35R-CC, 0-1	551.95		1.70		14.2
36R-CC, 0-1	557.11		5.10		42.5
37R-4, 140-150	568.40	1.99	2.03	0.00	16.9
37R-CC, 0-1	571.62		1.17		9.8
37R-CC, 0-1	571.62	1.35	1.31	0.04	10.9
38R-CC, 0-1	580.60	3.03	2.97	0.06	24.7
38R-CC, 0-1	580.60		1.09		9.1
39R-6, 24-26	589.54	1.66	1.63	0.03	13.6
39R-6, 76-78	590.06	7.59	7.52	0.07	62.6
39R-CC, 0-1	591.43		6.66		55.5
40R-CC, 0-1	593.36		6.84		57.0
41R-5, 140-150	608.50	4.79	4.78	0.01	39.8
41R-CC, 0-1	610.26		3.38		28.2
42R-CC, 0-1	617.63		3.33		27.7
43R-3, 110-111	624.40		9.66		80.5
43R-3, 120-121	624.50		3.44		28.7
43R-4, 24-25	625.04		6.80		56.6
43R-4, 35-36	625.15		2.89		24.1
43R-CC, 0-1	628.20		7.86		65.5
44R-4, 140-150	635.90	9.35	9.16	0.19	76.3
44R-CC, 0-1	637.43		3.92		32.7
45R-CC, 0-1	640.15		8.94		74.5
46R-CC, 0-1	651.95		6.96		58.0
47R-CC, 0-1	662.48		5.20		43.3
48R-2, 22-23	669.62	5.40	5.33	0.07	44.4
48R-CC, 0-1	671.69		8.24		68.6
49R-CC, 0-1	685.84		8.49		70.7
50R-CC, 0-1	695.73		9.33		77.7
51R-3, 37-38	699.57	0.09	0.03	0.06	0.3
51R-CC, 0-1	701.58		10.24		85.3
52R-2, 23-24	707.63	1.65	1.61	0.04	13.4
52R-CC, 0-1	711.23		7.97		66.4

Ceratium pentagonum (generally found close to the Antarctic Convergence Zone; E. Balech, pers. comm., 1975), as well as the temperature of the surface water, it is assumed that during this time the site location was close to, but somewhat north of, the dynamic boundary of the Antarctic Convergence Zone.

Other zonal markers in the plankton include *Thalassiosira tumida*, present in what Fryxell et al. (1986) considered the northern form, which is rarely found close to ice. *Rhizosolenia curvata* is also considered an antarctic indicator species (Hart, 1937). *Nitzschia kerguelensis* was found frequently. This characteristic antarctic species was found by Abbott (1974) to compose up to 70% of the Pleistocene assemblage in the Subantarctic Zone of the southeastern Indian Ocean. Another characteristic antarctic species, *Thalassiosira lentiginosa*, appeared in the plankton; Fenner et al. (1976) found it also to be widespread in the Subantarctic Zone.

Eucampia antarctica was in the vegetative state at this site, with both heavily and lightly silicified spiraling chains having low and moderate polar elevations similar to the Gombos (1977) illustrations (pls. 1 and 11). The potential for spirals is evident in the asymmetry of individual valves, as well as of girdle bands, and can be differentiated in the sediment from straight-sided winter forms. Although this species has been used for tracing the sea-ice front, Gombos (1977) considered its distribution to be independent of the ice. Its abundance at Sites 736 and 737 would support that idea, although differentiation between forms might indicate another kind of boundary.

Several species appeared to be in sexual reproduction, including *Gymnodinium* species, which was commonly observed with two cells enclosed in a mucous sphere. In later samples, these cells were found dividing twice to release eight cells. *T. tumida* was found with diameters up to 176 μm in a bimodal distribution, apparently after auxospore production, and *T. lentiginosa* was found up to 95 μm in diameter. *Rhizosolenia alata* was also found with truncated processes and expanded diameters in the hypothecae, indicating auxospore production.

In the sediments, the species found at the mud line and at the 2 cm level of the first core include those in Table 10. Farther downcore, the flora changed to apparently date from the Pliocene, rich in *Thalassiosira* species (such as one described as *Coscinodiscus kolbei* Jouse, *Thalassiosira* sp. cf. *trifulta*, *Thalassiosira oestrupii*, *Thalassiosira gracilis*, *T. gracilis* var. *expecta*, *Thalassiosira oliverana*, *T. lentiginosa*, one large species with eccentric areola pattern, and several small species). Also present were *Chaetoceros* resting spores not seen in the living plankton.

PHYSICAL PROPERTIES

The objective of the physical-properties program at Site 737 was to add to the limited data base of physical properties of high-latitude sediments, particularly those containing abundant biogenic silica. The physical-properties program was also to provide reference data for geophysical and stratigraphic evaluation of the sedimentary section at the site. Furthermore, Site 737 was expected to give more data on the somewhat unusual physical behavior of diatom ooze, which was noted at Site 736 (see "Physical Properties" section, "Site 736" chapter, this volume).

Physical properties evaluated included (1) index properties (water content, porosity, bulk density, and grain density), (2) undrained shear strength, (3) compressional-wave velocity, and (4) thermal conductivity. General techniques and laboratory procedures are discussed in the "Explanatory Notes" chapter. Two holes (737A and 737B) were drilled at this site. The APC was used at Hole 737A down to 166.5 mbsf, and the XCB was used from that depth to the bottom of the hole, at 273.2 mbsf. Hole 737B was cored with RCB to 715.5 mbsf. The same change in degree of disturbance of the diatomaceous oozes between the different coring techniques that was observed at Site 736 was also noted at this site. However, as most of the RCB coring was performed in lithified sediments, disturbance was effective only in the upper part of Hole 737B.

The physical-properties data are presented in Figure 33 and Tables 11 through 16. Temperature measurements are presented in Figures 34 and 35 and Table 17.

Index Properties

The index properties can be roughly subdivided into three geotechnical units.

Geotechnical Unit G1

From the seafloor to approximately 200 mbsf, all index-property values are fairly constant, although a large scatter is observed in the grain densities. The scatter in grain densities may be a function of the calculation method, which is particularly imprecise when the sample has a high porosity (Boyce, 1973). Therefore, only average values and main trends in the grain density values should be used. Water content generally varies between 70% and 80%, porosity between 80% and 90%, bulk density is mostly between 1.2 and 1.3 g/cm³, and the calculated grain density is scattered around 2.0 g/cm³. The high-density/low-water-content zone is in a sandy lag at the seafloor to 1 mbsf. In the lower part of the interval, from 170 mbsf, there are few measurements as a result of the poor recovery.

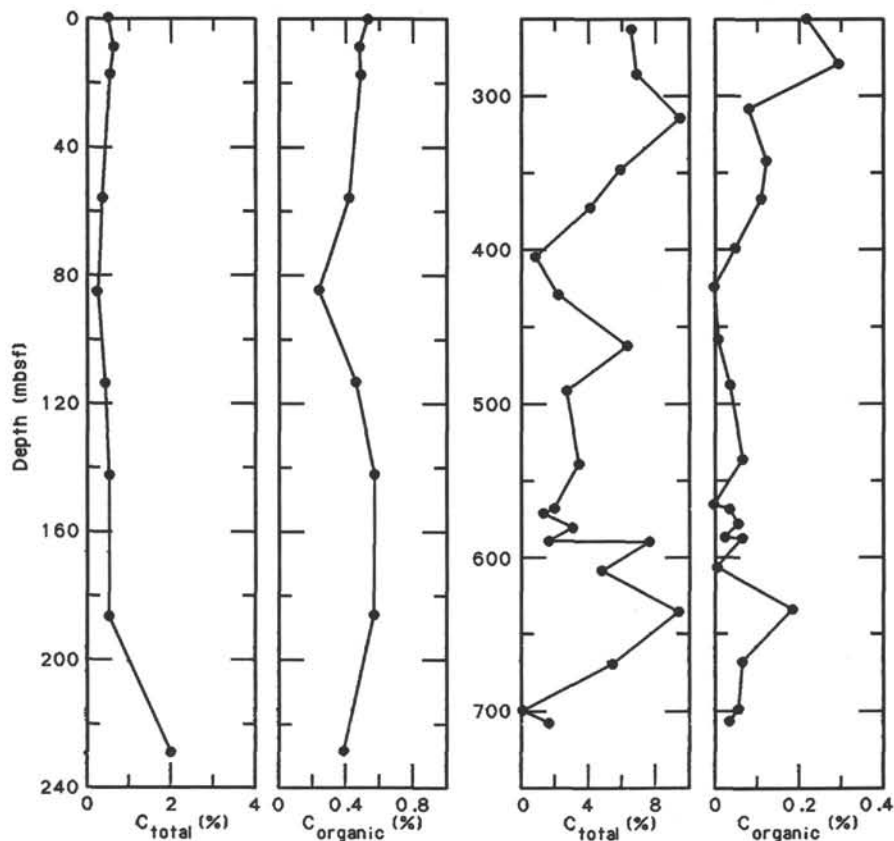


Figure 27. Total carbon (C_{total}) and organic carbon ($C_{organic}$) from squeeze-cake and core-catcher sediment samples, Holes 737A and 737B.

Geotechnical Unit G2

The interval from around 200 to 670 mbsf shows relatively linear decreases in water content and porosity to about 15% and 25%, respectively, and a similar increase in bulk density from 1.2 to 2.4 g/cm³. Within this interval, however, there are large oscillations between 200 and 350 mbsf and 480 and 570 mbsf. At about 500 mbsf there is a notable decrease of 10% in water content and porosity (relative to the overall trend, despite the local oscillations), and a similar increase in bulk density. Grain density increases to about 2.6 g/cm³ down to 400 mbsf and is constant to 550 mbsf, where there is a drop to about 2.5 g/cm³.

Geotechnical Unit G3

The lower interval, from 670 mbsf to the bottom of the hole, shows some oscillations, but with an overall trend of more constant values for water content (10%–20%), porosity (20%–40%), and bulk density (2.4 g/cm³). The grain density increases slightly, from about 2.5 to about 2.6 g/cm³. Bulk density obtained by the GRAPE confirms the pattern obtained by the gravimetric methods. The scatter in the upper interval is caused mainly by coarser material in the uppermost section of each of the cores. This is material that fell from higher levels in the hole. The large scatter between 300 and 400 mbsf is caused by varying sample diameter. The sediment became more lithified below 300 mbsf, and discrete measurements made by 2-min GRAPE counts instead of continuous runs on whole-round cores from 325 mbsf clearly confirm the linearly increasing trend of this interval.

These three geotechnical units roughly correlate to the different lithologies (see "Lithostratigraphy and Sedimentology" section, this chapter), although the geotechnical and lithologic boundaries do not match completely. Unit G1 corresponds to

the diatom ooze that dominates the upper 234 mbsf. The sequence from 234 to 295 mbsf is characterized as a diatom/calcareous nannofossil ooze. The increasing content of calcareous nannofossils may cause the increase in density and the rate of decrease in water content/porosity noted for geotechnical unit G2. Because of the change in coring technique from APC to XCB at 166.5 mbsf, the variations in properties may be due in part to the varying degree of core disturbance. The diatom/nannofossil chalk between 295 and 307 mbsf is underlain by a diatom/nannofossil chalk, below which there is a nannofossil chalk, with an increase in lithification down through the sequence. The increased lithification explains the gradually increasing density and decreasing water content/porosity values of geotechnical unit G2. In the region of higher variability from 670 mbsf to the bottom of the cored sequence, the scatter in index properties may be a function of the transition into clayey limestone material.

Undrained Shear Strength

Because of lithification, shear-strength measurements were made only in the upper 300 m of the cored sequence. The large variations in values in the lower part of the plots are mainly caused by coring disturbance as a result of changing from APC to XCB to RCB methods. The upper 170 m of sediments, however, shows a distinct trend of increasing values with depth, from 5–10 kPa at the top to approximately 50–60 kPa at 170 mbsf. The two methods show somewhat different results in that values of vane shear strength record a distinct increase at 110 mbsf whereas the values of shear measured with the fall cone have a wider scatter but show a more linear trend overall. At Site 736, both instruments showed a relatively constant linear increase down to 100 mbsf, although the gradient was smaller for the Wykeham Farrance device.

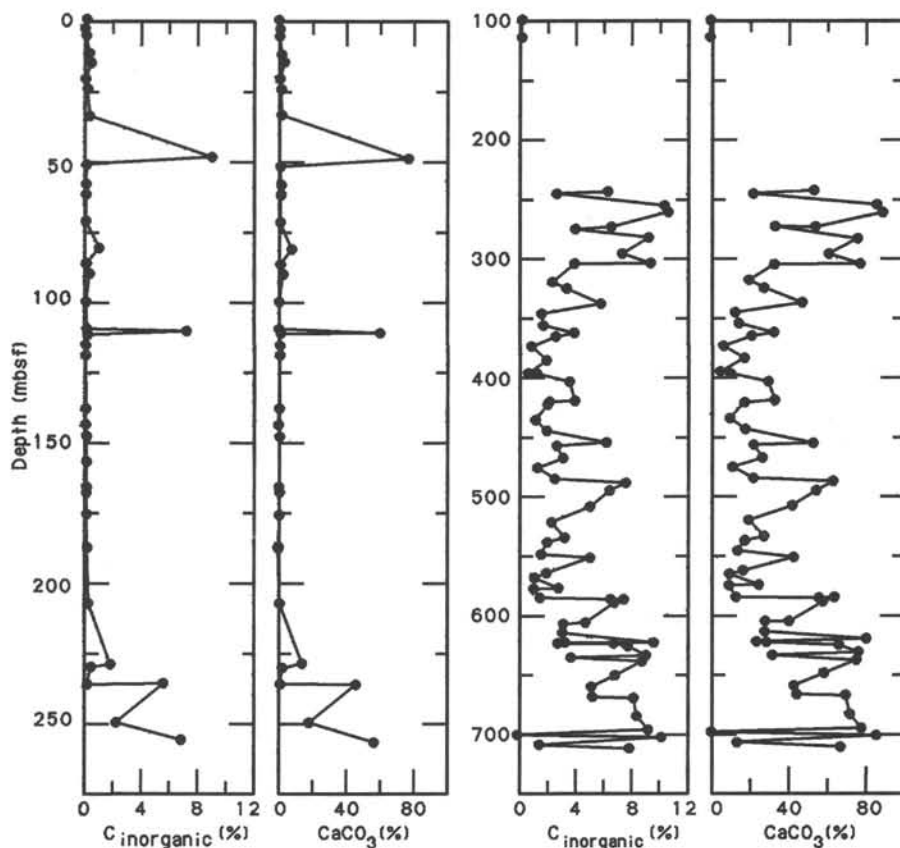


Figure 28. Inorganic carbon and percent calcium carbonate from squeeze-cake and core-catcher sediment samples, Holes 737A and 737B.

Table 7. Rock-Eval summary, Site 737.

Sample no.	Weight (mg)	T _{max} (°C)	S1 (mg HC/g)	S2 (mg HC/g)	S3 (mg CO ₂ /g)	Productivity index	Pyrolyzied carbon		TOC (wt%)	Hydrogen index (mg HC/g C _{org})	Oxygen index (mg CO ₂ /g C _{org})
							S2/S3	(0.08 [S1 + S2])			
29	100.5	581	0.08	0.15	0.40	0.36	0.37	0.01	0.04	375	1000
28	100.1	558	0.01	0.87	0.25	0.01	3.48	0.07	0.06	1450	417
27	101.9	288	0.03	0.00	0.38	1.00	0.00	0.00	0.07	0	543
26	99.4	224	0.05	0.00	0.30	1.00	0.00	0.00	0.19	0	158
25	98.3	230	0.06	0.00	0.39	1.00	0.00	0.00	0.01	0	3900
24	101.1	444	0.01	0.00	0.31		0.00	0.00	0.07	0	443
23	99.1	566	0.02	0.27	0.61	0.07	0.44	0.02	0.03	900	2033
22	100.1	583	0.04	0.09	0.57	0.33	0.15	0.01	0.06	150	950
21	105.0	224	0.01	0.00	0.82		0.00	0.00	0.00	0	
20	100.6	435	0.03	0.00	0.58	1.00	0.00	0.00	0.04	0	1450
19	98.0	230	0.03	0.00	0.64	1.00	0.00	0.00	0.07	0	914
18	97.3	222	0.01	0.00	1.38		0.00	0.00	0.04	0	3450
17	107.6	230	0.08	0.00	0.71	1.00	0.00	0.00	0.01	0	7100
16	103.0	222	0.03	0.00	0.71	1.00	0.00	0.00	0.00		
15	100.5	228	0.02	0.00	0.62	1.00	0.00	0.00	0.05	0	1240
14	104.6	228	0.09	0.00	0.96	1.00	0.00	0.00	0.11	0	872
13	108.4	284	0.09	0.00	0.66	1.00	0.00	0.00	0.12	0	550
12	99.2	245	0.08	0.03	0.50	0.80	0.06	0.00	0.08	38	625
11	96.2	368	0.10	0.09	0.58	0.56	0.15	0.01	0.29	31	200
10	94.8	403	0.12	0.25	0.63	0.33	0.39	0.03	0.22	114	286
9	101.3	399	0.18	0.51	0.67	0.26	0.76	0.05	0.39	131	172
8	81.2	391	0.76	2.36	0.13	0.24	18.15	0.26	0.57	414	23
7	95.9	392	0.36	1.52	0.12	0.19	12.66	0.15	0.57	267	21
6	97.2	392	0.43	2.21	0.24	0.16	9.20	0.22	0.46	480	52
5	98.6	543	0.08	0.62	0.05	0.11	12.40	0.05	0.24	258	21
4	99.2	401	0.34	1.25	0.13	0.22	9.61	0.13	0.42	298	31
3	99.6	399	0.41	1.24	0.18	0.25	6.88	0.13	0.49	253	37
2	55.2	396	1.35	2.42	0.77	0.36	3.14	0.31	0.48	504	160
1	104.0	558	0.26	0.75	0.19	0.26	3.94	0.08	0.53	142	36

Note: See Figure 29 for sample depths (mbsf).

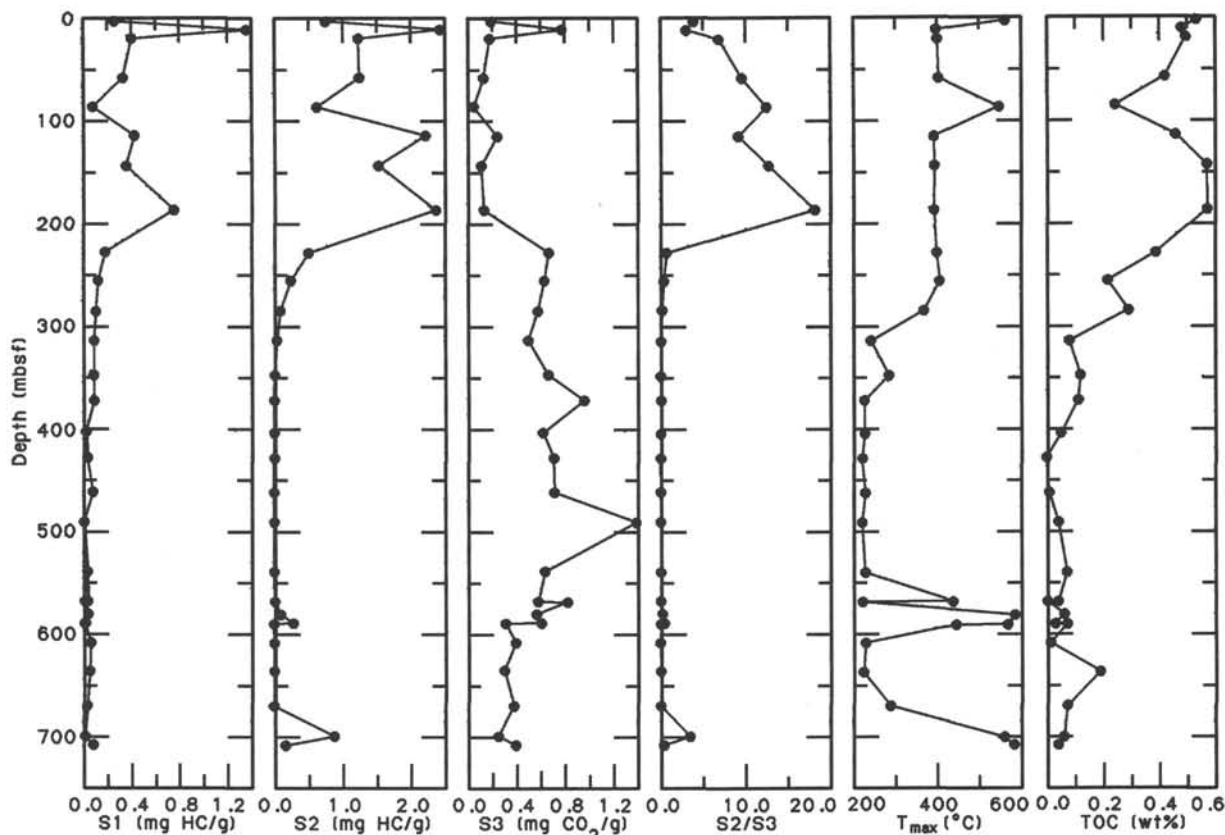


Figure 29. Comparison of Rock-Eval parameters S1, S2, S3, S2/S3, T_{max} , and TOC for Site 737. TOC was determined as the difference between total carbon and inorganic carbon.

As no apparent compaction effect can be seen in the upper 200 mbsf from the index properties, the cause of the shear-strength increase may be found in the composition and shape of the grains. Pore-water chemistry (see "Inorganic Geochemistry" section) shows a downcore increase in silica content in the diatom oozes, which points toward increasing dissolution of diatoms. This may reduce the surface area of the individual diatoms and cause more grain-to-grain contacts, thereby also increasing the strength of the sediment. A gradual increase in the amount of calcareous nannofossils relative to diatoms may also be of importance.

Compressional-Wave Velocity

Compressional-wave velocities, as determined by the Hamilton Frame and *P*-wave logger, confirm the trends of the index properties. There is, however, no noticeable velocity discontinuity between geotechnical units G1 and G2. Both methods show a constant velocity between 1500 and 1550 m/s down to 300 mbsf, which includes both of the units. Because of poor contact between the liner and sample in the lithified material, use of the *P*-wave logger ended at 350 mbsf.

The velocity peak (2596 m/s) at 310 mbsf represents a thin layer of calcareous siltstone, embedded in the less lithified sediment. There is a marked increase of 250 m/s to velocities on the order of 1900 m/s at 375 mbsf. This change corresponds well with a marked decrease in the quality of preservation of the calcareous microfossils ("Biostratigraphy" section). Below this boundary, the foraminifers are filled to a large degree with cement. There is also a marked color change. The degree of cementation may be responsible for the velocity increase. However, there is no corresponding discontinuity in the bulk densities. The veloc-

ities are relatively constant down to 540–550 mbsf, where there is an increase to 2000–2100 m/s, but with large variations to 620 mbsf. In the clayey limestone at the bottom of Hole 737B, the velocities vary between 3450 and 2400 m/s.

For comparison, velocities from downhole logging and sonobuoys are projected onto Hamilton Frame velocities (see "Logging" section). These two other methods clearly confirm the described trends.

Thermal Conductivity

Thermal-conductivity values were measured on APC, XCB, and RCB cores, with the most variation occurring in the RCB cores. Rates of temperature drift during the conductivity measurements ranged from 0.008 to 0.69 and generally exceeded the 0.01 value recommended by the instrument manual. High drift gradients may explain why several conductivity values are lower than 0.59 W/m/°C, the conductivity of water at ambient conditions (Clark, 1966); however, the lowest drift (0.008), which is within specified drift limits, also gave a conductivity value below 0.59 W/m/°C.

The conductivity values at Site 737, like those at Site 736, appear to have a bimodal distribution, although it is not as apparent at Site 737. Lower values (e.g., below 0.6 W/m/°C) are unrealistically small, but higher values (e.g., 0.6 to 1.5 W/m/°C) appear reasonable because they are similar to those obtained from other areas with highly porous diatomaceous oozes (see the discussion in "Physical Properties" section, "Site 736" chapter). The thermal-conductivity values at Site 737 average about 0.8 W/m/°C to about 380 mbsf, where they begin to increase uniformly to about 1.3 W/m/°C at about 610 mbsf. Below 590 mbsf, conductivities are more variable because good contact be-

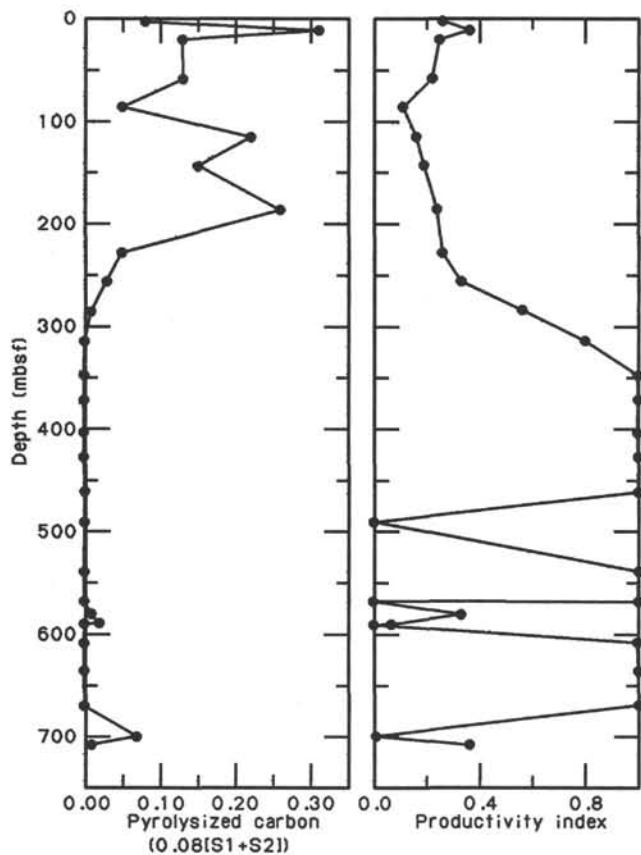


Figure 30. Comparison of Rock-Eval parameters pyrolyzed carbon and productivity index, Site 737.

tween the needle probe and the indurated and silicified rocks was difficult to achieve. A zone of locally higher conductivities may occur around 300 mbsf.

The two principal breaks in the curve of conductivity vs. depth (300 and 380 mbsf) generally correspond with boundaries at the tops of downhole logging units 2 and 4 ("Logging" section). The correspondence suggests that the observed conductivity variations are due to geologic (rather than instrumental) factors.

Temperature and Heat Flow

Temperatures were measured at 81.5, 128.5, and 226.5 mbsf in Hole 737A using the Uyeda probe and standard operational procedures (see "Explanatory Notes" chapter) (Fig. 34).

All measurements are affected to varying degrees by ship surges of up to 5–7 m that most likely resulted in vertical motion of the probe while in the sediment. The apparent surge effects increase with depth, probably reflecting greater temperature loss at depth caused by gradual probe extraction, poorer sediment/probe contact, and an influx of water.

The temperature profile at 81.5 mbsf yields the most reliable equilibration temperature at Site 737 (12.0°C), based on projection of the $1/t$ equilibration curves (Fig. 35). The near linearity of the equilibration curve indicates that significant temperature variations did not occur during the 10 min that the probe was inserted.

The temperature profiles made at 128.5 and 226.5 mbsf have a jagged triangular shape during sediment penetration. Two equilibrium temperatures were estimated for 128.5 mbsf based on the initial (i.e., immediately after probe penetration) reading and from a later part of the temperature curve. The two equi-

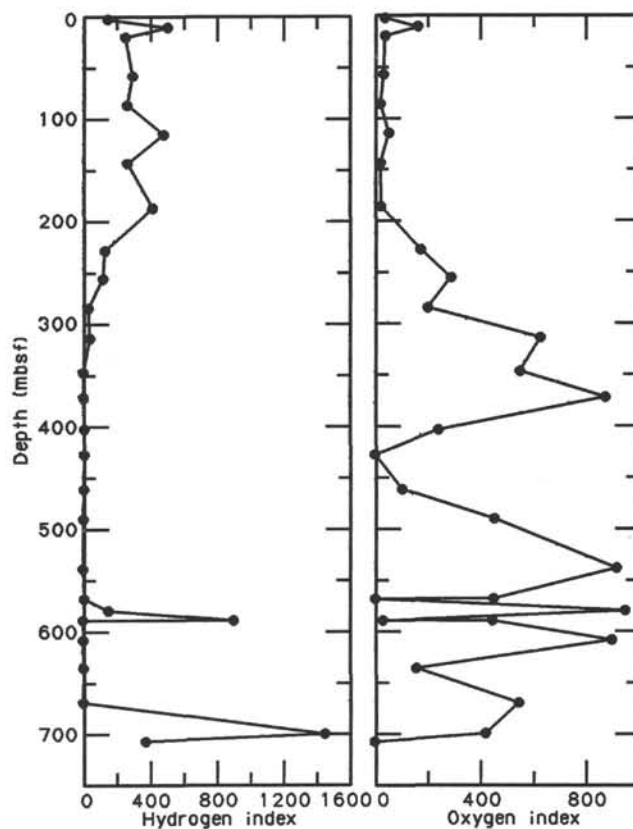


Figure 31. Comparison of Rock-Eval parameters hydrogen index and oxygen index, Site 737.

bration curves for 128.5 mbsf do not yield the same equilibration temperature, which suggests that the probe had moved to shallower, or different, positions in the hole. The higher equilibration temperature (17.1°C) is more probable because it gives the first undisturbed measurement. The estimated equilibration temperature derived for 226.5 mbsf is based on the first and second(?) penetrations of the probe, as described previously. Here, however, the two equilibration temperatures are nearly identical (23.5°C), which gives greater reliability to the measurement.

Temperatures at Site 737 are high, ranging from about 1.3°C at the seafloor to 12°C at 81.5 mbsf to 23.5°C at 226.5 mbsf. The average temperature gradient is 98°C/km. The sedimentary section at this interval is composed of diatomaceous oozes with conductivity values averaging about 0.8 W/m°C. The heat flow, based on these average values for temperature gradient and thermal conductivity, is 78.2 W/m² (1.87 HFU). This value is high in comparison to that at Site 736 (52.8 W/m², 1.26 HFU).

Temperatures were measured during a downhole logging run below 280 mbsf. The recorded temperatures increased from 11°C at 280 mbsf to 22°C at the end of the run at 680 mbsf (see "Logging" section). The logging temperatures are significantly lower than those measured by the *in-situ* probe because cold high-density mud had been circulated through the hole about 1 hr before the logging run. In addition, the fast logging speed was not long enough for the thermistor to reach equilibrium temperatures.

In summary, good temperature readings were measured at three depths within the upper 227 m of the sediment at Site 737 to give an average temperature gradient of 98°C/km and a heat flow of 78.2 W/m² (1.87 HFU).

Table 8. Weather summary for JOIDES Resolution at Site 737.

Time (hr)/date	Winds (kt)	Sea-surface temperature (°C)	Waves (m)	Sky
00-23/30 Dec.	NW 22-30	3.4-3.5	7-8	Mostly clear; clouds covered less than half the sky
00-09/31 Dec.	W 30-35, with gusts to 45	3.2-3.5	7-8	Overcast with isolated light rain showers. Pressure begins to fall.
10-15/31 Dec.	NW 20-25, with gusts to 30	3.4	5-6	Overcast with continuous light rain. Pressure still falling.
16-21/31 Dec.	SE 5-10	3.2-3.4	4	Overcast with continuous light rain. Lowest pressure at 17 hr.
22/31 Dec. to 09/1 Jan.	SW veering to NW 12-18	3.1	6	Mostly cloudy with scattered light rain showers. Pressure rising.
10-20/1 Jan.	N-NW 10-15 to <5 at 18 hr	3.5	4-5	Overcast with light rain and fog. Pressure falling.
21/1 Jan. to 03/3 Jan.	SW 22-28	3.0-3.5	5	Mostly cloudy to overcast with light rain showers. Pressure rising.
04/3 Jan. to 03/4 Jan.	W 20-30, with gusts to 35	3.0-3.5	5	Overcast with light rain showers. Pressure rising.
04-21/4 Jan.	NE 10-18	3.3-4.0	2-3	Overcast with fog and occasional light rain. Pressure falling.

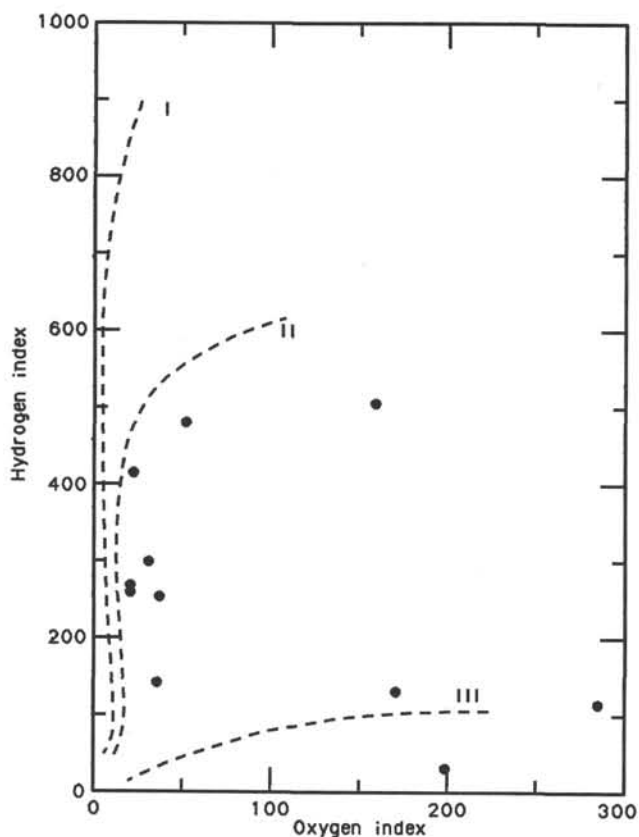


Figure 32. Hydrogen and oxygen indices obtained from Rock-Eval pyrolysis of squeeze-cake sediment samples from Site 737 plotted on a van Krevelen-like diagram (Tissot and Welte, 1984).

Discussion

Site 737 demonstrated the same physical behavior for the diatom oozes as observed at Site 736: low velocity, low density, high water content, and seeming consistency of these parameters with depth, at least to 200 mbsf. However, the increasing shear strength downcore implies that some change

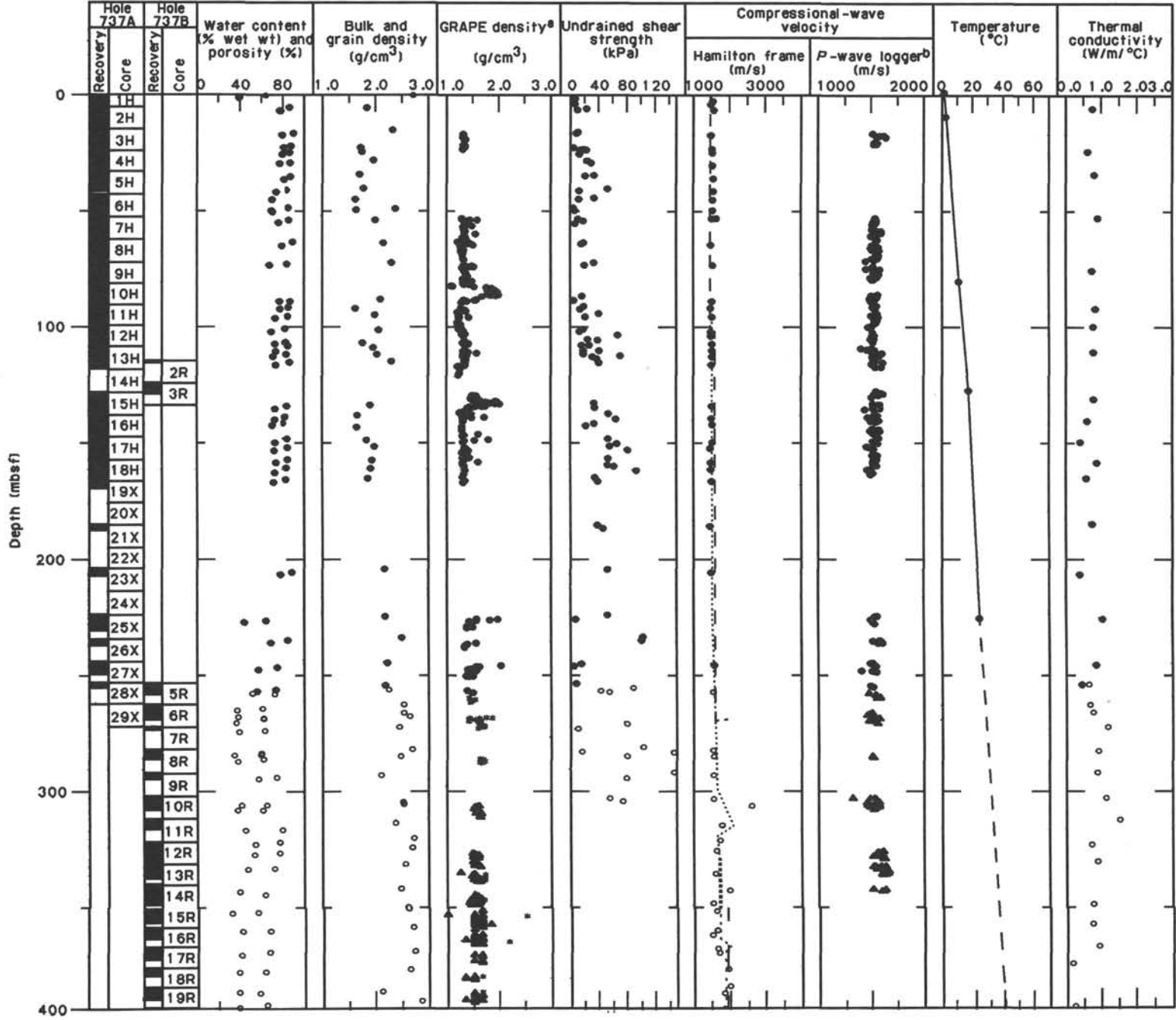
Table 9. Planktonic diatom species not noted at Site 736.

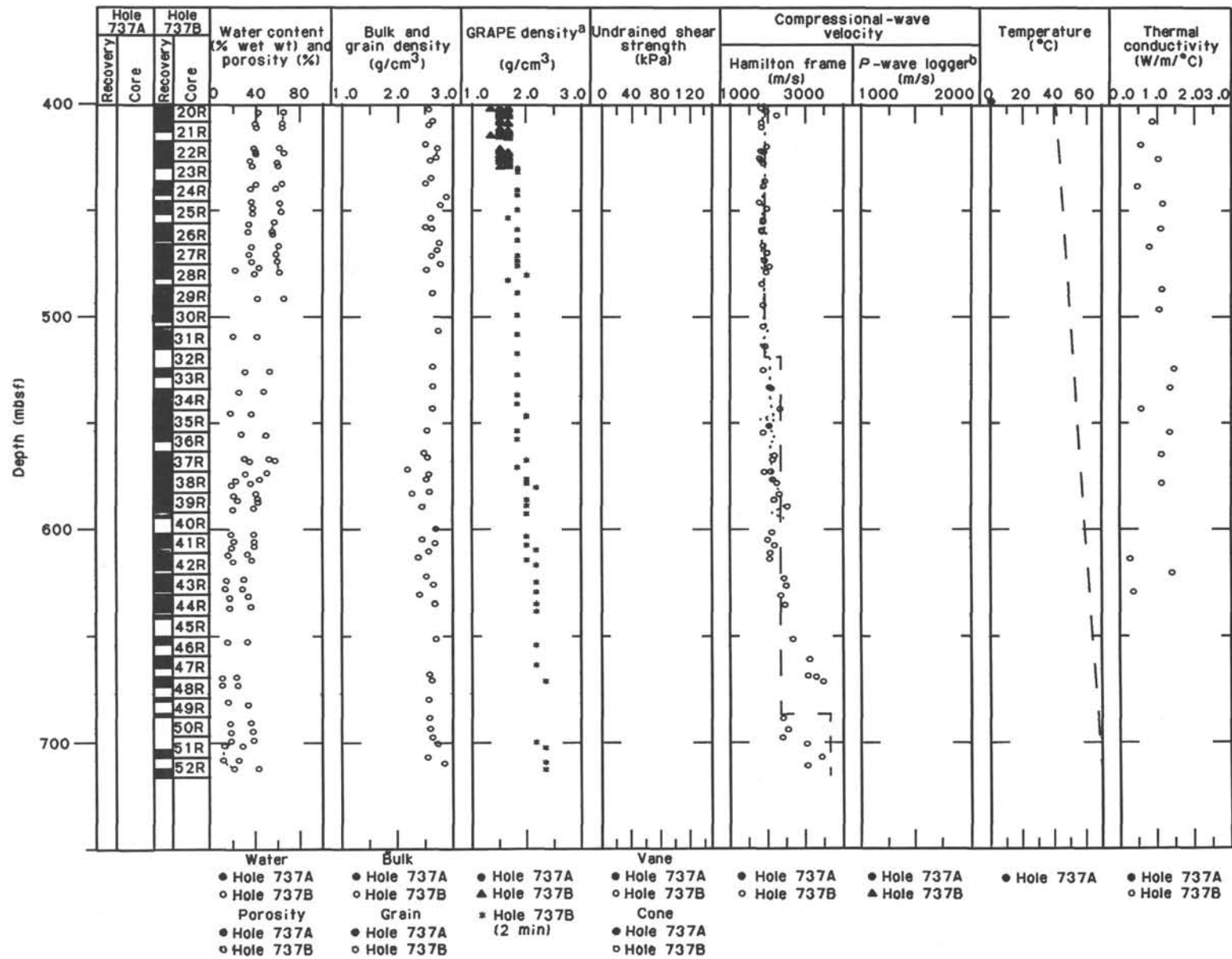
Actinocyclus ehrenbergii
Asteromphalus hyalinus
Chaetoceros atlanticus
Chaetoceros bulbosus
Chaetoceros neglectus
Coscinodiscus curvatulus
Haslea sp.
Navicula directa
Nitzschia angulata
Nitzschia lineola?
Nitzschia ritscheri
Rhizosolenia curvata
Synedra reinholdii?
Thalassiosira frequelii

Table 10. Species found at the mud line and in Sample 119-737A-1H-1, 2 cm.

Actinocyclus actinochilus
Actinocyclus ehrenbergii
Asteromphalus hookeri
Azpeitia tabularis
Chaetoceros resting spores
Coscinodiscus curvatulus
Coscinodiscus oculoides
Dactiliosolen antarcticus (heavy bands only)
Eucampia antarctica
Nitzschia angulata
Nitzschia curta
^a*Nitzschia kerquelensis* (coarse, fine, and long forms)
Nitzschia panduriformis
Nitzschia ritscheri
Nitzschia separanda
Nitzschia spp. (Pseudonitzschia chains!)
Odontella weissflogii
Paralia sulcata
Rouxia spp.
Thalassionema nitzschioides
Thalassiosira gracilis
^a*Thalassiosira lentiginosa*
Thalassiosira oestrupii?
Thalassiosira oliverana
Thalassiosira scottia
Thalassiosira trifulta
Thalassiosira tumida
Thalassiosira sp. cf. *trifulta*

^a Abundant.





^aData filtered for values <1.0 and >2.5 g/cm³ and blocked in 0.2-m averages.
^bData filtered for signal strengths <150 m/s and blocked in 0.2-m averages.

Figure 33. Physical-property profiles, Site 737.

Table 11. Water content, porosity, bulk density, dry-bulk density, and grain density, Hole 737B.

Core, section, interval (cm)	Depth (mbsf)	Water content (%)	Porosity (%)	Bulk density (g/cm ³)	Dry-bulk density (g/cm ³)	Grain density (g/cm ³)
10R-4, 30	306.60	39.60	62.40	1.72	1.04	2.52
11R-3, 50	315.00	46.37	79.88	1.53	0.82	2.37
12R-1, 39	321.49	54.97	76.74	1.49	0.67	2.72
12R-4, 47	326.07	54.48	76.11	1.47	0.67	2.68
13R-2, 50	332.80	49.4	71.5	1.51		2.55
14R-3, 10	343.50	41.8	63.6	1.64		2.46
15R-2, 23	351.83	33.7	56.6	1.55		2.60
16R-2, 8	361.38	43.8	67.5	1.65		2.69
17R-3, 17	372.57	43.3	67.3	1.63		2.72
18R-3, 10	382.20	40.8	64.1	1.70		2.63
19R-3, 43	392.13	40.6	58.9	1.60		2.11
20R-1, 55	398.95	40.17	65.33	1.67	1.00	2.84
20R-4, 99	403.89	42.88	65.44	1.66	0.95	2.55
21R-2, 45	410.05	40.44	63.80	1.68	1.00	2.63
21R-3, 34	411.44	41.03	63.70	1.78	1.05	2.55
22R-3, 48	421.18	39.14	61.33	1.70	1.04	2.49
22R-5, 22	423.92	40.96	64.99	1.69	1.00	2.71
23R-1, 39	427.79	35.42	59.31	1.80	1.16	2.69
23R-2, 18	429.08	37.05	59.93	1.75	1.10	2.57
24R-1, 49	437.49	40.41	63.52	1.66	0.99	2.60
24R-3, 24	440.24	36.42	58.37	1.74	1.11	2.48
25R-1, 46	447.16	36.93	62.42	1.75	1.10	2.87
25R-3, 105	450.75	38.39	63.02	1.75	1.08	2.77
26R-1, 33	456.73	34.40	57.29	1.76	1.15	2.59
26R-3, 143	460.83	33.34	55.23	1.83	1.22	2.50
26R-4, 77	461.67	32.33	55.18	1.86	1.26	2.61
27R-1, 141	467.41	36.67	61.13	1.76	1.11	2.75
27R-4, 71	471.21	34.71	58.58	1.92	1.25	2.70
27R-6, 73	474.23	36.81	59.89	1.75	1.11	2.60
28R-2, 72	477.92	22.10	43.56	2.01	1.57	2.76
28R-4, 18	480.38	39.11	61.51	1.66	1.01	2.52
29R-5, 5	491.45	42.5	65.8	1.65		2.63
30R-2, 29	496.79	23.3	47.4	2.33		3.01
31R-4, 35	508.96	21.0	41.8	2.08		2.74
33R-2, 23	525.73	30.5	53.2	1.99		2.63
34R-2, 3	535.13	25.6	47.3	1.95		2.64
35R-2, 4	544.84	18.6	37.2	2.10		2.63
36R-2, 23	554.63	28.0	49.3	1.91		2.53
37R-2, 143	565.43	31.03	52.45	1.97	1.36	2.48
37R-4, 55	567.55	35.62	58.14	1.89	1.21	2.54
38R-1, 88	573.08	32.25	50.58	1.88	1.27	2.18
38R-3, 82	576.02	23.53	43.75	2.07	1.58	2.56
38R-5, 31	578.51	19.17	37.01	2.11	1.71	2.51
39R-2, 56	583.86	21.64	41.23	1.96	1.54	2.58
39R-3, 80	585.60	24.81	42.54	1.91	1.43	2.27
39R-6, 71	590.01	21.03	39.07	2.08	1.64	2.44
41R-1, 76	601.86	19.62	39.37	2.10	1.69	2.70
41R-3, 114	605.24	21.90	40.36	2.14	1.68	2.45
41R-5, 24	607.34	20.27	40.16	2.13	1.70	2.68
42R-1, 102	611.72	16.88	33.97	2.14	1.78	2.57
42R-3, 49	614.19	20.45	37.50	2.12	1.69	2.37
43R-2, 141	623.21	15.15	30.62	2.15	1.82	2.51
43R-5, 90	627.20	13.85	29.60	2.33	2.01	2.66
44R-1, 148	631.48	18.22	34.55	2.16	1.76	2.40
44R-4, 110	635.60	18.01	36.62	2.19	1.80	2.67
46R-2, 101	651.81	16.13	33.80	2.34	1.96	2.70
48R-1, 118	669.08	11.12	24.05	2.48	2.20	2.57
48R-CC, 17	671.86	11.25	24.64	2.39	2.12	2.62
49R-2, 147	680.57	16.95	33.97	2.82	2.34	2.56
50R-2, 147	689.47	18.55	36.69	2.38	1.94	2.58
50R-5, 147	693.97	19.75	38.54	2.37	1.90	2.59
51R-1, 146	697.66	19.63	38.82	2.24	1.80	2.64
51R-4, 1	700.71	13.48	29.47	2.49	2.15	2.72
52R-1, 142	707.32	11.95	25.35	2.32	2.04	2.54
52R-4, 41	710.81	21.80	43.82	2.33	1.82	2.84

occurs in the material. Factors that possibly are of importance are diagenetic processes and variations in other constituents, such as nanofossils, clay minerals, or volcanic fragments. One should also note that the increase in shear strength is significantly smaller than would be expected in a clay, for instance.

Recorded changes in seismic velocity and bulk density generally follow lithologic changes as described in the core descrip-

Table 12. Bulk density from 2-min GRAPE counts of discrete samples, Hole 737B.

Core, section, interval (cm)	Depth (mbsf)	GRAPE density (g/cm ³)
13R-2, 38-48	332.68	1.73
13R-4, 17-18	335.47	1.63
14R-2, 146-147	343.36	1.71
14R-CC, 1-4	348.04	1.71
15R-1, 46-49	350.56	1.73
15R-2, 21-22	351.81	2.49
16R-1, 148-150	361.28	1.67
16R-3, 101-103	363.81	2.24
17R-1, 143-145	370.83	1.72
17R-4, 21-22	374.11	1.60
18R-2, 49-52	381.09	1.65
19R-1, 38-40	389.08	1.73
19R-3, 73-75	392.43	1.69
20R-1, 115-117	399.55	1.68
20R-3, 113-118	402.53	1.69
21R-2, 44-48	410.04	1.73
21R-3, 33-35	411.43	1.73
22R-3, 48-51	421.18	1.69
22R-5, 22-25	423.92	1.73
23R-1, 36-39	427.76	1.80
23R-2, 16-19	429.06	1.77
24R-1, 49-51	437.49	1.89
24R-3, 20-24	440.20	1.77
25R-1, 47-50	447.17	1.82
25R-3, 105-108	450.75	1.72
26R-1, 35-38	456.75	1.81
26R-3, 142-146	460.82	1.81
26R-6, 70-71	464.61	1.76
27R-2, 143-147	468.93	1.76
27R-4, 72-75	471.22	1.82
27R-6, 70-73	474.20	1.78
28R-2, 72-75	477.92	1.98
28R-4, 18-22	480.38	1.65
29R-1, 70-73	486.10	1.83
30R-1, 108-111	496.08	1.75
31R-1, 88-91	505.58	1.78
31R-CC, 19-22	514.57	1.79
33R-1, 146-150	525.46	1.77
34R-1, 30-32	533.90	1.77
34R-4, 11-13	538.21	1.85
35R-1, 114-117	544.44	2.02
35R-6, 7-8	550.87	1.76
36R-1, 147-150	554.37	1.82
37R-2, 143-146	565.43	1.92
37R-4, 55-59	567.55	1.86
38R-1, 89-93	573.09	1.93
38R-3, 83-86	576.03	1.99
38R-5, 32-36	578.52	2.09
39R-2, 57-61	583.87	2.07
39R-3, 82-86	585.62	1.92
39R-6, 72-76	590.02	2.08
41R-1, 77-80	601.87	2.05
41R-3, 115-118	605.25	2.06
41R-5, 26-29	607.36	2.12
42R-1, 98-101	611.68	2.07
42R-3, 50-53	614.20	2.09
43R-2, 142-146	623.22	2.22
43R-5, 86-89	627.16	2.21
44R-1, 148-150	631.48	2.10
44R-4, 110-114	635.60	2.19
46R-2, 101-106	651.81	2.15
47R-2, 147-150	661.57	2.24
48R-1, 118-121	669.08	2.37
48R-CC, 17-21	671.07	2.32
49R-2, 147-148	680.57	2.37
50R-2, 147-148	689.47	2.19
50R-5, 147-148	693.97	2.22
51R-1, 146-150	697.66	2.15
51R-4, 1-4	700.71	2.33
52R-1, 142-145	707.32	2.31
52R-4, 41-44	710.81	2.26

Table 13. Undrained shear strength from vane measurements, Site 737.

Core, section, interval (cm)	Depth (mbsf)	Undrained shear strength (kPa)
119-737A-		
1H-2, 86	2.36	6.2
1H-3, 3	3.03	7.2
2H-1, 110	6.10	10.8
3H-2, 80	16.80	8.9
3H-CC, 7	24.29	18.2
3H-6, 110	23.10	22.6
4H-1, 100	25.00	12.8
4H-4, 80	29.30	29.6
5H-2, 75	35.75	20.9
5H-6, 40	41.40	13.4
6H-2, 80	45.30	12.4
6H-5, 85	49.85	6.2
7H-1, 114	53.64	11.8
7H-2, 101	55.01	8.1
8H-2, 80	64.30	16.1
9H-2, 80	73.80	20.3
10H-6, 76	89.26	5.2
11H-2, 90	92.90	14.5
11H-4, 117	96.17	21.3
12H-2, 76	102.26	13.4
12H-4, 112	105.62	24.8
12H-6, 26	107.76	26.9
13H-1, 86	110.36	18.6
13H-1, 86	110.36	41.3
13H-3, 96	113.46	32.1
13H-3, 96	113.46	71.1
13H-5, 118	116.68	40.8
15H-5, 71	135.21	35.6
16H-2, 71	140.21	65.3
16H-4, 51	143.01	22.3
17H-2, 123	150.23	66.8
17H-4, 96	152.96	81.2
18H-2, 81	159.31	52.2
18H-4, 78	162.28	92.8
19X-1, 70	167.20	39.4
21X-1, 94	186.84	46.4
25X-1, 136	226.06	8.1
26X-1, 120	235.60	100.9
27X-2, 75	246.35	5.8
119-737B-		
5R-3, 94	257.44	43.1
5R-3, 120	257.70	55.1
7R-1, 58	273.48	11.5
8R-1, 64	283.14	17.0
8R-3, 13	285.63	80.0
9R-2, 40	294.10	78.9
10R-2, 63	303.93	55.7

tions for Site 737. In particular, velocity discontinuities seem to correspond well with apparent hiatuses. The high velocity of the calcareous siltstone at about 310 mbsf corresponds to a break in sedimentation from 15 to 24 Ma, and the increase at 540–550 mbsf corresponds to a possible break from 30 to 34 Ma (see "Biostratigraphy" section). The onset of higher velocities toward the bottom of the cored section, in the clayey limestones, roughly corresponds to a middle to lower Eocene hiatus. The main velocity discontinuities measured in the laboratory are seen both in the seismic reflection (see "Site Geophysics" section, this chapter) and in the downhole logging results (see "Logging" section).

LOGGING

Operations

Logging operations at Hole 737B began at 2130 hr on 2 January 1988 and were completed at 0430 hr on 4 January, corre-

Table 14. Undrained shear strength from fall cone measurements, Site 737.

Core, section, interval (cm)	Depth (mbsf)	Undrained shear strength (kPa)
119-737A-		
1H-2, 90-91	2.40	7.3
1H-3, 91-92	3.91	6.6
2H-1, 110-111	6.10	24.0
3H-2, 81-82	16.81	12.0
3H-6, 110-111	23.10	5.1
4H-1, 100-101	25.00	15.0
4H-4, 80-81	29.30	24.0
5H-2, 75-76	35.75	34.0
5H-6, 40-41	41.40	53.0
6H-2, 80-81	45.30	34.0
6H-5, 85-86	49.85	4.2
7H-1, 114-115	53.64	9.0
7H-2, 101-102	55.01	19.0
8H-2, 80-81	64.30	19.0
9H-2, 80-81	73.80	34.0
10H-6, 76-77	89.26	17.0
11H-2, 91-92	92.91	19.0
11H-4, 114-115	96.14	41.0
12H-2, 78-79	102.28	19.0
12H-4, 110-111	105.60	67.0
12H-6, 25-26	107.75	39.0
13H-1, 87-88	110.37	17.0
13H-3, 100-101	113.50	19.0
13H-5, 121-122	116.71	39.0
15H-5, 74-75	135.24	34.0
16H-2, 73-74	140.23	54.0
16H-4, 54-55	143.04	34.0
17H-2, 120-121	150.20	54.0
17H-4, 93-94	152.93	56.0
18H-2, 78-79	159.28	54.0
18H-4, 80-81	162.30	62.0
19X-1, 72-73	167.22	35.0
21X-1, 97-98	186.87	39.0
23X-1, 90-91	206.20	53.0
25X-1, 136-137	226.06	53.0
26X-1, 120-121	235.60	103.0
27X-2, 75-76	246.35	17.0
28X-2, 20-21	255.50	9.3
119-737B-		
5R-3, 123-124	257.73	89.0
7R-1, 61-62	273.51	80.0
8R-1, 71-72	283.21	103.0
8R-3, 17-18	285.67	145.0
9R-2, 40-41	294.10	145.0
10R-4, 30-31	306.60	75.0

sponding to a total logging time of 31 hr. The hole was cleaned by dropping the pipe to the bottom of the hole. Seawater was circulated for about 15 min, and then the pipe was pulled up and left at 124 mbsf for the logging operations.

The seismic stratigraphic combination (see "Explanatory Notes" chapter), which included long-spacing sonic (LSS), dual induction (DIL), gamma-ray (GR), and caliper (MCD) tools, was rigged at 0115 hr on 3 January. The log was recorded in two runs because a bridge was encountered as the tool was going downhole at 250 mbsf. The first logging run was recorded from 250 to 94 mbsf (Fig. 36). The bridge was crossed by lowering the pipe to 296 mbsf, and the second logging run was recorded from 616 to 296 mbsf. This second run did not reach the bottom of the hole (715.5 mbsf) because a second bridge was encountered at 616 mbsf.

Before running the second tool combination, the hole was conditioned by circulating a freshwater mud composed of bentonite and barite with a density of 19.5 lb/gal. The geochemical combination (see "Explanatory Notes" chapter) was rigged at 1800 hr on 3 January. The prelogging tests indicated that the

Table 15. Compressional-wave velocity determined with the Hamilton Frame, Site 737.

Core, section, interval (cm)	Depth (mbsf)	Direction ^a	Compressional-wave velocity (m/s)
119-737A-			
1H-2, 82-84	2.32	C	1532
1H-3, 86-86	3.86	C	1477
2H-1, 110-113	6.10	C	1569
3H-2, 80-83	16.80	C	1492
3H-6, 110-113	23.10	C	1513
4H-1, 100-103	25.00	C	1525
4H-4, 80-83	29.30	C	1527
5H-2, 75-78	35.75	C	1547
5H-6, 40-43	41.40	C	1564
6H-2, 83-85	45.33	C	1529
6H-5, 85-88	49.85	C	1529
7H-1, 114-117	53.64	C	1532
7H-1, 101-104	53.51	C	1631
8H-2, 80-83	64.30	C	1492
9H-2, 80-83	73.80	C	1530
10H-6, 76-79	89.26	C	1520
11H-2, 90	92.90	C	1471
11H-4, 114	96.14	C	1516
12H-2, 74	102.24	C	1474
12H-4, 110	105.60	C	1498
12H-6, 30	107.80	C	1496
13H-1, 90	110.40	C	1502
13H-3, 100	113.50	C	1502
13H-5, 124	116.74	C	1495
15H-5, 75	135.25	C	1513
16H-2, 73	140.23	C	1507
16H-4, 54	143.04	C	1536
17H-2, 120	150.20	C	1517
17H-4, 85	152.85	C	1459
18H-2, 77	159.27	C	1492
18H-4, 74	162.24	C	1476
19X-1, 65	167.15	C	1495
21X-1, 99	186.89	C	1448
23X-1, 90	206.20	C	1495
27X-2, 75	246.35	C	1574
119-737B-			
5R-3, 98	257.48	C	1513.0
5R-3, 116	257.66	C	1528.0
8R-1, 72	283.22	C	1523.0
8R-3, 16	285.66	C	1541.0
9R-2, 40	294.10	C	1543.0
10R-2, 63	303.93	C	1557.0
10R-4, 44	306.74	C	2596.0
11R-3, 50	315.00	C	1775.0
12R-1, 39	321.49	C	1717.0
12R-4, 47	326.07	C	1630.0
13R-4, 10	335.40	C	1599.0
14R-2, 146	343.36	C	1973.0
14R-CC, 1	348.04	A	1526.0
15R-1, 46	350.56	A	1568.0
15R-2, 21	351.81	A	1623.0
16R-1, 148	361.28	A	1616.0
16R-3, 101	363.81	A	1500.0
17R-1, 143	370.83	A	1646.0
17R-3, 81	373.21	A	1693.0
18R-2, 49	381.09	A	1933.0
19R-1, 38	389.08	A	1967.0
19R-3, 73	392.43	A	1817.0
20R-1, 115	399.55	C	1812.5
20R-2, 145	401.35	C	1909.8
20R-4, 107	403.97	C	1951.6
20R-6, 33	406.23	C	2216.7
20R-3, 113	402.53	A	1843.4
21R-2, 44	410.04	C	1830.7
21R-3, 33	411.43	C	1826.4
22R-3, 48	421.18	C	1962.0
22R-3, 48	421.18	A	1949.3
22R-5, 22	423.92	C	1887.3
22R-5, 22	423.92	A	1812.5
23R-1, 36	427.76	C	1777.5
23R-1, 36	427.76	A	1805.2
23R-2, 16	429.06	A	1877.0
24R-1, 49	437.49	A	1900.0

Table 15 (continued).

Core, section, interval (cm)	Depth (mbsf)	Direction ^a	Compressional-wave velocity (m/s)
119-737B- (Cont.)			
24R-1, 49	437.49	C	1908.4
24R-3, 20	440.20	A	1871.9
25R-1, 47	447.17	A	1781.1
25R-3, 105	450.75	A	1971.6
26R-1, 35	456.75	A	1880.2
26R-3, 142	460.82	A	1837.7
26R-4, 76	461.66	A	1836.6
27R-2, 143	468.93	A	1878.9
27R-4, 72	471.22	A	1973.0
27R-6, 70	474.20	A	1900.8
28R-2, 72	477.92	A	2035.5
28R-4, 18	480.38	A	1939.7
29R-1, 70	486.10	A	1838.0
30R-1, 108	496.08	A	1887.2
31R-1, 88	505.58	A	1873.4
31R-CC, 19	514.57	A	1916.7
33R-1, 146	525.46	A	1871.6
34R-1, 11	533.71	A	2094.7
34R-1, 30	533.90	A	2046.9
35R-1, 114	544.44	A	2335.7
35R-6, 7	550.87	A	2047.6
36R-1, 147	554.37	A	1869.9
37R-2, 143	565.43	A	2171.6
37R-4, 55	567.55	A	2118.9
38R-1, 89	573.09	A	1901.0
38R-1, 89	573.09	A	2073.9
38R-3, 83	576.03	A	2134.5
38R-5, 32	578.52	A	2238.5
39R-2, 57	583.87	A	2302.9
39R-3, 82	585.62	A	2164.9
39R-6, 72	590.02	A	2519.5
41R-1, 77	601.87	A	2112.4
41R-3, 115	605.25	A	2000.0
41R-5, 26	607.36	A	2177.4
42R-1, 98	611.68	A	2074.5
42R-3, 50	614.20	A	2055.6
43R-2, 142	623.22	A	2432.1
43R-5, 86	627.16	A	2500.0
44R-1, 148	631.48	A	2347.8
44R-4, 110	635.60	A	2455.7
46R-2, 101	651.81	A	2678.6
47R-2, 147	661.57	A	3108.1
48R-1, 117	669.07	A	3287.7
48R-1, 118	669.08	A	3066.0
48R-CC, 10	671.79	A	3458.0
49R-2, 147	680.57	A	3029.6
50R-2, 147	689.47	A	2423.9
50R-5, 147	693.97	A	2540.4
51R-1, 146	697.66	A	2411.8
51R-4, 1	700.71	A	3033.3
52R-1, 142	707.32	A	3417.4
52R-4, 41	710.81	A	3056.2

^a A = perpendicular to split-core surface; B = parallel to split-core surface; C = axial.

gamma-ray spectrometry tool (GTS), one of the main components of the geochemical combination, was not working properly in either the primary or the spare tools. The geochemical logging run was not made, and the lithoporosity combination was rigged at 2215 hr.

The lithoporosity combination consisted of spectral gamma-ray (NGT), neutron porosity (CNT-G), lithodensity (LDT), and temperature (AMS) tools (see "Explanatory Notes" chapter). The pipe was lowered to 294 mbsf to prevent the unstable upper part of the hole from collapsing. The log was recorded from the bottom of the hole (715.5 mbsf) up to the base of the pipe (294 mbsf) without any problem or delay (Figs. 37 and 38). The third logging run ended at 0130 hr on 4 January.

Table 16. Thermal conductivity and temperature drift rate, Site 737.

Core, section, interval (cm)	Depth (mbsf)	Thermal conductivity (W/m/°C)	Temperature drift rate (°C/min)
119-737A-			
2H-1, 100	6.00	0.738	0.035
4H-1, 50	24.50	0.603	-0.008
5H-1, 50	34.00	0.792	0.009
7H-1, 50	53.00	0.901	0.097
9H-3, 75	75.25	0.724	0.068
11H-2, 50	92.50	0.831	0.037
12H-1, 50	100.50	0.767	0.056
13H-2, 50	111.50	0.757	0.020
15H-3, 50	132.00	0.779	-0.039
16H-3, 70	141.70	0.577	0.012
17H-3, 70	151.20	0.405	-0.030
18H-3, 70	160.70	0.869	0.060
19X-1, 70	167.20	0.570	0.058
21X-1, 100	186.90	0.737	0.045
23X-2, 60	207.40	0.389	-0.096
25X-2, 70	226.90	1.019	0.028
27X-2, 80	246.40	0.844	0.038
28X-1, 70	254.50	0.441	-0.13
119-737B-			
5R-2, 70	255.70	0.623	0.004
6R-1, 80	264.00	0.657	-0.053
6R-3, 80	267.00	0.749	-0.029
7R-1, 70	273.60	1.158	0.04
8R-2, 70	284.70	0.885	0.064
9R-2, 40	294.10	0.860	0.023
10R-2, 70	304.00	1.105	0.056
11R-2, 70	313.70	1.493	0.042
12R-3, 70	324.80	0.697	0.041
13R-1, 75	331.55	0.871	0.014
15R-1, 75	350.85	0.740	-0.11
16R-1, 75	360.55	0.722	-0.064
17R-1, 80	370.20	0.887	0.022
18R-1, 80	379.90	0.159	-0.086
20R-2, 50	400.40	0.227	-0.69
21R-2, 50	410.10	0.873	0.044
22R-3, 50	421.20	0.568	-0.048
23R-1, 40	427.80	1.035	0.026
24R-3, 60	440.60	0.475	-0.028
25R-2, 70	448.90	1.156	0.049
26R-3, 87	460.27	1.094	0.041
27R-3, 84	469.84	0.789	0.047
28R-2, 81	478.01	1.307	0.022
29R-3, 70	489.10	1.113	0.029
30R-3, 75	498.75	1.056	0.016
33R-2, 80	526.30	1.466	0.02
34R-2, 10	535.20	1.336	0.029
35R-2, 50	545.30	0.583	-0.008
36R-3, 50	556.40	1.348	0.060
37R-3, 50	566.00	1.124	0.041
38R-6, 50	580.20	1.120	0.036
42R-4, 60	615.80	0.285	-0.28
43R-2, 45	622.25	1.385	0.042
44R-1, 45	630.45	0.368	-0.34

The heave compensator system was used at the beginning of the logging, but was soon turned off because the motion of the compensated heave did not correspond to the heave of the ship. During the two logging runs the tension on the cable was relatively steady, indicating that the heave of the ship was not adversely affecting the data.

Log Quality

Most of the logs were of good quality (Figs. 36 through 39); nevertheless, some of them were affected by the hole conditions or by heave motion and have bad responses. This was particularly the case for the photoelectric effect, which is strongly in-

fluenced by barite in the mud. However, the data from the upper part of the logging section above 550 mbsf seem usable, because the high-density barite concentrated mainly at the bottom of the hole after circulation was stopped. In this interval the photoelectric effect curve increases with increasing depth from a value at 94 mbsf of 3.3, which is close to the index of siliceous sedimentary rocks, to a value at 550 mbsf of 4.6, which corresponds to the index of carbonate rocks (Fig. 37).

The caliper response during the first run of the seismic stratigraphic combination appears as a straight line at 33 cm which probably indicates that it was fully opened in a washed and caved section. Although the caliper curve remained fairly constant during the second run, it gives an average value of 30.4 cm, which is close to the expected hole diameter (28 cm). The synthetic caliper computed from the four transit times recorded with the sonic tool (Fig. 36) confirms that the hole is strongly caved in the upper part of the drilled section, from 94 to 385 mbsf.

The velocity and bulk-density curves obtained with the logging tools are in good agreement, with the same measurements made continuously on the cores. The bulk densities read by the logging tool increase from 1.51 g/cm³ at 300 mbsf to 2.19 g/cm³ at the bottom of the hole (715.5 mbsf). For comparison, laboratory measurement of bulk density on the cores increases from 1.5 g/cm³ at 300 mbsf to about 2.3 g/cm³ in the lower part of the hole. The density trough of 2.19 g/cm³ given by the logging tool in the lower section of the hole (670 mbsf) is probably due to the existence of washed zones. Big deviations can be seen on the quality curve of the density tool, confirming existing caved zones at this depth (Fig. 37).

The velocity increases on the logging curve from 1417 m/s at 100 mbsf to 2257 m/s at 600 mbsf. In the same interval, the laboratory core measurements have close values that increase from 1500 m/s at 100 mbsf to 2250 m/s at 600 mbsf. Cycle skipping (e.g., first arrival, sonic wave train, or detection error at the tool receivers causing measurement of an erroneously long or short time) is rare on the sonic record—occurring only between 574 and 596 mbsf—which attests to the good results of this acoustic logging tool.

The neutron porosity tool indicates that porosity values for the interval from 300 to 700 mbsf decrease from 60% to 44% (Fig. 37). The porosities measured from core samples decrease from about 60% to 30% for the corresponding interval. The high porosities given by the neutron tool in the lower part of the hole do not give a good fit with the laboratory core measurements. The neutron tool measures the hydrogen content of the formation, and the porosity calculated from this measurement is based on the equivalent water content. However, the presence of clay minerals in the lower section of the hole (see "Lithostratigraphy and Sedimentology" section) causes the neutron tool to overestimate the porosity as a result of the hydrogen atoms in the clays. The porosity calculated from the density logging tool fits better than the neutron porosity, with the porosity core measurements decreasing from 68% to 28% from 300 to 700 mbsf.

Deep and medium resistivities from the dual induction tool are similar for the entire logged section, increasing from 0.3 ohm-m at 100 mbsf to about 1.0 ohm-m at 600 mbsf. The focused resistivity curve from the SFLU gives higher values than those of the induction tool along the entire logged section, with a consistent difference of about 0.15 μm . This difference in the resistivity values from the focused tool and from the induction tool suggests that the salinity of the formation was higher than the salinity of the drilling water at Site 737. The data measurements from the SFLU contain high-frequency peaks as a result of the heave influence during recording of the log. Figure 36 shows the SFLU curve without the high-frequency peaks after smoothing the data using a filtering program.

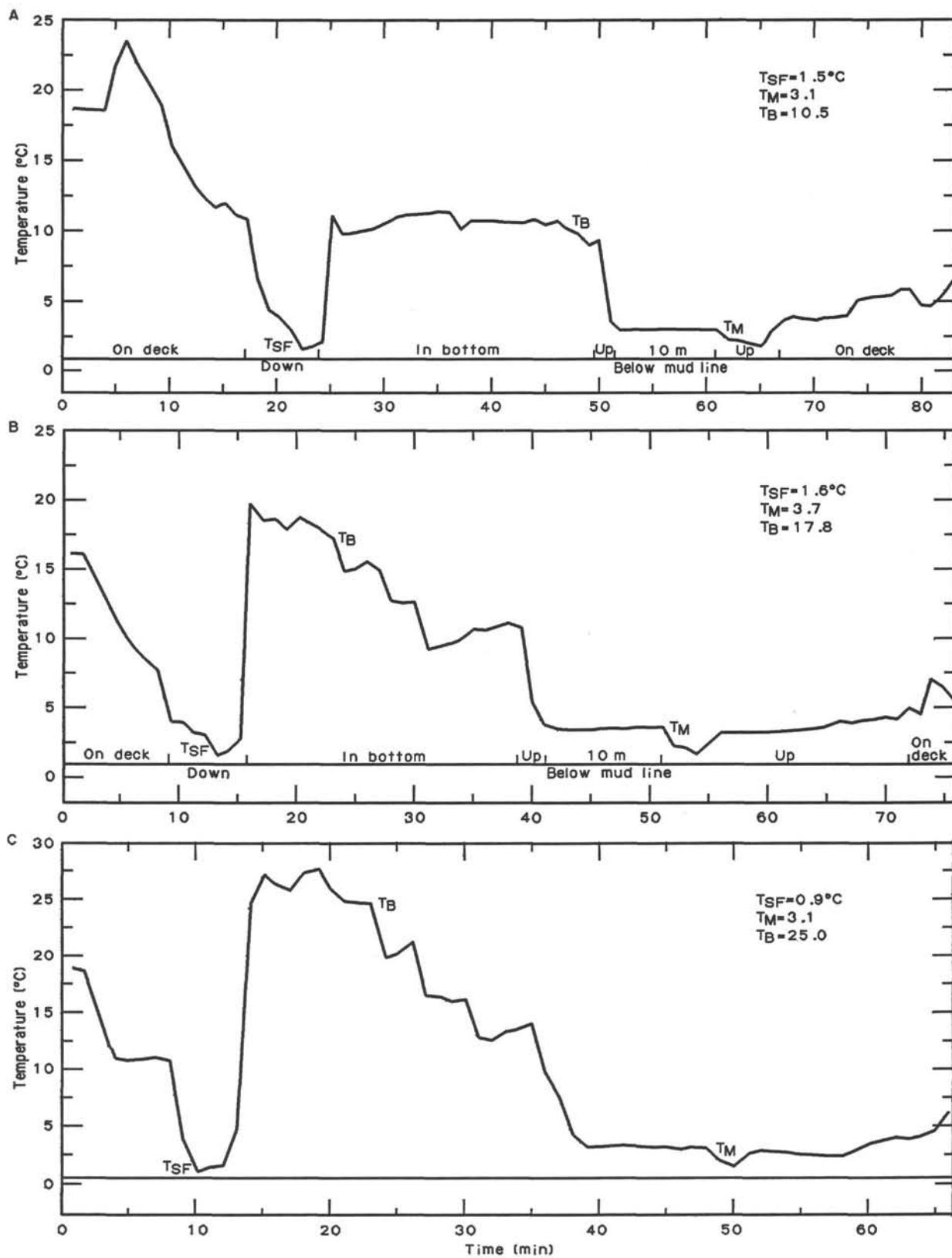


Figure 34. Temperature vs. measurement time curves for the three Uyeda probe deployments in Hole 737A. T_M = temperature at mud line (10 mbsf); see Table 17 for measurement data. A. 81.5 mbsf. B. 128.5 mbsf. C. 226.5 mbsf.

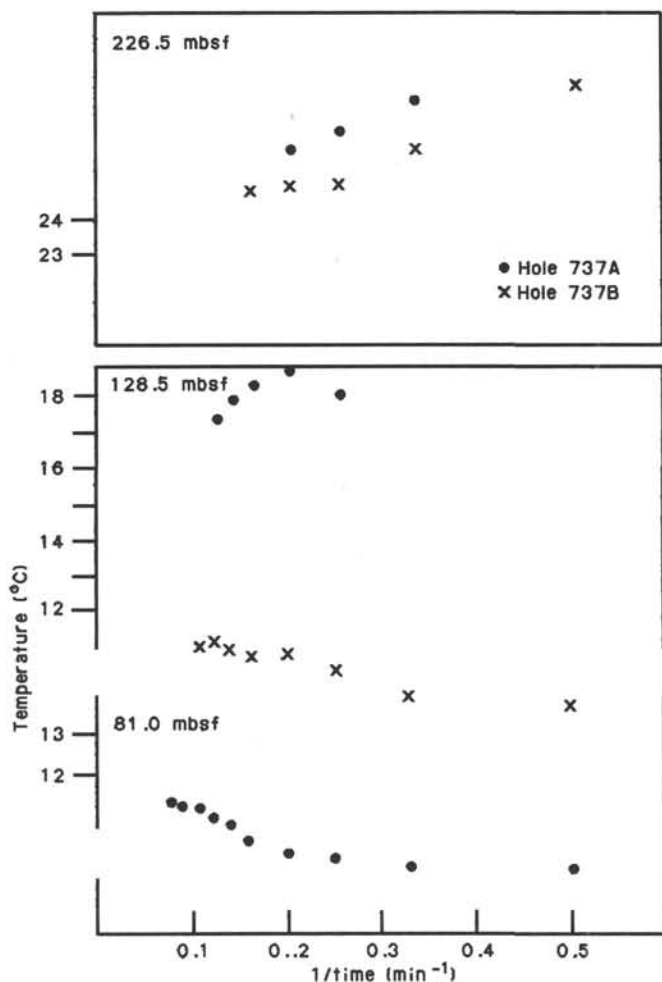


Figure 35. Equilibration curves of three temperature probe deployments.

Table 17. Temperature measurements, Hole 737A.

Core	Depth (mbsf)	Probe in sediment (min)	Probe equilibration time (min)	Temperatures ^a	
				T _{SF} (°C)	T _B (°C)
9H	81.5	25	10	1.5	12.0
14H	128.5	22	7	1.6	21.1–17.1
24X	226.5	22	8	0.9	23.5–23.7

^a T_{SF} = lowest temperature immediately prior to probe penetration;
T_B = equilibration temperature in sediment.

Logging Units

Six logging units were identified in Hole 737B (Fig. 39). Significant boundaries were identified in each of the units based on simultaneous variations on different logs. The following is a listing and interpretation of these boundaries.

Logging Unit 1 (94 to 250 mbsf)

Logging unit 1 appears as a low-resistivity (3.5 ohm-m) low-velocity (1417 m/s) section that corresponds to the high-porosity diatomaceous oozes. The gamma ray increases slightly down-hole in this section from 10 to 20 API units. This increase could be interpreted as a rise in the percentage of clay minerals or volcanic minerals toward the lower part of the unit. Two peaks of higher velocity, 1550 m/s, that occur at 125 and 190 mbsf prob-

ably represent layers that are more lithified than the surrounding sediment. The hole was not logged between logging units 1 and 2 because of the bridge encountered at 250 mbsf; thus, the exact depth where logging unit 1 ends and where logging unit 2 begins is not known.

Logging Unit 2 (300 to 320 mbsf)

In comparison with logging unit 1, logging unit 2 is characterized by an increase in the average velocity and resistivity of the sediments. The average velocity is about 1682 m/s, and the resistivity ranges from about 0.5 to 0.6 ohm-m. Several peaks within the unit that correspond to an increase in the resistivity, sonic velocity, and density indicate the presence of sediments more consolidated than the surrounding material. These layers also give a strong peak of radioactivity, particularly in a layer at 313 mbsf, the boundary of logging units 2 and 3. This layer seems thicker and more consolidated than the other layers. The response of the gamma spectrometry shows that both potassium and uranium are enriched in the material of this layer. The increase of the radioactivity indicated by the gamma-ray tool is due either to clay minerals or to the presence of potassium feldspar.

The kind of lithology that fits the logging response of this unit is probably an alternation of consolidated detrital layers and soft sediments. The soft sediments could correspond to the nannofossil ooze identified at this depth in the lithologic description. The boundary between logging units 2 and 3 is identified in the lithologic and stratigraphic section as a hiatus from 15 to 23 Ma between the upper Oligocene and the middle Miocene.

Logging Unit 3 (320 to 377 mbsf)

The top of logging unit 3 is characterized by the disappearance of the localized peaks described for logging unit 1. Only a few variations affect the logging curves in this interval, and the records appear mainly as straight lines. The values of logging parameters are close to the average values at logging unit 2. Logging unit 3 corresponds to the upper part of the glauconitic calcareous claystones described in the lithologic section.

Logging Unit 4 (377 to 515 mbsf)

The top of logging unit 4 (377 mbsf) is differentiated from logging unit 3 on the resistivity and sonic curves. The velocity and resistivity show a strong increase from 1682 to 1892 m/s and from 0.5 to 1.0 ohm-m, respectively. The other parameters, particularly the density, also indicate a change at this depth (Fig. 39). The abrupt increase in resistivity, sonic, and density values at the top of logging unit 4 is evidence for the existence of sediments that are more lithified than in the previous logging units. A diagenetic front or a compaction effect could explain this boundary, although the description of the cores at this depth mentions only the same lithology as that above (calcareous claystone) but without diatoms. The density curve begins to increase regularly with depth from the top of logging unit 4, attesting to the existence (for the first time in this hole) of a distinct compaction trend.

Thus, the point where diatoms disappear from the sediments corresponds on the logging records to a diagenetic effect and the beginning of a compaction trend.

A peak of higher velocity occurs in this logging unit at 426 mbsf, which also corresponds to an increase in density. This peak could be interpreted in the present sedimentary context as a thin layer of chert.

The transition between logging units 4 and 5 based on the log responses again occurs within a rather short interval and is deduced mainly from the resistivity and velocity curves.

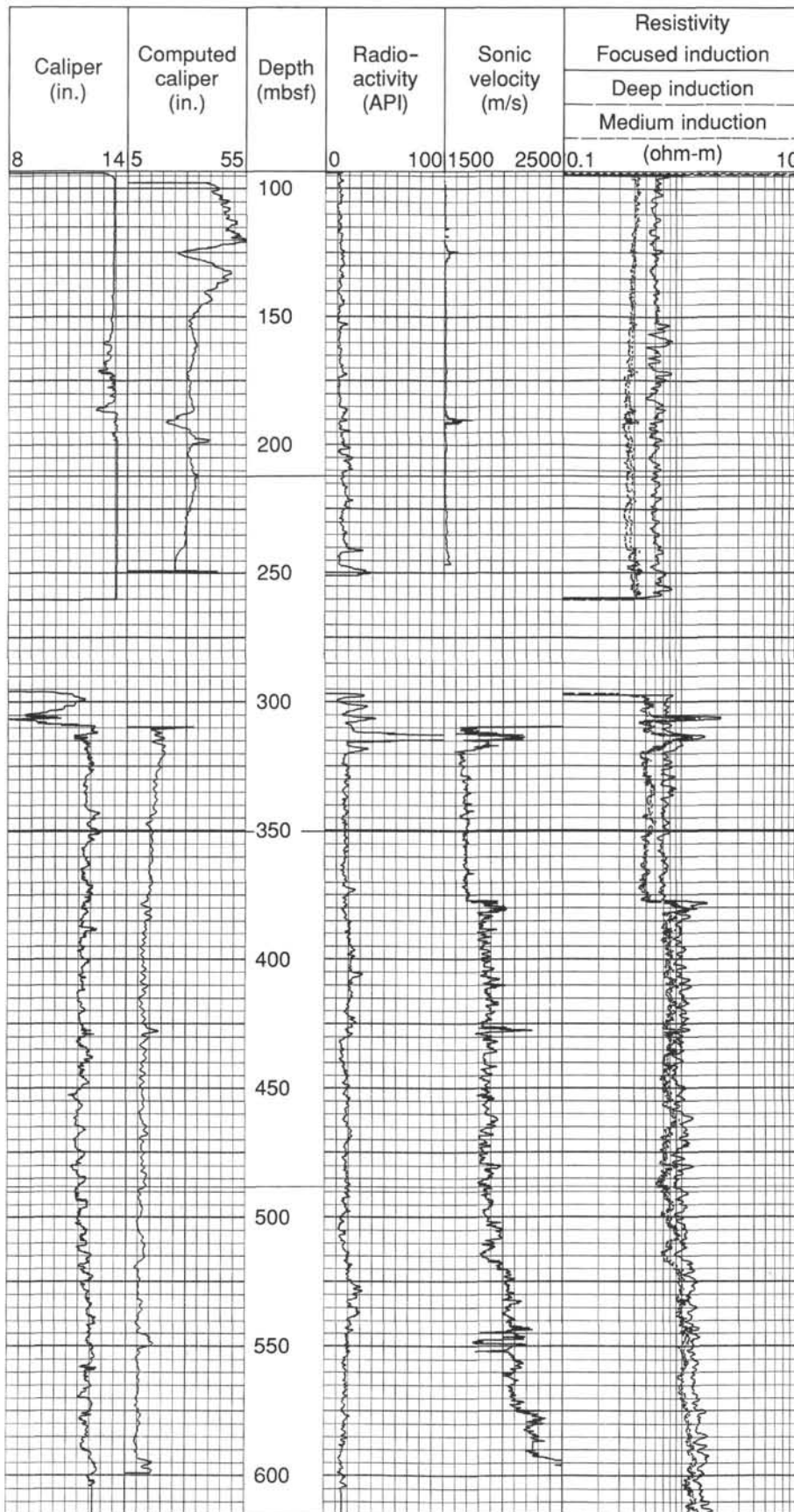


Figure 36. Downhole logs for the seismic stratigraphic combination: caliper, gamma ray, sonic, and medium-deep-focused resistivity for the interval from 94 to 610 mbsf, Hole 737B.

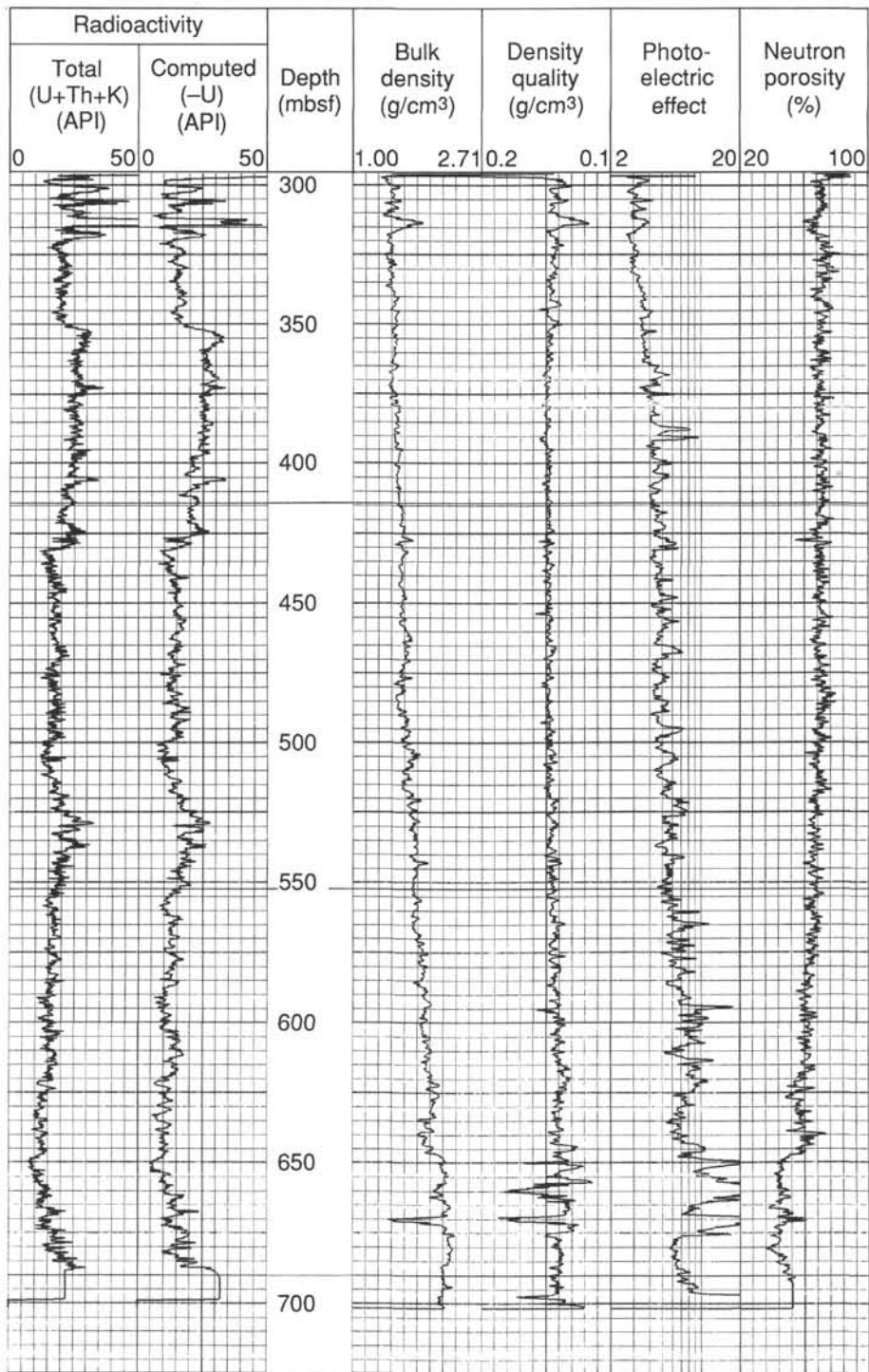


Figure 37. Downhole logs for the lithoporosity combination: total gamma ray, computed gamma ray, density, density calibration, photoelectric effect, and neutron porosity for the interval from 280 to 690 mbsf, Hole 737B.

Logging Unit 5 (515 to 645 mbsf)

The abrupt increase in resistivity and velocity at the top of logging unit 5 is less strong than that between logging units 3 and 4, but the increase in density as a function of depth becomes higher in this unit, indicating a new compaction trend stronger than that in the previous unit. Increases in velocity and

resistivity with increasing depth also show this compaction trend. Logging unit 5 constitutes the lower part of the calcareous claystone described in the lithologic section, and it is differentiated from logging unit 4 on the basis of a higher carbonate content. Although the porosity calculated from the density log is high in this interval, the porosity decreases from 56% at the top to 40% at the bottom of the unit.

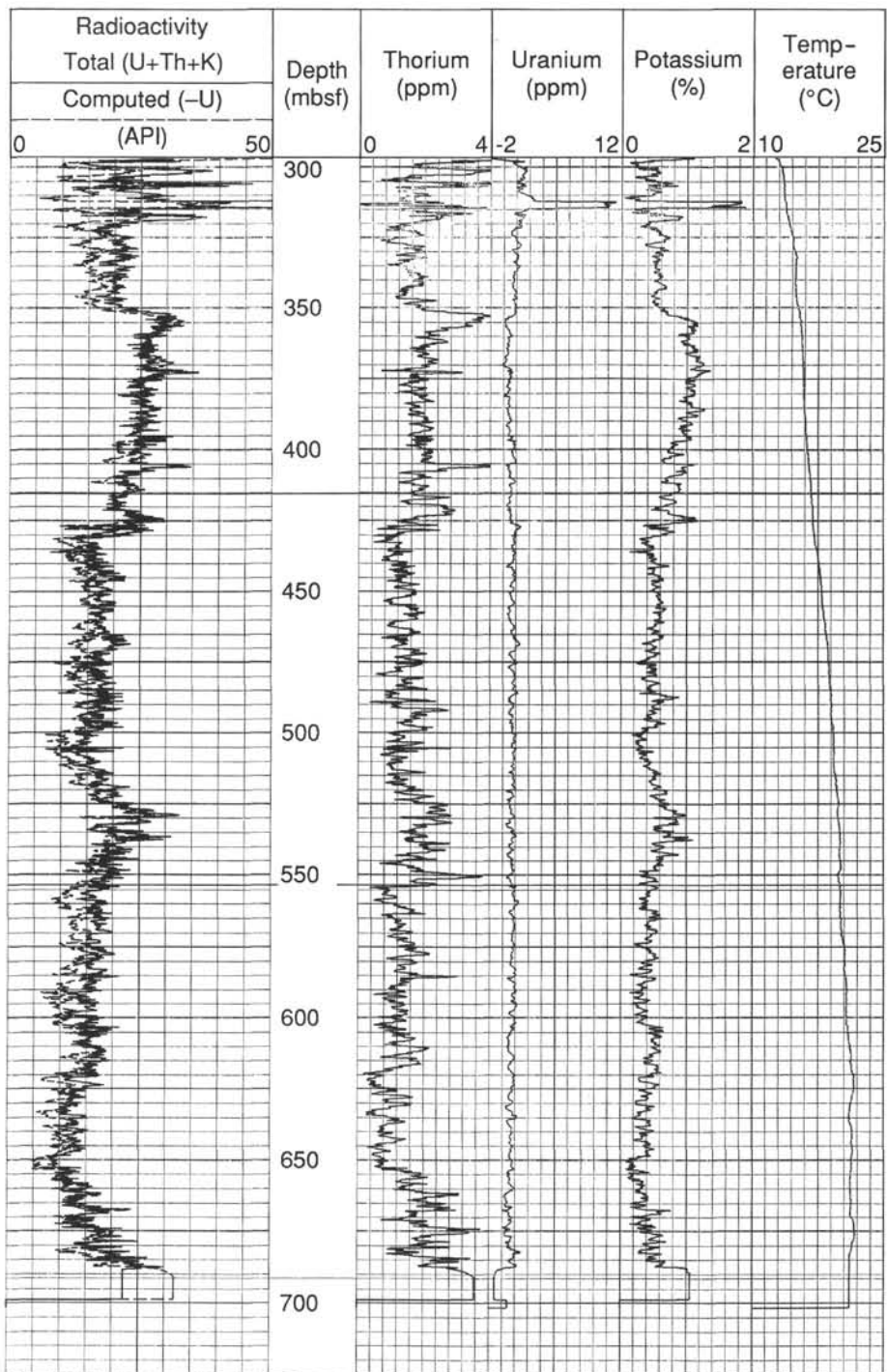


Figure 38. Downhole total gamma-ray, computed gamma-ray, thorium, uranium, potassium, and temperature logs for the interval from 300 to 690 mbsf, Hole 737B.

Logging Unit 6 (645 to 701 mbsf)

The definition of this last logging unit is based only on the porosity and density curves because no data from the seismic stratigraphic combination were recorded at the bottom of the hole. At the boundary between logging units 5 and 6 the porosity calculated from the density log drops from 40% to 28% and the density increases from 1.93 to 2.19 g/cm³ (645 mbsf). These values are close to those for a consolidated rock and are in good agreement with the limestone described in the "Lithostratigra-

phy and Sedimentology" section. A thin low-density-high-porosity layer occurs within logging unit 6 (670 mbsf) and corresponds to the unconformity between middle and upper Eocene rocks.

Poor Core-Recovery Intervals

Two intervals of poor core recovery at 118-128 and 166-224 mbsf in the diatomaceous ooze unit of the lithologic section correspond to a logging section of low sonic velocity and low resistivity. The increase in resistivity and sonic velocity recorded

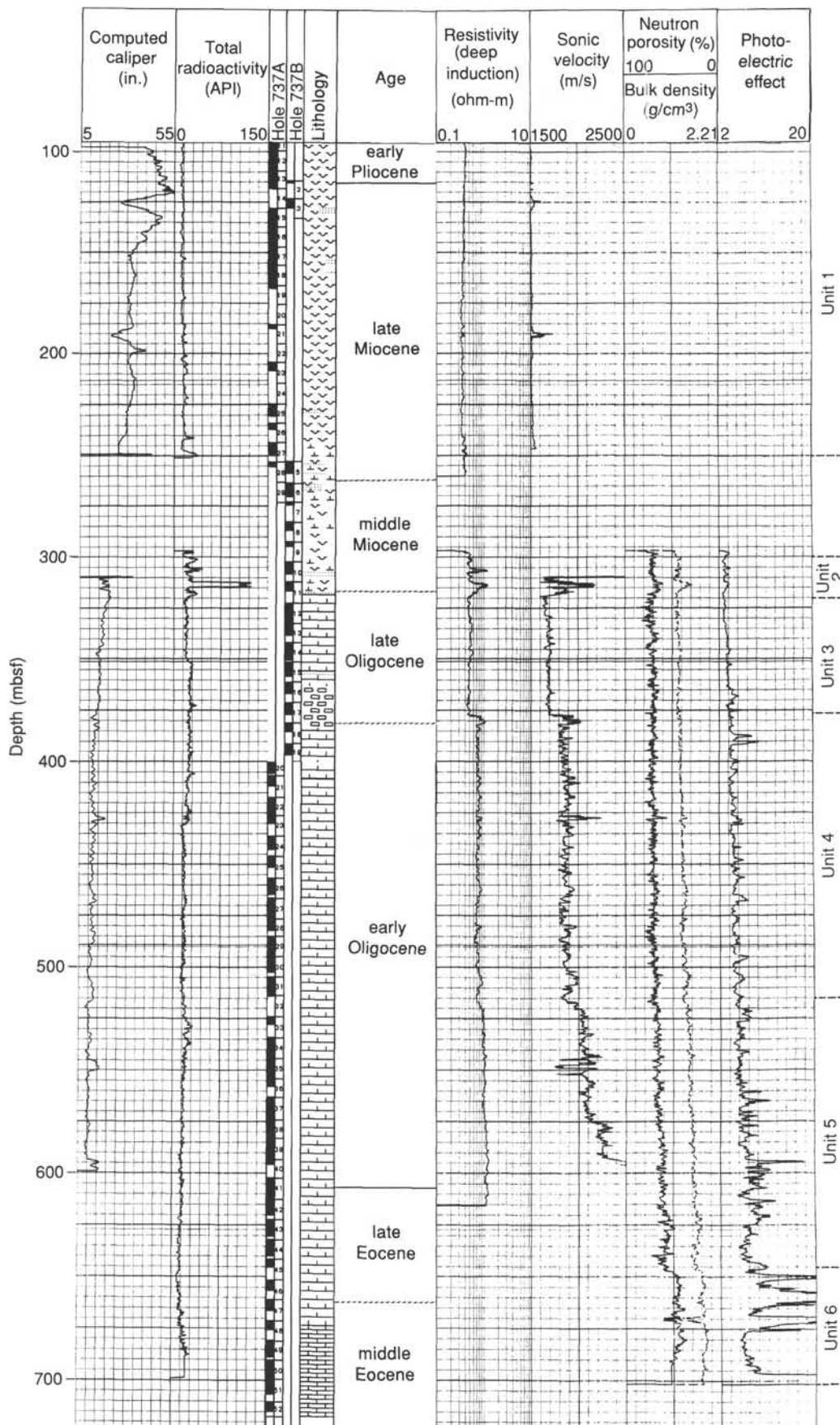


Figure 39. Summary compilation of downhole logs used to define the six logging units at Site 737.

with the logging tools at 125 and 190 mbsf also attests to the presence of thin lithified layers that probably correspond to sand or gravel layers in these intervals.

The interval at 514–524 mbsf at the top of logging unit 5 was not well sampled by coring. As described in the previous section, density, porosity, sonic velocity, resistivity, and photoelectric effect logging records indicate a rise in the lithification rate and carbonate content in this unit.

Synthetic Seismogram

A synthetic seismogram was computed for Site 737 to accurately tie the drilled sequence in the hole to seismic-reflection data over the site (Fig. 40A). The seismogram is based on velocity and density data from several sources (Fig. 40B).

The velocity data are compiled from downhole sonic logs (94–245 and 310–595 mbsf) and laboratory compressional-wave measurements (Hamilton Frame; 245–310 and 595–715 mbsf). A uniform velocity of 1500 m/s, from average laboratory measurements, is assumed for the interval 0–94 mbsf. A comparison

of the different velocity measurements made at Site 737 is shown in Figure 33 (short-dashed line = velocities from sonic logs, solid line = laboratory measurements, and long-dashed line = sonobuoy seismic data). Variations in the carbonate content profile shown in Figure 28 are probably responsible for many log variations and reflectors beneath Site 737.

Good density measurements are available only from down-hole logging in the lower part of the hole (300–700 mbsf). The laboratory bulk-density measurements were not used because they are too sparse to give a reliable synthetic seismogram (small density variations that are sparsely sampled give spurious reflection events). Instead, a uniform density was assumed for 0–300 mbsf. The synthetic seismogram is computed from the composite velocity and density curves (Fig. 40).

The synthetic seismogram illustrates the significant points that (1) for intervals in the upper 235 m of the hole, where few velocity (i.e., lithologic) variations are found, the synthetic seismogram shows only a few isolated low-amplitude reflections and (2) the largest reflection events (315 and 590 mbsf) result from uncorrected effects of layer dips and from use of the Dix

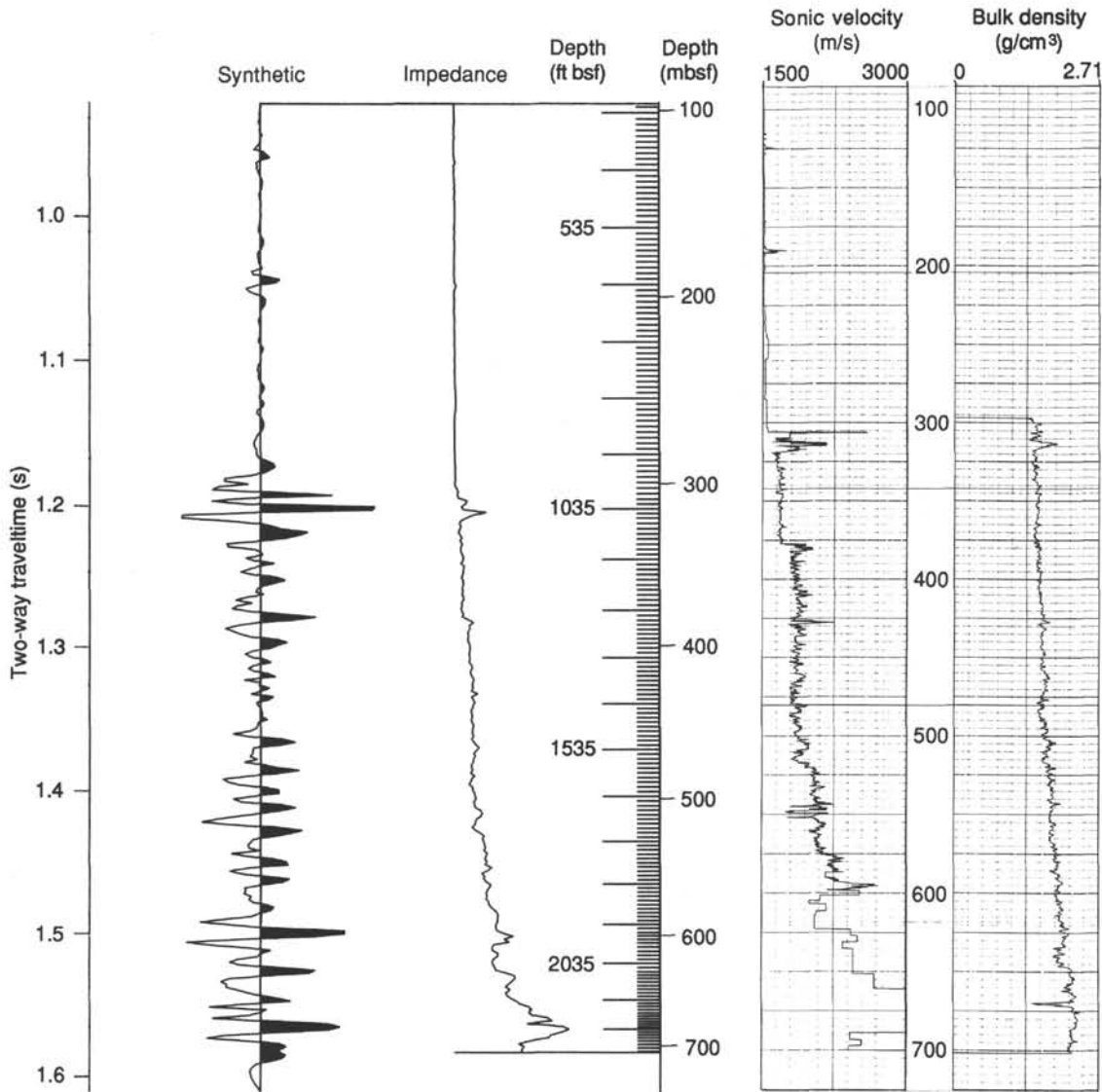


Figure 40. Synthetic seismic trace computed using impedance curve and the values of velocity (inverse of sonic log values) and density used to compute impedance for synthetic seismic trace (see text).

equation to compute interval velocities using large-offset reflection data (Shah and Levin, 1973). The depths shown in Figure 40 are from the synthetic seismogram.

In general, there is a good match between the width and relative amplitude of reflection peaks in the synthetic and observed seismic traces at Site 737 (Fig. 41). In part, the good correlation of peak spacing results from the band-pass filters used; however, the similarity in locations of high-amplitude peaks down the core is due to variations in acoustic impedance (i.e., lithology). Abrupt changes in reflection amplitude are more sensitive to the relative change in acoustic impedance than to the absolute

magnitude of the impedance. For example, the zone of large-amplitude reflections at 1.5 s (290–330 mbsf) is caused by two or three thin (less than 3–4 m thick) layers with velocities up to 2.6 km/s. Within this zone, the impedance contrasts between the layers of low-velocity (diatom ooze = 1.5 km/s; calcareous ooze = 1.7 km/s) ooze and high-velocity (2.1–2.6 km/s) silica-carbonate at 306 and 313 mbsf produce the major set of reflectors at 1.18–1.23 s. These reflectors are essentially an amplified image of the 0.07-s-long water gun signature, but with a double central peak (compare with the small isolated reflector at 190 mbsf).

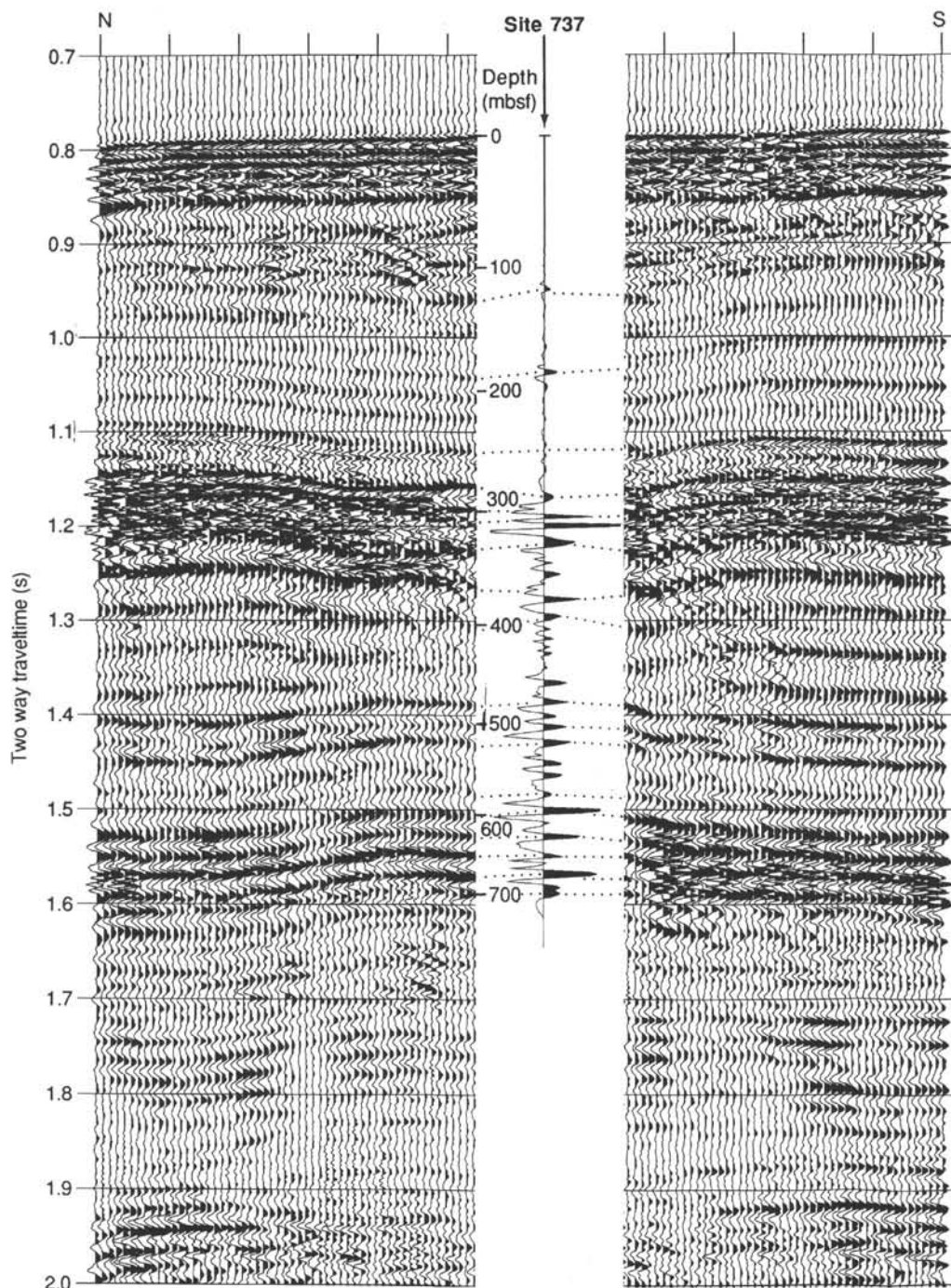


Figure 41. Comparison of vertical-incident seismic-reflection data recorded over Site 737 with the synthetic seismic-reflection trace computed from downhole and laboratory velocity and density measurements.

An abrupt increase in velocity at 380 mbsf (1.28 s) causes a similar shaped, but lower amplitude, band of reflectors to those at 313 mbsf. The increases in velocity (0.2 km/s) are similar at both levels, but no interbedded layers are present at 380 mbsf to produce the high-reflection amplitudes seen at 290–330 mbsf.

Reflection waveforms in the interval from 450 to 590 mbsf are more complex, in contrast to those at shallower levels. In this interval, downhole logs indicate oscillations in velocity of up to 0.3 km/s over distances of 5 to 10 m. These oscillations are superimposed on a gradual increase of velocity with increasing depth. Similar velocity variations are seen in the laboratory measurements. These velocity variations cause composite synthetic reflections that cannot be correlated with specific layers. The spacing of the reflectors is, to a greater extent than for the upper part of the well, controlled by the band-pass filter applied to the data (e.g., filtering for lower frequencies would produce a similar wave train but with wider spacing between peaks). The observation that some of these reflection peaks can be traced for at least 1.5 km across Site 737 indicates that the depositional (or diagenetic?) processes responsible for the velocity variations were probably widespread in their effect.

A prominent zone of high-amplitude reflectors characterizes the interval from 590 to 715 mbsf. These reflections occur where interbedded layers have greater velocity variations (0.4–0.5 km/s) than above, and these variations are superimposed on a steep velocity gradient at the lithologic boundary between overlying claystone and underlying limestone. The large reflection peak at 600 mbsf in the synthetic data does not occur at the claystone/limestone boundary—instead, the peak results from a single 5–10-m-thick layer (limestone?) within the claystone unit. The major lithologic (and velocity) boundary lies about 70 m deeper, at 670 mbsf, and corresponds with a strong, continuous, double-peak reflector in the seismic-reflection profile (1.55 s; Fig. 41) crossing Site 737. The synthetic profile indicates high-amplitude reflections of greater complexity than the seismic profile at this major boundary.

Summary

In summary, a suite of 10 downhole logs was successfully recorded at Site 737, leading to identification of six distinct logging units. These logging units indicate that significant lithologic variations are likely in the shallow diatomaceous and deep calcareous sedimentary sections (Fig. 42). Distinctive inflections in the logging curves are also observed at unconformities.

A good correlation can be made between the synthetic and observed seismic-reflection traces at Site 737. In the upper part of the hole (94–450 mbsf) the synthetic trace is dominated by reflection events resulting from thin (less than 3–4-m-thick), isolated, higher-velocity layers within the diatom and nannofossil oozes and from small (0.2–0.3 km/s), abrupt increases in velocity at lithologic boundaries (two are unconformities). Below 450 mbsf, the waveforms are more complex, resulting from numerous oscillations in velocity (up to 0.3 km/s) occurring over 5–10-m-thick intervals and superimposed on a gradual increase in velocity with depth. These oscillations and reflections suggest that lithologic or diagenetic variations, of widespread extent, occur within the calcareous claystone section. From 590 to 715 mbsf, high-amplitude reflectors characterize the synthetic and observed seismic traces.

The principal reflection peak in the synthetic data (600 mbsf) occurs over an isolated high-velocity (limestone?) layer in the claystone, about 45 m above the principal reflector in the observed data, which follows the major lithologic (and velocity) boundary between claystone and limestone. The possible unconformity between upper and middle Eocene rocks at 670 mbsf

lies within the complex waveform of the synthetic and observed data near the claystone/limestone boundary.

SEISMIC STRATIGRAPHY

The geologic structure of Site 737 and the surrounding region has been elucidated by analysis of seismic sections along the tracks shown on Figure 1. The upper seismic sequence is displayed in detail on the 3.5-kHz precision depth recorder (PDR) record (Fig. 43). The deeper structures are seen on the single-channel seismic lines recorded by *JOIDES Resolution* (Figs. 44 and 4). The correlation between the stratigraphic section recovered from the Holes 737A and 737B with the seismic sections is discussed in the “Logging” section (Figs. 41 and 42).

The seismic sequence is divided into three major units (Table 18). The major reflectors and seismic units are designated according to Munsch and Schlich (1987), but depths at the site and datings are based on the results of this leg (see “Biostratigraphy” and “Logging” sections and Fig. 42).

The major reflections do not correspond in detail to the major sedimentation breaks but seem to be more closely related to the changes of sedimentary facies associated with unconformities. Reflector A1, which is dated to approximately 2.6 Ma at Site 736 (see “Summary and Conclusions” section, “Site 736” chapter), and the overlying seismic unit S1 are represented at Site 737 by only a 1.5-m-thick cover of Pleistocene lag sand (lithologic Unit I; “Lithostratigraphy and Sedimentology” section).

Units S1 and S2

Well-defined reflectors within unit S2 are observed on the 3.5-kHz PDR record to a depth of 200–300 mbsf near Site 737 (Fig. 44), assuming a mean sound velocity of 1550 m/s (see “Physical Properties” section). They show a basically horizontal and parallel—but moderately wavy—stratification pattern near the site in the upper Miocene to lower Pliocene (3.4–8.2 Ma) sequence of soft diatom ooze. However, local moundlike structures of uncertain origin are observed approximately 5 km away from the site. The one to the northwest seems related to local elevations of the basement, as seen on the nearby multichannel line MD 26-13.

The upper sequence (S2) at Site 737 thickens to northwest and is covered by younger sediments (Fig. 44). The sequence of reflectors is almost concordant, but the amplitude of the waves decreases upward. This suggests pelagic-type sedimentation, forming blanketing sheets of sediment over the bottom topography (Sangree and Widmier, 1977). This pattern is superimposed upon large-scale sigmoidal prograding units forming the slope of the former trough between the huge sedimentary accumulations at Sites 736 and 737. The toes of the prograding units downlap onto reflector A. The floor of the former trough lay approximately 700 m below the top level of the surrounding sedimentary accumulations. The prograding sequence is also observed on seismic line MD 26-4 (Munsch and Schlich, 1987), so its total width exceeds 30 km. The oldest prograding unit west of Site 737 is probably correlated with the middle Miocene sequence observed between 263 and 315 mbsf in Hole 737B, but older prograding units might be present east of the site. The topmost prograding unit may, with some doubt, be traced to a reflector a small distance above reflector A1, which has an estimated age of 2.6 Ma in Hole 736.

Above the 2.6-Ma level a marked change from prograding fill to onlap fill and general leveling of the topography is observed in that part of the trough, which was left unfilled. A similar change in deposition pattern was described north of Site 736 (see “Seismic Stratigraphy” section, “Site 736” chapter). The

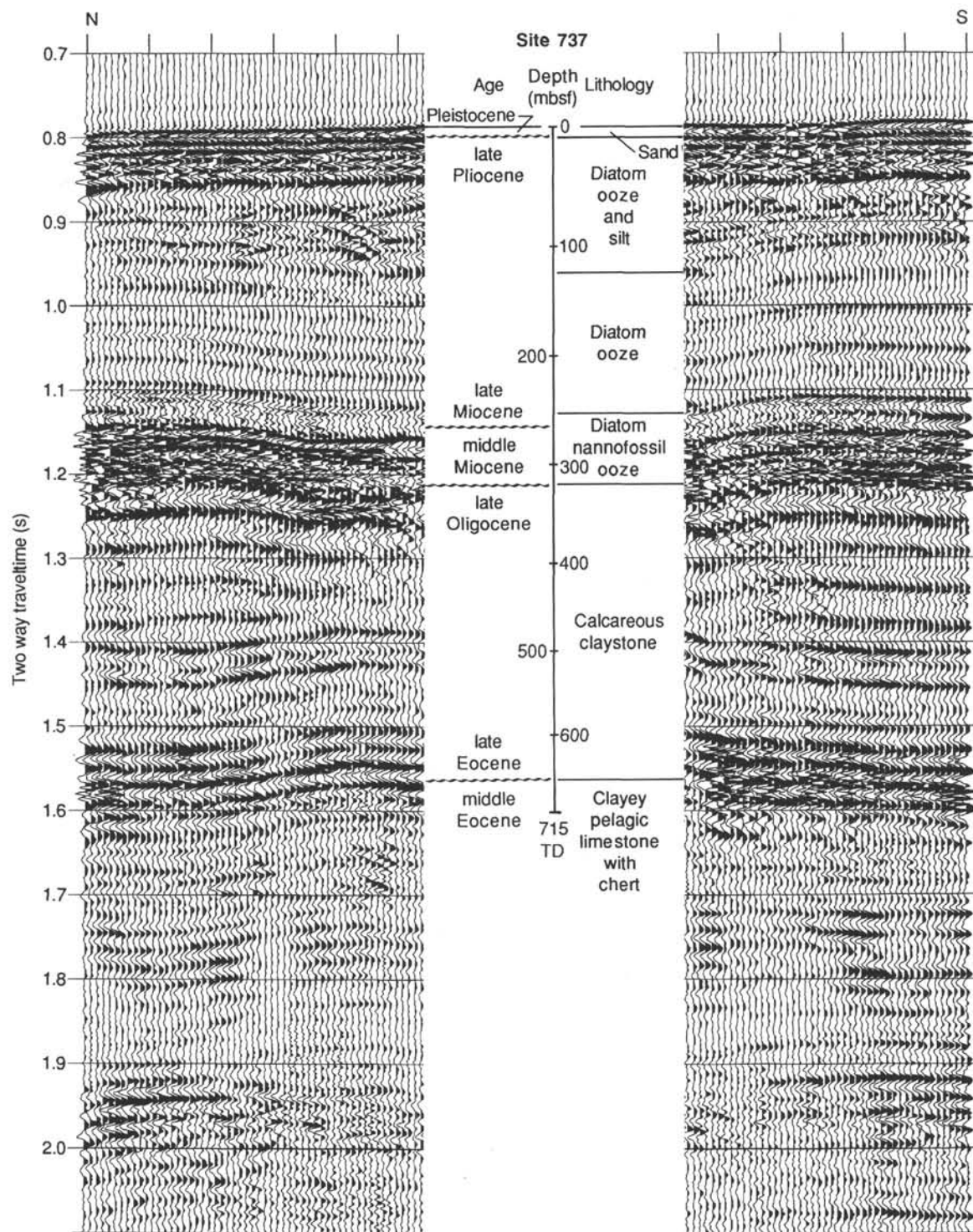


Figure 42. Seismic section over Site 737 showing depths to major lithologies and unconformities. Depths are from synthetic seismic trace in Figure 41.

new fill seems to consist of a pile of lenticular sediment bodies that are thickest on the southeastern flanks of the paleotrough, displacing the deepest part of the trough to the northwest through time. Complete infilling eventually leads to the nearly level present-day seafloor.

The "topsets" of the prograding units are commonly preserved near the level of the present-day seafloor, indicating little erosion since deposition in the late Miocene. However, from a

point roughly 14 km northwest of Site 737, truncation of reflections at the seafloor and the hiatus observed at about 1 mbsf at the site indicate an erosional unconformity at or just below the seafloor in this area. This unconformity probably extends to the eastern edge of the Kerguelen-Heard Plateau, about 50 km east of the site, where it merges with reflector A.

The overall pattern of sedimentation during the middle Miocene to early Pliocene seems to have been pelagic sedimentation

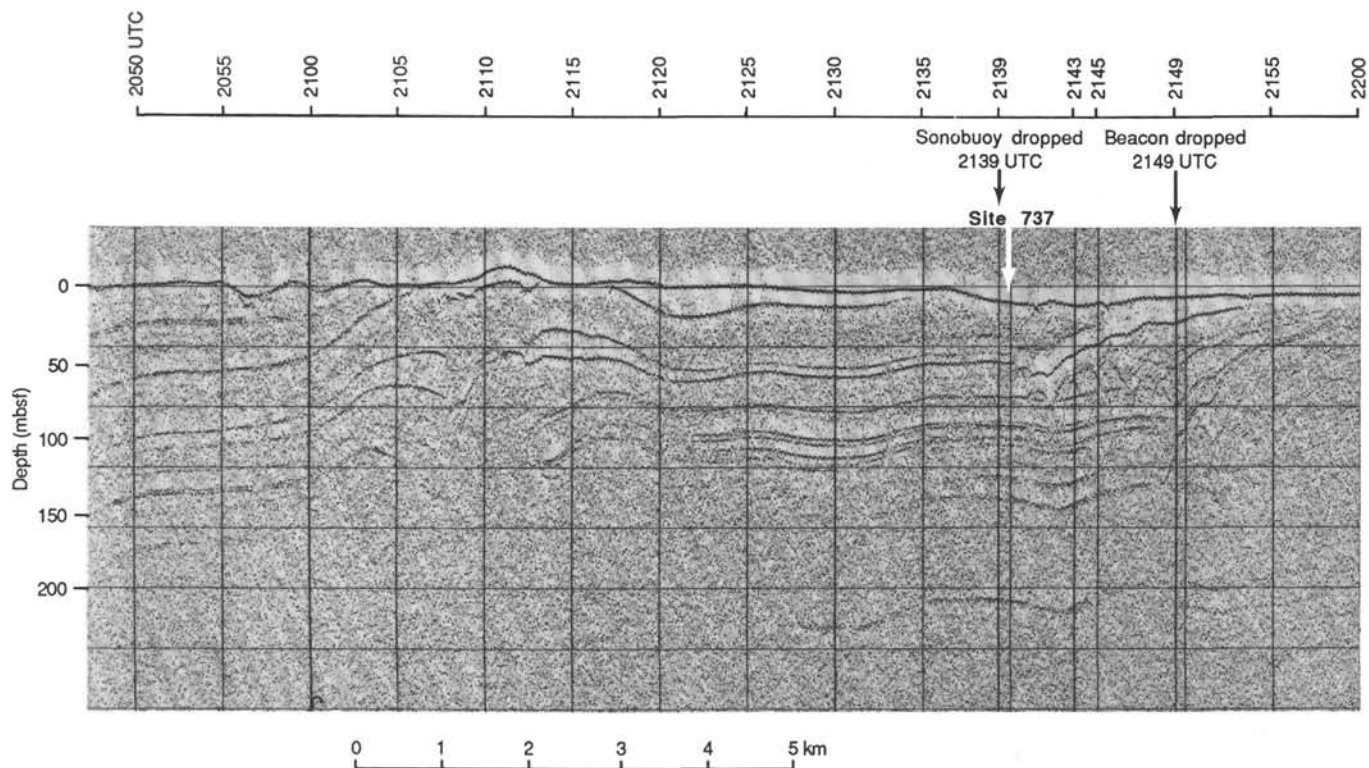


Figure 43. Five-kHz echo-sounder record over Site 737. The track is marked on Figure 1. Note the deep penetration in the water-rich diatom ooze. Moundlike structures are on both sides of the site. An erosional unconformity is shown by truncated reflections at the seafloor.

modified by a weak current from a southerly direction. The maximum accumulation rate of the diatom ooze occurred over the lee slope of the sediment-drift areas on the plateau, while weak nonerosive currents prevented net sedimentation in the trough between the drifts. The microfossil assemblages do not indicate much reworking of older strata, and the seismic data seem to indicate that erosion contemporaneous with the deposition of the prograding sequence was limited. The dominant source of sediment grains was mainly pelagic production, especially from water over and southeast of the northern plateau. The latter area, at the edge of the plateau, could possibly be associated with the upwelling suggested by the radiolarian assemblage ("Biostratigraphy" section).

The change in the sedimentation pattern at approximately 2.6 Ma corresponds to the latest Cenozoic time of increased intensity of Antarctic glaciation and initiation of glaciation in the Northern Hemisphere (Kerr, 1987) and may signal a change in intensity and flow path for the Antarctic surface-water masses at the plateau. At roughly the same time an influx of terrigenous material from Kerguelen and its surrounding shelf areas is recorded in the sediments in Site 736. This influx could be related to a lowering of the sea level caused by increased glaciation and increased intensity of ice rafting.

It is remarkable that the level to which the upper Miocene through Holocene sediments were deposited, forming the present-day nearly level seafloor, seems to have varied little through time. This could suggest that the magnitude of the water depth above this level has not changed much from that of today. Consequently, the level of the unconformity marked by reflector A appears to have subsided to its present-day level before the middle Miocene. However, some presumably small-scale faulting may have occurred since the middle Miocene (Fig. 45).

SUMMARY AND CONCLUSIONS

Site 737 (target Site KHP-3; 50°13.67'S, 73°01.95'E, water depth 564 m) lies on the northern Kerguelen-Heard Plateau about 130 km southeast of Site 736. The 714-m-thick middle Eocene to lower Pliocene section cored (overlain by a 1.5-m-thick Quaternary sand) in two holes at Site 737 begins almost exactly (3.4 Ma) where coring was terminated at Site 736. Thus, together the two sites form a composite reference section for the upper part of the sedimentary section of the northern part of the Kerguelen-Heard Plateau, and they constitute a valuable paleoceanographic reference section for the late Paleogene and Neogene at about 50°S.

Lithostratigraphy

Six lithologic units are recognized at Site 737: Unit I is a 1.5-m-thick Quaternary black calcareous and pumiceous sand mixed with diatom ooze that unconformably overlies Unit II, a lower Pliocene and upper Miocene olive to olive gray diatom ooze (1.5–244.1 mbsf), which conformably overlies the upper and middle Miocene diatom-nannofossil ooze (244.1–306.6 mbsf) of Unit III. Unit III conformably overlies the middle Miocene Unit IV, a sandy porcelaneous siltstone with mixed volcanic sand and diatom-nannofossil ooze (306.6–312.8 mbsf), which unconformably overlies (in sharp contact) Unit V, a lowermost Miocene to upper Eocene calcareous claystone (313–671.7 mbsf), with clayey limestone at the unit base. The basal Unit VI cored at Site 737 is an upper middle Eocene clayey limestone (677.6–715.5 mbsf) that contains some thin chert layers and is separated by a hiatus from the overlying Unit V.

The sedimentary record at Site 737 is characterized by an early phase of carbonate-clay deposition (late middle Eocene to

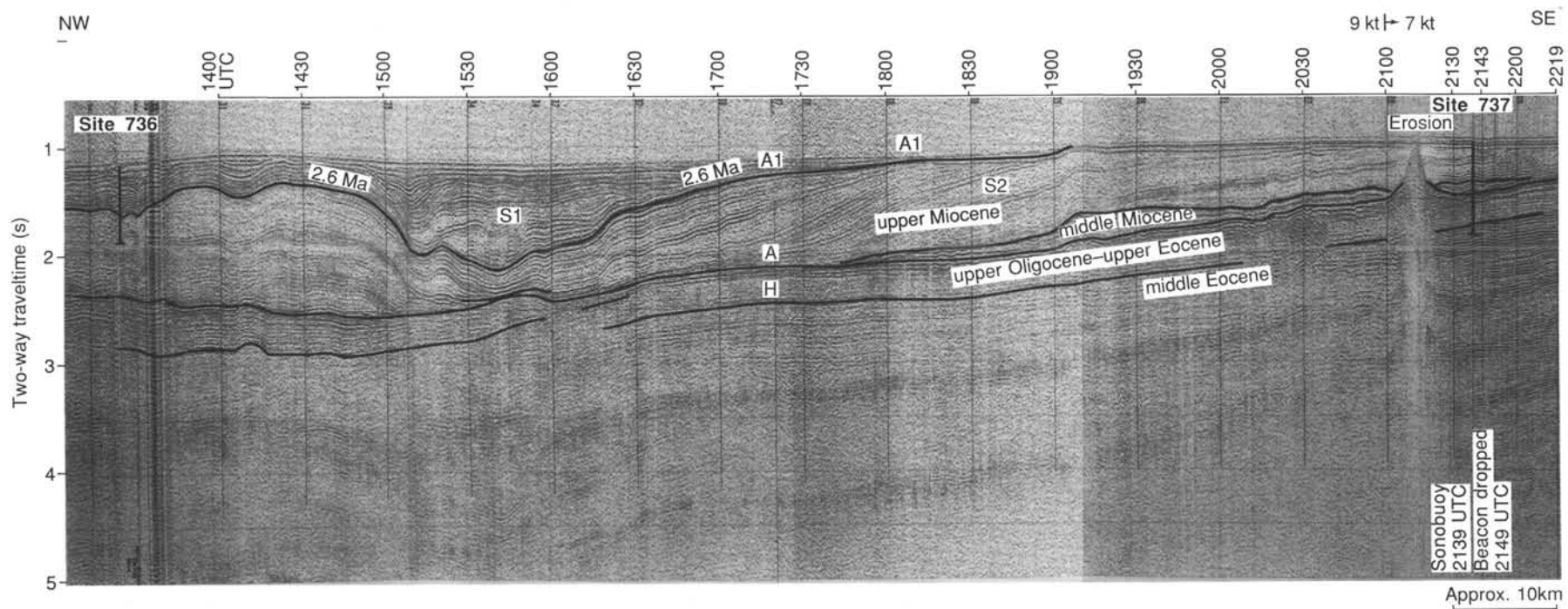


Figure 44. Single-channel seismic record between Site 736 and 737 (track shown on Figure 1) with the major seismic units marked. The horizontal scale varies slightly as a result of variation in ship's speed. The prograding sequence is seen between reflectors A and A1 at 2.6 Ma. Note the elevation on reflector A approximately 5 km north of Site 737.

Table 18. Major seismic units at Site 737.

Reflector	Unit	Depth (mbsf)	Age (Site 737)	Age (Ma)
Seafloor		0	Holocene	0–3.4 hiatus
A	S2	320	late Pliocene–middle Miocene	15–23 hiatus
H	II	670	late Eocene–late Oligocene	
Basement	I2-3	~1430	–middle Eocene	

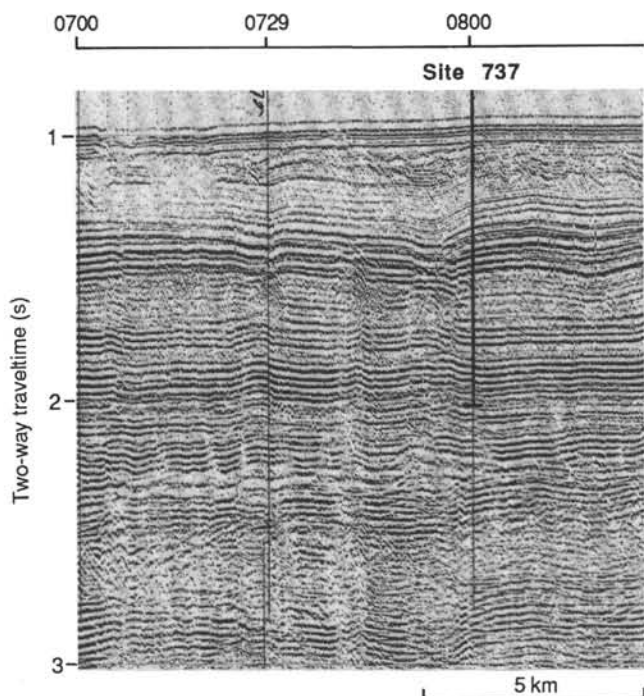


Figure 45. Single-channel seismic record from north to south across Site 737. Note the possible small-scale normal faulting of reflector A (Fig. 44) and deeper levels. The draping of the Miocene sediments over the fault scarps may be depositional structures, but a tectonic origin is also possible. Faulting has not been recognized on the nearby MD 26-13 line.

late Oligocene), a middle phase of mixed diatom and nannofossil ooze production with a significant volcanic sand input (late Oligocene to late Miocene), a late phase of diatom ooze sedimentation (late Miocene to early Pliocene), and a final phase during the late Pliocene and Quaternary of either slow sedimentation combined with bypassing of sediments by bottom currents or, less likely, uplift and removal of sediments. Disseminated volcanic glass and/or minerals first occur in uppermost Eocene sediments and reach their peak in Unit III (middle to upper Miocene, or about 13.8–7.8 Ma). These ages are significant, because Nougier (1972) dated two extrusive basalts on Kerguelen Island at 13.3 and 11.5 Ma and dated phonolitic extrusions in southeastern part of the island at 8–9 Ma.

Seismic Stratigraphy

The middle Eocene to lower Miocene unconformity proposed by Munschy and Schlich (1987), based on seismic interpretation for the northern Kerguelen-Heard Plateau, was not recognized at Site 737. An unconformity, however, is probably present between the middle Eocene and upper Eocene where

nannofossil Subzone CP15a is extremely compressed, and it is possible that this relatively brief hiatus (estimated duration 2 m.y.) may correspond to the time when Broken Ridge was rifted away from the Kerguelen-Heard Plateau along the Southeast Indian Ridge. This unconformity is also recognized as a seismic reflector by sonobuoy studies, and it corresponds to a downhole increase in sonic velocities measured by physical properties and by logging. If this unconformity does represent the time of rifting, rapid subsidence of Site 737 followed and pelagic sedimentation apparently continued uninterrupted from the latest Eocene to the latest Oligocene.

A second unconformity at about 312.8 mbsf, which separates lowermost Miocene calcareous claystone from middle Miocene nannofossil-diatom ooze containing siltstone and volcanic sandstone (23–15 Ma), may correspond to seismic discordance A of Munschy and Schlich (1987). A reflector corresponding to this unconformity is traceable regionally by seismic stratigraphy and also coincides with a seismic velocity peak measured in a calcareous siltstone at 310 mbsf. The seismic unit overlying this reflector (unit S2 of Munschy and Schlich, 1987) progrades regionally onto this reflector, and it is possible that units older than middle Miocene may also prograde onto it east of the site. Thus, locally, sediment was deposited onto the surface corresponding to reflector A prior to the middle Miocene. The regional expression of this discordance may be related to increased volcanism and intrusions on Kerguelen Island. Nougier (1972) reported that the eruption of plateau basalts on Kerguelen Island began at 30 Ma but increased between 25 and 19 Ma. Rhyolitic injections dated at 25.9 (maximum age) and 15.6 Ma cut across the northern and central parts of Kerguelen Island, respectively.

Biostratigraphy and Magnetostratigraphy

Calcareous microfossils are present and generally abundant from the upper middle Eocene to the middle upper Miocene. A complete Eocene/Oligocene boundary appears to be present at about 606 mbsf, and no abrupt environmental change is evident in nannofossil assemblages across the boundary. A good magnetostratigraphic record was obtained for the Eocene and Oligocene which supports the biostratigraphic evidence that the section is complete from the lower upper Eocene to the lowermost Miocene. Nannofossil diversity and abundances in the Eocene and Oligocene are similar to those in assemblages studied by W. Wei (unpubl. data) from Maud Rise (ODP Leg 113) and the Falkland Plateau (ODP Leg 114).

Diatoms and radiolarians are present and generally abundant and well preserved from the uppermost Oligocene to the Quaternary surficial lag sand. Diatom assemblages are dominated by Southern Ocean species above 3.9 Ma, but temperate species make up an important component of middle Miocene through lowermost Pliocene assemblages. Indeed, low-latitude diatoms are consistently present in the upper Miocene 8.2 to 5.1 Ma interval recovered at Site 737. Radiolarian assemblages show no low-latitude affinities, but they are low in diversity, probably reflecting the shallow water depth of Site 737.

In addition to unconformities detected between the middle Eocene and upper Eocene and between the upper Oligocene and the middle Miocene, an unconformity spanning the interval between 10 and 8.2 Ma is recognized by diatom and radiolarian biostratigraphy at 263 mbsf. This unconformity coincides with combined widespread Neogene deep-sea hiatuses NH5 and NH4 of Barron and Keller (1982).

Magnetostratigraphy is of good quality and straightforward in the upper Miocene and lower Pliocene, but poor recovery and the presence of the two recognized hiatuses (23.7–15 and 8.2–10 Ma) make interpretation of magnetostratigraphy in the middle Miocene difficult.

Geochemistry

A low organic carbon content (0.5%–0.3% TOC in the upper 225 mbsf, decreasing to <0.1% TOC below that depth) characterizes Site 737 sediments. Combined with relatively inactive methanogenic bacteria, this low organic carbon content has a major effect on the geochemistry of Site 737 sediments. Interstitial-water phosphate and ammonium concentrations are relatively low, and no gas pockets were observed. Dissolved sulfate concentrations decrease with depth, but they do not reach sufficiently low levels to indicate extensive sulfate reduction. Sharp discontinuities of calcium, magnesium, silica, and pH occur in Site 737 pore waters with depth at about 400 mbsf, corresponding with the uppermost Oligocene transition from nanofossil-rich clays and oozes below to mixed diatom and nanofossil oozes and clays above. Calcium and pH increase with depth to 380–400 mbsf and remain high. Magnesium and silica show opposite trends, although silica is variable between 285 and 380 mbsf.

REFERENCES

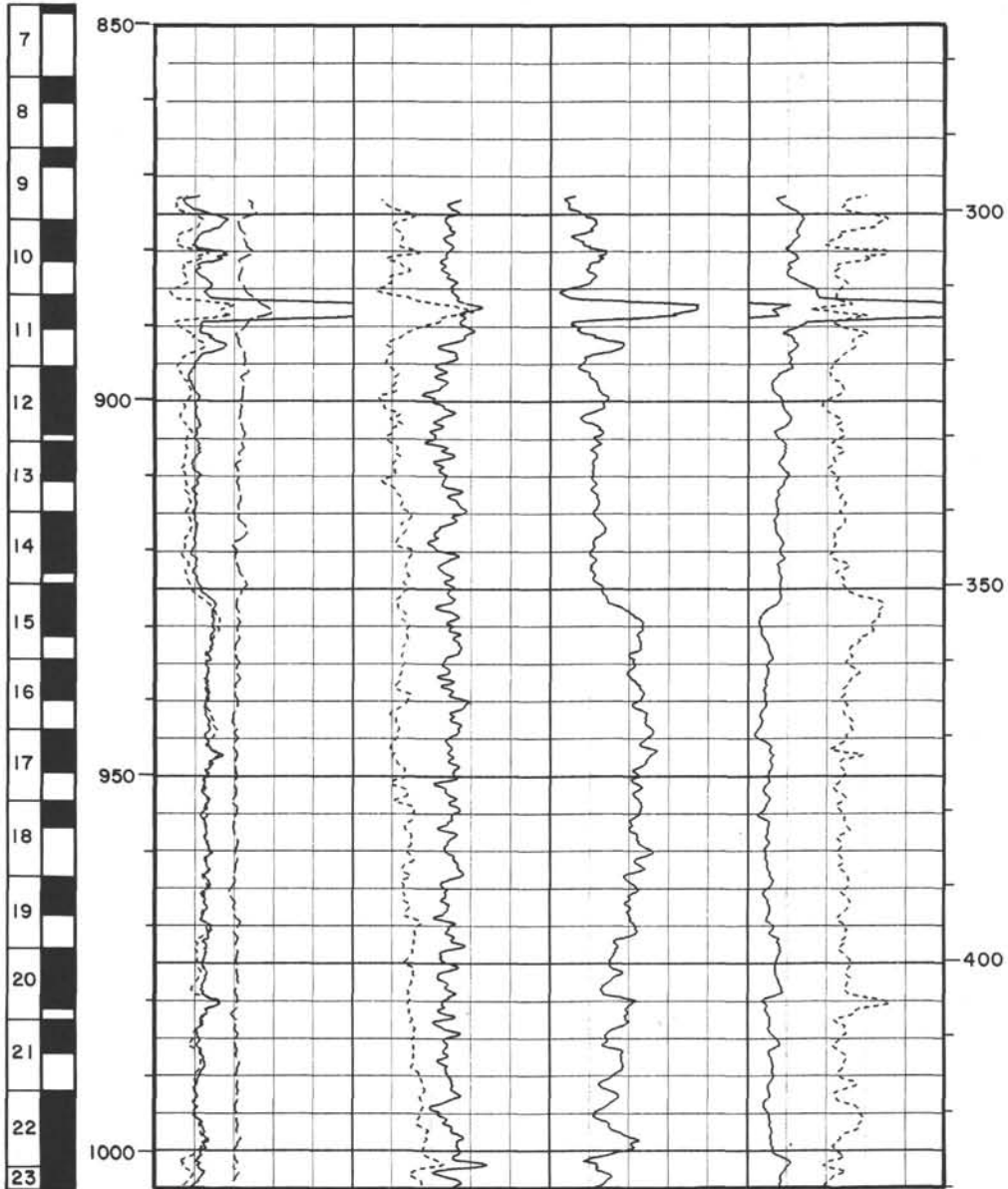
- Abbott, W. H., 1974. Temporal and spatial distribution of Pleistocene diatoms from the southeast Indian Ocean. *Nova Hedwigia*, 25:291–347.
- Balech, E., 1975. Clave ilustrada de dinoflagelados Antárticos. *Inst. Antart. Argent. Publ.*, 11:1–99.
- Barron, J. A., 1985. Miocene to Holocene planktonic diatoms. In Bolli, H. M., Saunders, J. B., and Perch-Nielsen, K. (Eds.), *Plankton Stratigraphy*: Cambridge (Cambridge Univ. Press), 763–809.
- Barron, J. A., and Keller, G., 1982. Widespread Miocene deep-sea hiatuses: coincidence with periods of global cooling. *Geology*, 10:577–581.
- Barron, J. A., Keller, G., and Dunn, D. A., 1985. A multiple microfossil biochronology for the Miocene. In Kennett, J. P. (Ed.), *The Miocene Ocean: Paleoceanography and Biogeography*: Mem. Geol. Soc. Am., 163:21–36.
- Bathurst, R. G. C., 1975. *Carbonate Sediments and Their Diagenesis*: Amsterdam (Elsevier).
- Berggren, W. A., Kent, D. V., and Van Couvering, J. A., 1985. The Neogene: part 2. Neogene geochronology and chronostratigraphy. In Snelling, N. J. (Ed.), *The Chronology of the Geological Record*: Geol. Soc. London Mem., 10:211–260.
- Bolli, H. M., and Saunders, J. B., 1985. Oligocene to Holocene low latitude planktonic foraminifera. In Bolli, H. M., Saunders, J. B., and Perch-Nielsen, K. (Eds.), *Plankton Stratigraphy*: Cambridge (Cambridge Univ. Press), 155–262.
- Boyce, R. E., 1973. Physical properties—methods. In Edgar, N. T., Saunders, J. B., et al., *Init. Repts. DSDP*, 15: Washington (U.S. Govt. Printing Office), 1115–1127.
- Bukry, D., 1973. Low-latitude coccolith biostratigraphic zonation. In Edgar, N. T., Saunders, J. B., et al., *Init. Repts. DSDP*, 15: Washington (U.S. Govt. Printing Office), 685–704.
- , 1975. Coccolith and silicoflagellate stratigraphy, northwestern Pacific Ocean, Deep Sea Drilling Project, Leg 32. In Larson, R. L., Moberly, R., et al., *Init. Repts. DSDP*, 32: Washington (U.S. Govt. Printing Office), 677–702.
- Ciesielski, P. F., 1983. The Neogene and Quaternary diatom biostratigraphy of subantarctic sediments, Deep Sea Drilling Project Leg 71. In Ludwig, W. J., Krashennnikov, V. A., et al., *Init. Repts. DSDP*, 71: Washington (U.S. Govt. Printing Office), 635–665.
- Clark, S. P., 1966. Handbook of physical constants. *Mem. Geol. Soc. Am.*, 97:459–482.
- Claypool, G. E., and Kvenvolden, K. A., 1983. Methane and other hydrocarbon gases in marine sediments. *Annu. Rev. Earth Planet. Sci.*, 11:299–327.
- Corliss, B. H., 1979a. Recent deep-sea benthonic foraminiferal distributions in the southeast Indian Ocean: inferred bottom water routes and ecological implication. *Mar. Geol.*, 31:115–138.
- , 1979b. Taxonomy of Recent deep-sea benthonic foraminifera from the southeast Indian Ocean. *Micropaleontology*, 25:1–19.
- Deroo, G., Herbin, J.-P., Roucache, J. R., and Tissot, B., 1979. Organic geochemistry of Cretaceous mudstones and marly limestones from DSDP Sites 400 and 402, Leg 48, eastern North Atlantic. In Montadert, L., Roberts, D. G., et al., *Init. Repts. DSDP*, 48: Washington (U.S. Govt. Printing Office), 921–930.
- Deroo, G., Herbin, J.-P., Roucache, J. R., Tissot, B., Albrecht, P., and Dastillung, M., 1978. Organic geochemistry of some Cretaceous claystones from Site 391, Leg 44, western North Atlantic. In Benson, W. E., Sheridan, R. E., et al., *Init. Repts. DSDP*, 44: Washington (U.S. Govt. Printing Office), 593–598.
- Ehlmann, A. J., 1978. Glauconite. In Fairbridge, R. W., and Bourgeois, J. (Eds.), *Encyclopedia of Sedimentology*: Stroudsburg, PA (Dowden, Hutchinson, and Ross), 364–366.
- Ekdale, A. A., Bromley, R. G., and Pemberton, S. G., 1984. *Ichnology: The Use of Trace Fossils in Sedimentology and Stratigraphy*: SEPM Short Course, 15.
- Fenner, J., Schrader, H.-J., and Wienigk, H., 1976. Diatom phytoplankton studies in the Southern Ocean, composition, and correlation to the Antarctic Convergence and its paleoecological significance. In Hollister, C. D., Craddock, C., et al., *Init. Repts. DSDP*, 35: Washington (U.S. Govt. Printing Office), 757–813.
- Fryxell, G. A., Hasle, G. R., and Carty, S. V., 1986. *Thalassiosira tumida* (Janisch) Hasle: observations from field and clonal cultures. *Proc. 8th Int. Diatom Symp.*, 8:11–21.
- Gieskes, J. M., 1983. The chemistry of interstitial waters of deep sea sediments: interpretation of deep sea drilling data. In Riley, J. P., and Chester, R. (Eds.), *Chemical Oceanography* (vol. 8): New York (Academic Press), 221–269.
- Gombos, A. M., Jr., 1977. Paleogene and Neogene diatoms from the Falkland Plateau and Malvinas Outer Basin: Leg 36, Deep Sea Drilling Project. In Barker, P., Dalziel, I. W. D., et al., *Init. Repts. DSDP*, 36: Washington (U.S. Govt. Printing Office), 575–687.
- Hart, T. S., 1937. *Rhizosolenia curvata* Zacharias, an indicator species in the Southern Ocean. *Discovery Rep.*, 16:413–446.
- Jenkins, D. G., 1985. Southern mid-latitude Paleocene to Holocene planktonic foraminifera. In Bolli, H. M., Saunders, J. B., and Perch-Nielsen, K. (Eds.), *Plankton Stratigraphy*: Cambridge (Cambridge Univ. Press), 263–282.
- Kennett, J. P., and Srinivasan, M. S., 1983. *Neogene Planktonic Foraminifera*: Stroudsburg, PA (Hutchinson Ross).
- Kerr, R. A., 1987. Ocean drilling details steps into an icy world. *Science*, 236:912–913.
- Martini, E., 1971. Standard Tertiary and Quaternary calcareous nannoplankton zonation. In Farinacci, A. (Ed.), *Proc. Planktonic Conf. II Rome 1970*: Rome (Edizioni Technoscienza), 2:739–785.
- Martini, E., and Müller, C., 1986. Current Tertiary and Quaternary calcareous nannoplankton stratigraphy and correlations. *Newsl. Stratigr.*, 16:99–112.
- McCrae, S. G., 1972. Glauconite. *Earth Sci. Rev.*, 8:397–440.
- McDuff, R. E., 1978. Conservation behavior of calcium and magnesium in interstitial waters of marine sediments: identification and interpretation [Ph.D. dissert.]. Univ. of California, San Diego.
- McDuff, R. E., and Gieskes, J. M., 1976. Calcium and magnesium profiles in DSDP interstitial waters: diffusion or reaction? *Earth Planet. Sci. Lett.*, 33:1–10.
- Munsch, M., and Schlich, R., 1987. Structure and evolution of the Kerguelen-Heard Plateau (Indian Ocean) deduced from seismic stratigraphic studies. *Mar. Geol.*, 76:131–152.
- Nougier, J., 1972. Geochronology of the volcanic activity in Iles Kerguelen. In Adie, R. J. (Ed.), *Antarctic Geology and Geophysics*: Oslo (Universitetsforlaget), 803–808.
- Okada, H., and Bukry, D., 1980. Supplementary modification and introduction of code numbers to the low latitude coccolith biostratigraphic biozonation (Bukry, 1973; 1975). *Mar. Micropaleontol.*, 5: 321–325.
- Perch-Nielsen, K., 1985. Cenozoic calcareous nannofossils. In Bolli, H. M., Saunders, J. B., and Perch-Nielsen, K. (Eds.), *Plankton Stratigraphy*: Cambridge (Cambridge Univ. Press), 427–554.
- Rivkin, R. B., and Putt, M., 1987. Dual periodicity of photosynthesis in polar phytoplankton: influence on primary production. *Science*, 238:1285–1288.
- Sangree, J. B., and Widmier, J. M., 1977. Seismic stratigraphy and global changes of sea level, part 9: seismic interpretation of clastic depositional facies. In Payton, C. E. (Ed.), *Seismic Stratigraphy: Applications to Hydrocarbon Exploration*: AAPG Memoir, 26:165–184.
- Scholle, P. A., 1978. A color illustrated guide to carbonate rock constituents, textures, cements, and porosities. *AAPG Memoir*, 27.

- Shah, M. P., and Levin, F. K., 1973. Gross properties of time-distance curves. *Geophysics*, 38:643-656.
- Thomas, E., 1985. Late Eocene to Recent benthic foraminifers from the central equatorial Pacific Ocean. In Meyer, L., Theyer, F., Thomas, E., et al., *Init. Repts. DSDP*, 85: Washington (U.S. Govt. Printing Office), 655-694.
- Tissot, B. P., and Welte, D. H., 1984. *Petroleum Formation and Occurrence* (2nd ed.): Berlin (Springer-Verlag).
- Wei, W., and Wise, S. W., Jr., in press. Paleogene calcareous nannofossil magnetostratigraphy: results from South Atlantic DSDP Site 516. *Mar. Micropaleontol.*
- Welton, J. E., 1984. The SEM petrology atlas. *AAPG Methods Explor.*
- Wetzel, A., 1984. Bioturbation in deep-sea fine-grained sediment: influence of sediment texture, turbidite frequency and rates of environmental change. In Stow, D.A.V., and Piper, D.J.W. (Eds.), *Fine-Grained Sediments: Deep-Water Processes and Facies*: Oxford (Blackwell Scientific) 595-608.
- Wise, S. W., Jr., 1983. Mesozoic and Cenozoic calcareous nannofossils recovered in Deep Sea Drilling Project Leg 71 in the Falkland Plateau Region, southwest Atlantic Ocean. In Ludwig, W. J., Krashennikov, V. A., et al., *Init. Repts. DSDP*, 71: Washington (U.S. Govt. Printing Office), 481-550.

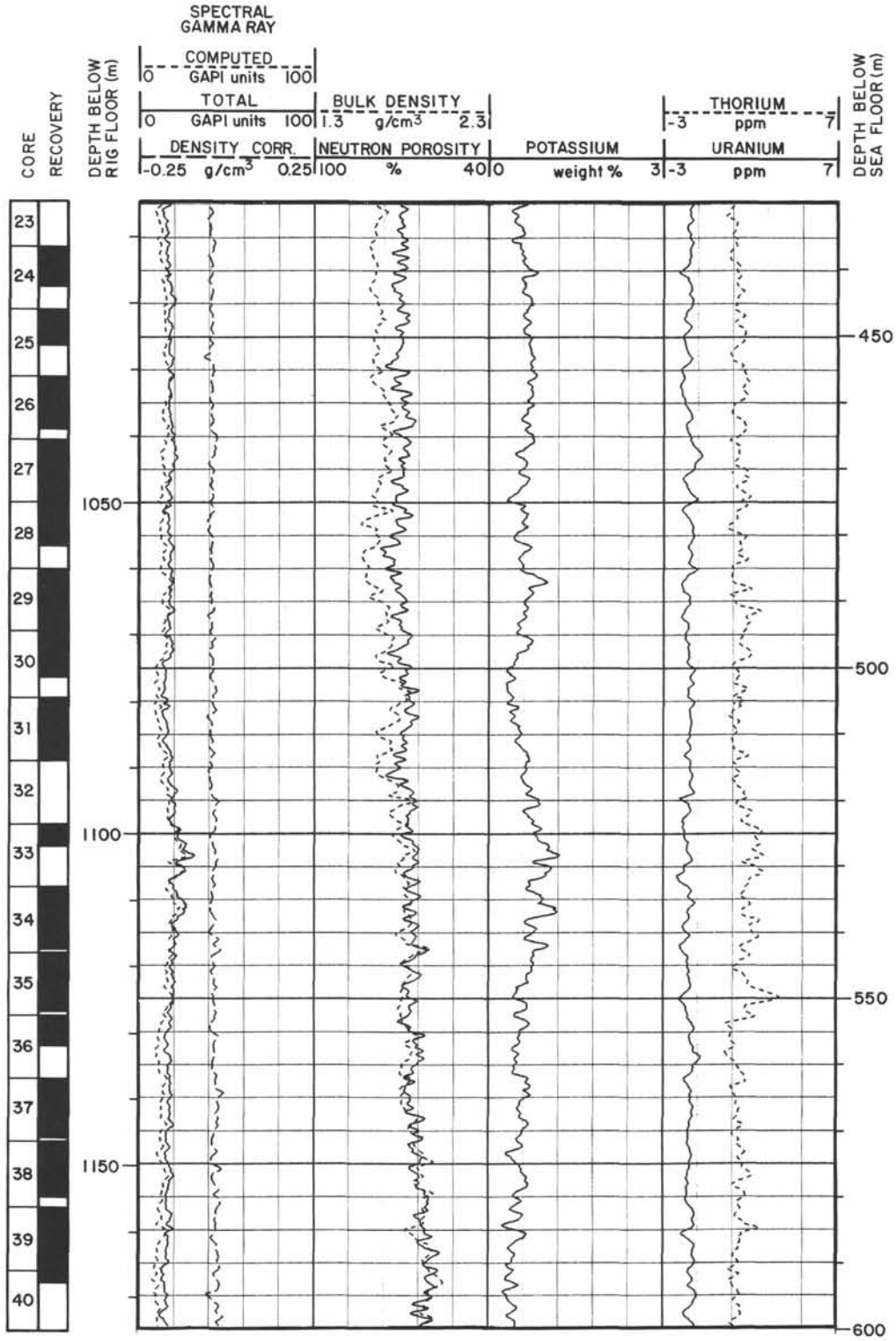
Ms 119A-105

Summary Log for Hole 737B

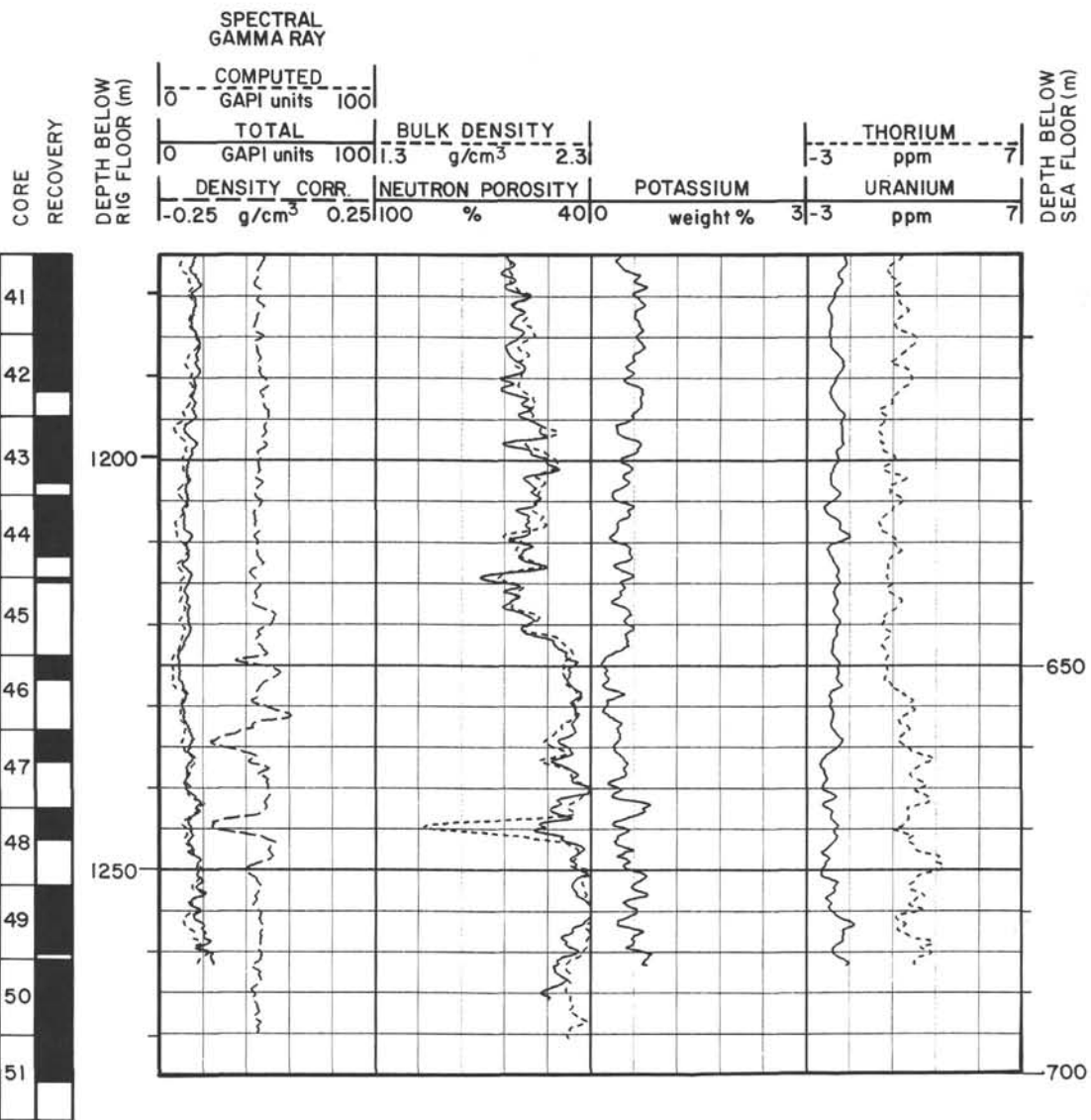
		SPECTRAL GAMMA RAY						
CORE RECOVERY	DEPTH BELOW RIG FLOOR (m)	COMPUTED GAPI units		BULK DENSITY		THORIUM		
		0	100	1.3	2.3	3	7	
		TOTAL GAPI units		g/cm ³		ppm		
		DENSITY CORR.	NEUTRON POROSITY	POTASSIUM	URANIUM			
		-0.25 g/cm ³	0.25	100 %	400	weight %	3	7
							ppm	



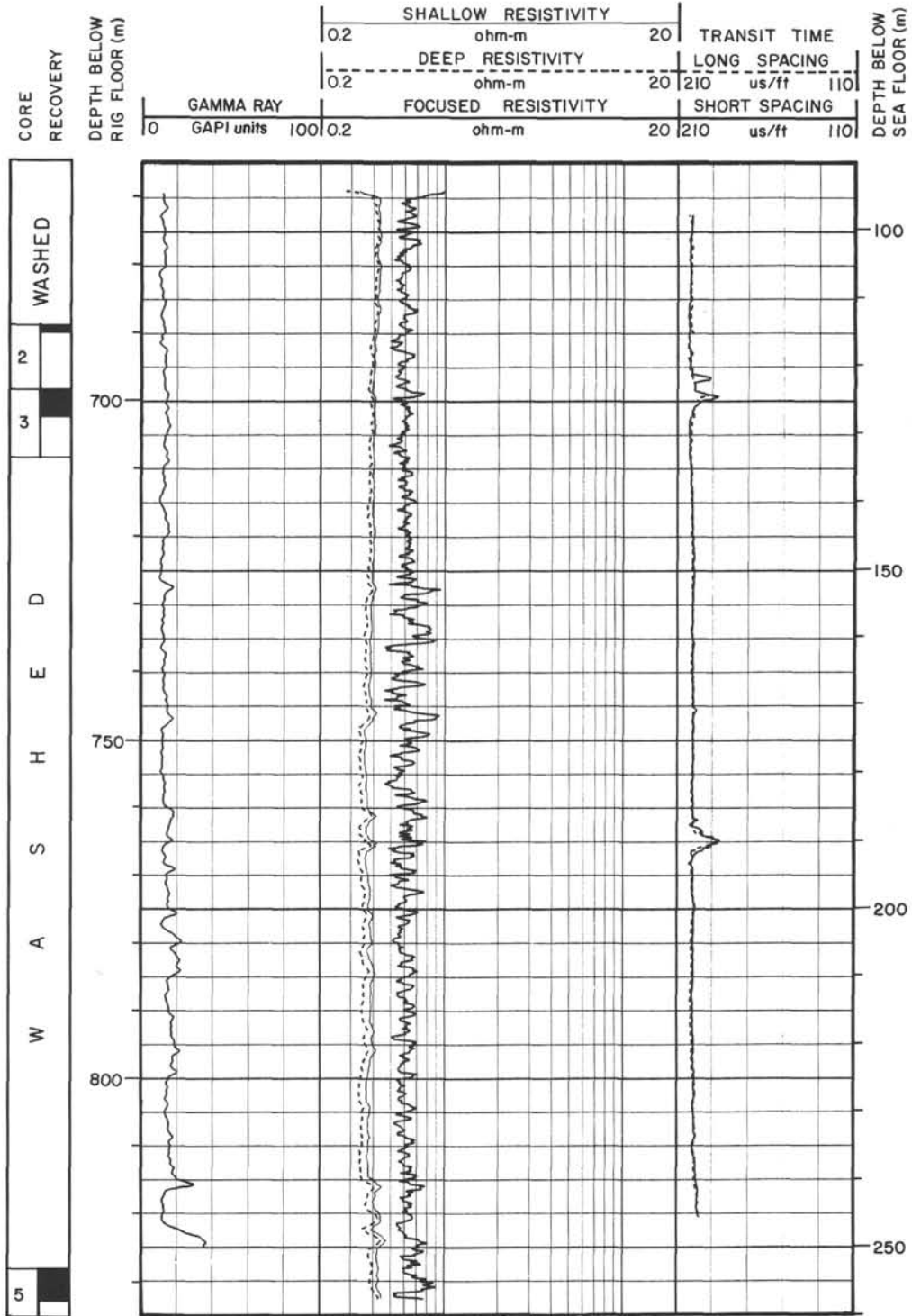
Summary Log for Hole 737B (continued)



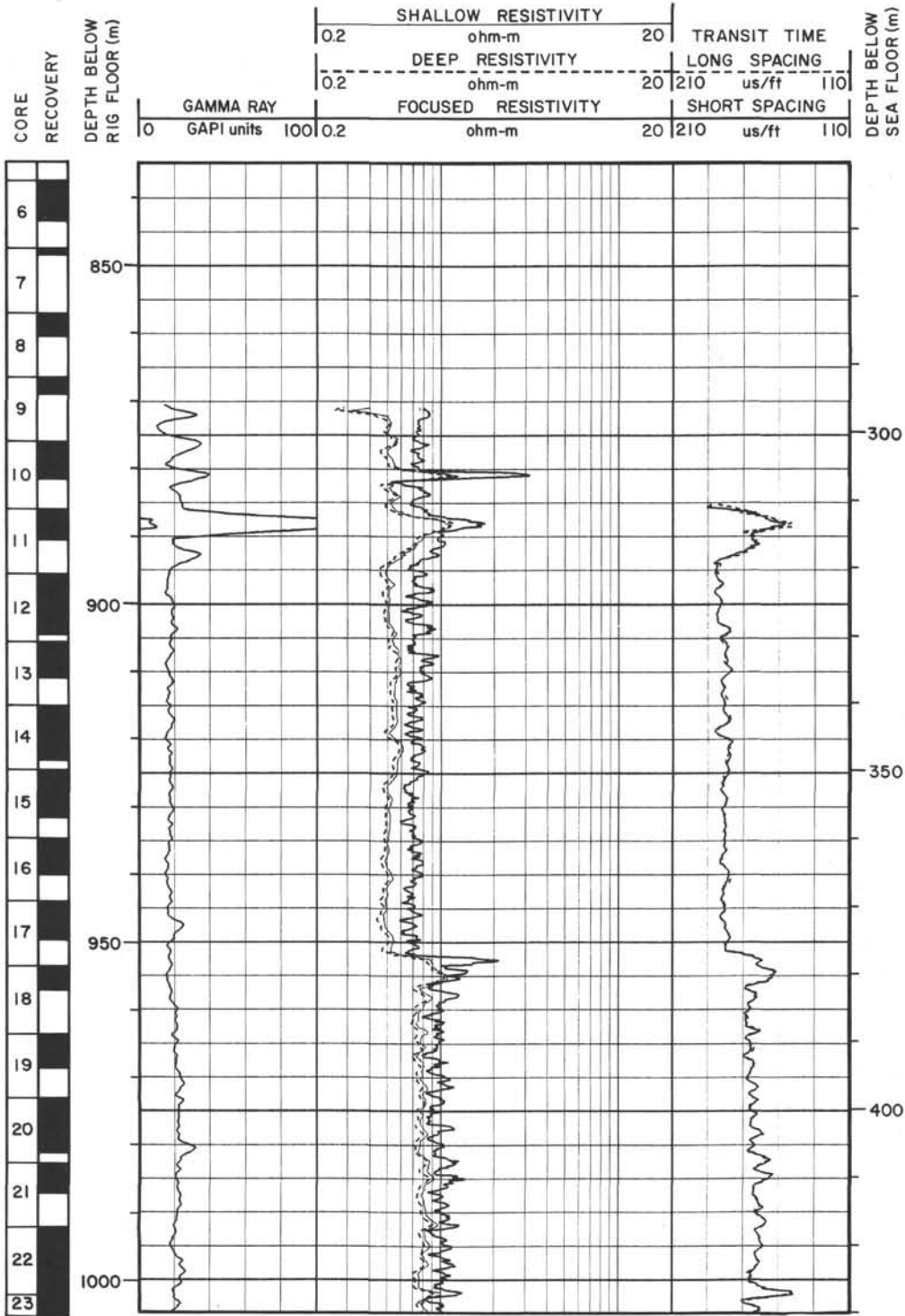
Summary Log for Hole 737B (continued)



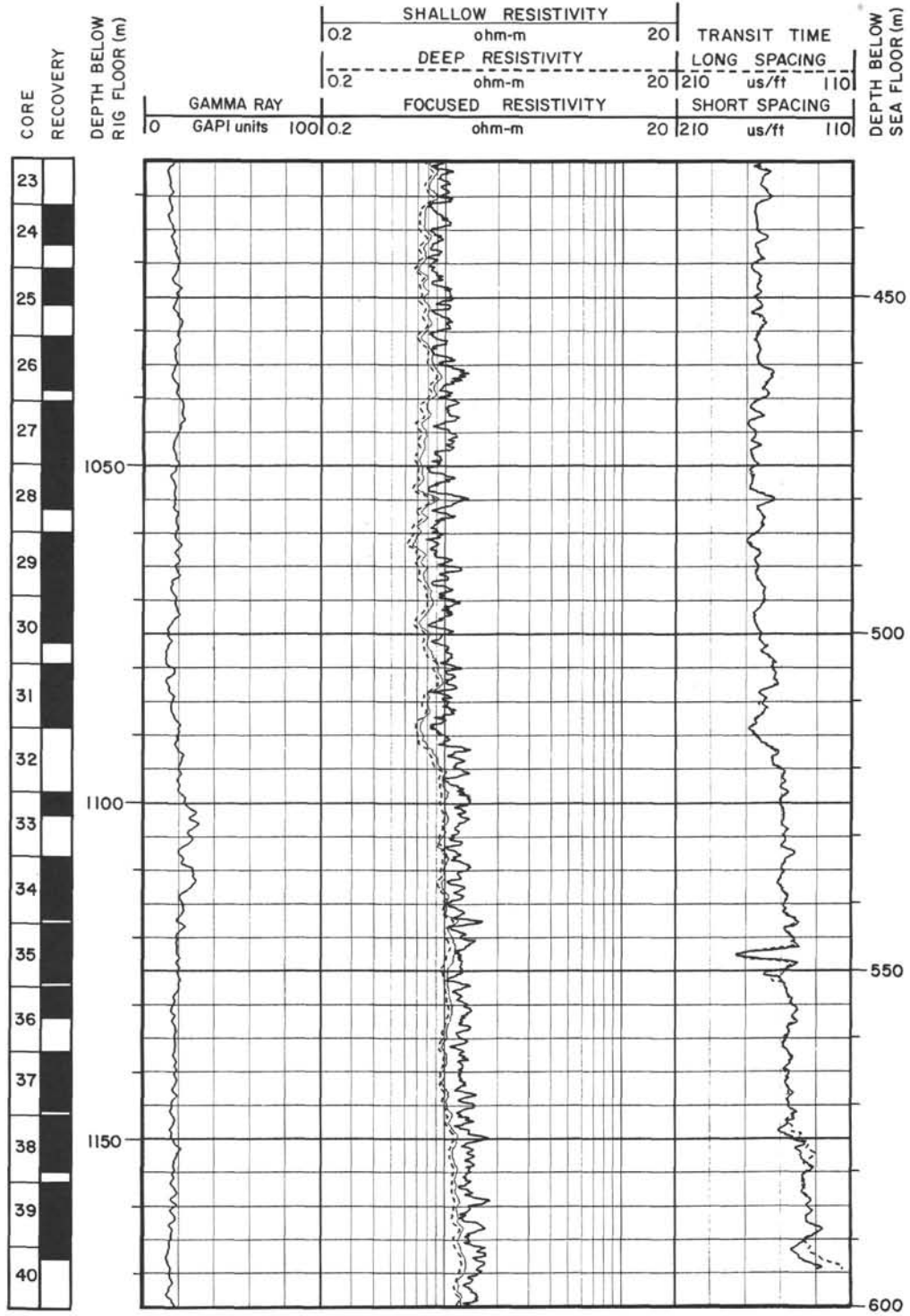
Summary Log for Hole 737B (continued)



Summary Log for Hole 737B (continued)



Summary Log for Hole 737B (continued)



Summary Log for Hole 737B (continued)

